THERMAL TURBULENT JETS

by

ANDREW H. WARREN

A dissertation submitted to the Graduate Faculty in Engineering in partial fulfillment of the requirements for the degree of Doctor of Philosophy, The City University of New York.

1976

This manuscript has been read and accepted for the Graduate Faculty in Engineering in satisfaction of the dissertation requirement for the degree of Doctor of Philosophy.

Dec 23, 1975
date

Chairman of Examining Committee

Jan 21, 1976
date

Jacques E Benvenuste
Executive Officer

Professor R.F. Dressler

Professor G.G. Ross

Professor N.C. Jen, Chairman
Supervisory Committee

The City University of New York

ABSTRACT

Thermal turbulent discharges are investigated. Numerical solutions are presented for two-dimensional time dependent jets. The governing equations are developed for a general three-dimensional, time dependent case. Equations of continuity, momentum, energy and turbulent intensity together with expressions evaluating eddy viscosity and mean square turbulent vorticity are formulated. Turbulent flow expressions are derived from an analysis of turbulent energy spectrum in the wave number space and with assumption of isotropic turbulence. Boussinesq approximation for the buoyancy force is applied. The equations are written in the finite difference form and the solutions are obtained through an explicit integration scheme with successive over-relaxation iteration method for the solution of the Poisson equation for the potential function on each time step. Free surface problems are investigated, although the solution may also be applied to open space problems. Temperature and velocity distributions are obtained for discharges to stationary or flowing ambients. Comparison of turbulent and laminar approximation of the flow is made.

Experiments were performed and data on velocity and temperature on vertical deep and shallow discharges were accumulated. A temperature compensated hot film probe and a special light technique were applied to gather the data. In order to test the accuracy of resulting solutions detailed comparisons were made with the experimental results. Very good agreement was achieved.

A C K N O L E D G E M E N T S

It is a pleasure for me to express my most sincere gratitude to my mentor, Professor Norman C. Jen. His friendly guidance, advice and high professional standards were most helpful in my work on this dissertation.

I am thankful to my Doctoral Committee members, Professors R.F. Dressler and G.G. Ross for their assistance and interest.

The discussions with Dr. J. Markowsky of American Electric Power Service Corporation and his comments on commercial application of this dissertation are greatly appreciated.

Special thanks are due to Professor C.M. Tchen for his comments and suggestions on the theory of turbulence. I am also thankful to Professor R.G. Stoneham and Mr. W. Lopinski for many valuable suggestions.

I wish to thank Messrs. W. Tendrich and W. Hall. Their ingenious and very high quality work was most helpful in building the apparatus and gathering the experimental data. The assistance of Mr. I. Mansfield in taking pictures is appreciated.

I am grateful to Ms. A. Novak for valuable comments and for proofing of the manuscript.

The financial aid and services provided by the City College and the Department of Civil Engineering are gratefully acknowledged.

TABLE OF CONTENTS

LIST OF FIGURES

LIST OF FIGURES - DEEP DISCHARGES

EXPERIMENTAL RESULTS

(*) - CJT-VDR - Constant Jet Temperature - Various Discharge Rates

Vjt-CDR - Various Jet Temperature - Constant Discharge Rate

LIST OF FIGURES - SHALLOW DISCHARGES

EXPERIMENTAL AND NUMERICAL RESULTS

LIST OF FIGURES - PHOTOGRAPHS

NOMENCLATURE

c_p	specific heat at constant pressure
E	three-dimensional energy-spectrum function
$F(k,t)$	three-dimensional transfer-spectrum function
F	densimetric Froude number
g_i	i-component of gravitational acceleration
K	thermal conductivity
K_k	diffusion by inhomogeneity
k	wave number
p	pressure
p'	fluctuating pressure component
$\bar{p}$	mean pressure component
$\tilde{p}$	pressure variations
T	absolute temperature
T'	fluctuating temperature component
$\bar{T}$	mean temperature component
T_r	ambient temperature
$\tilde{T}$	temperature variations
t	time
u_i	velocity component in i-direction
u_i'	fluctuating velocity component in i-direction
$\bar{u}_i$	mean velocity component in i-direction
U,u	velocity component in x-direction
V,v	velocity component in y-direction
W_k	transfer function
x_i	i-coordinate
x, y	horizontal and vertical coordinates respectively

α	thermal diffusivity $k/\rho c_p$
β	volumetric coefficient of thermal expansion
$\gamma', \gamma'', \gamma'''$	dimensionless constants
$\delta_{i,j}$	Kronecker operator
δt, dt	time step
δx, dx	space step in x-direction
δy, dy	space step in y-direction
ϵ	total dissipation
ϵ_{ijk}	alternating tensor
ϵ_m, ϵ_h	eddy diffusivity (momentum, thermal)
$\bar{\eta}$	mean vorticity
η'	fluctuating vorticity
$\varkappa_1, \varkappa_2, \varkappa_3$	dimensionless constants
μ	absolute viscosity
ν	kinematic viscosity
ρ	density
ρ_r	reservoir density
$\tilde{\rho}$	density variations
σ	ratio of eddy diffusivities (thermal to momentum)
φ	ratio of pressure to (constant) density p/ρ
Ψ_k	production function
$\zeta_1, \zeta_2, \zeta_3, \zeta_4$	numerical constants

Subscripts and Superscripts

i, j, n	correspondingly: space, space, time indexes in the finite difference equations
i, j, k, l	index of coordinate axis, Einstein (tensor) notation

Abbreviations

ODE	ordinary differential equation
PDE	partial differential equation
WRT	with respect to

I. INTRODUCTION AND LITERATURE REVIEW

The mathematical representation of the physical process of a thermal discharge is a complex one. Turbulence and interaction of inertia and buoyancy forces are the major factors in the structure of the flow. In addition to the velocity and temperature it is necessary to evaluate a number of correlations of turbulent quantities. This entails the analysis of the theory of turbulence and the closure problem. The governing equations are highly nonlinear and theoretical analysis is hardly possible. The earlier research in this area concentrated on approximated integral techniques to solve certain problems. The solutions were often applicable to a limited case only (e.g. simple jet, simple plume) barring a wider range of applications. Also, many terms were neglected as a necessity to simplify the governing equations.

The investigation of turbulent thermal discharges presented here resulted in the numerical solution of turbulent, time dependent buoyant jet. Equations of momentum, energy, turbulent intensity and other necessary expressions for turbulent flow were derived and solved. The solution covers the jet area, as well as, the far field of the thermal spread. This provides a solution for transient, or the steady flow of a discharge into a uniform or density stratified reservoir. Stationary environment, as well as, a cross flow for cases of vertical jets were investigated. Although the numerical procedure was developed for a two-dimensional case it may be extended to three dimensions, since the theory covers three-dimensional space.

The full impact of turbulence was taken under consideration for the case of isotropic turbulence. Thus, in addition to the velocity and temperature distribution, the turbulence intensity, eddy viscosity and turbulent vorticity were calculated for the entire field.

An approximated laminar flow case was also developed and a comparison between laminar and turbulent approach was made.

To assure correct numerical modeling and to test the accuracy of the resulting solutions, the parallel experimental investigation was performed. It provided data for the steady, two-dimensional flow of a vertical thermal discharge into water. Velocity and temperature distributions were obtained for a large variety of rates of flow and of discharge temperatures. The jet area and also the far field were investigated. The comparison of numerical results with the experiments was done for the near field and the far field. Good agreement with experimental data was found.

The typical field of a thermal discharge, that is already developed, can be divided into three major regions, each with its particular features. First is the region of a flow establishment with a potential flow core and a very large velocity and temperature gradients near the jet boundaries. The second is a region of an established flow where the velocity and temperature profiles of a jet cross-section could be roughly approximated by a Gaussian distribution curve, and the third is a region of thermal spread. The first two regions are usually turbulent; the region of thermal spread is rather laminar, although with a turbulent head in the initial stages of its development.

The trajectory of the jet axis and the size of the thermal discharge field are often characterized by the entrainment coefficient and densimetric Froude number.

The densimetric Froude number is particularly important in a case of horizontal, inclined jets. Its value reflects interaction between momentum and buoyancy forces, and is directly related to the shape of the jet axis.

The jet widens away from the discharge nozzle. This is due to a decreasing velocity of the jet and the entrainment of an ambient fluid. Rate of entrainment depends on velocity gradient and intensity of turbulence on jet borders, and, in a case of discharge to a stream, entrainment is due to a turbulence generated by the jet and the stream motion. In the initial stage of flow development, head entrainment is an additional source of entrainment.

The structure of the thermal jet is presented on the next page.

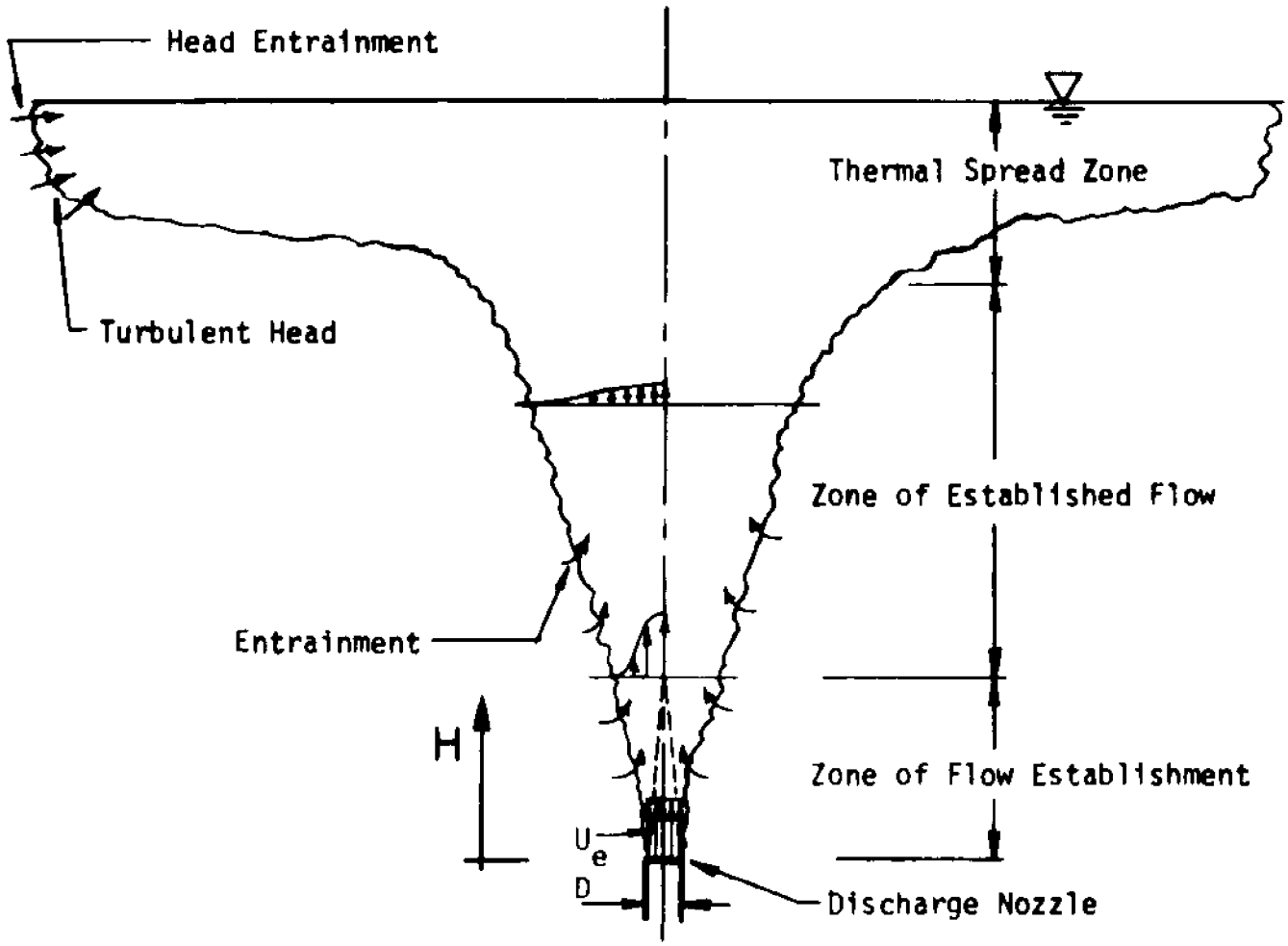

Fig. 1. Structure of Thermal Discharge

(symmetrical case)

U_e - entrance velocity

ρ_j - density of a discharge

In terms of the parameters shown above, the densimetric Froude number can be presented in a following form:

$$F = \frac{U_e^2}{D\, g\, \frac{\rho_r - \rho_j}{\rho_r}}$$

The theoretical and experimental work on a simple jet by Albertson, Dai, Jensen and Rouse (3) is the foundation of research in this area. The authors introduced the concept of zone of flow establishment and zone of established flow followed later by many writers. From theoretical investigation, it was found that velocity profiles are similar and follow a Gaussian distribution in the zone of established flow. They show also that there is a linear expansion of jet boundary, that center line longitudinal velocity is inversely proportional to the distance from the nozzle, and that volume flux over a cross-section increases linearly with the distance.

Albertson and others investigated simple steady jet without a any buoyancy impact. Morton, Taylor, and Turner (35) investigated in turn simple plumes in the environment with linear density stratification. In this case the flow field was developed through the impact of the buoyancy force alone with the absence of the initial momentum. They used the integral method for setting up the equations of volume, momentum, and density deficiency conservation. The main aspect of physical phenomenon in this case is that the plume, in a stably stratified environment, will not rise indefinitely, but only up to a certain level at which it will start to spread horizontally. It is due to a buoyancy force which will be decreasing with height until the point where it becomes slightly negative. With the entrainment coefficient assumed constant, the maximum height reached by the plume was predicted. Exact solution was obtained for the case of an instantaneous plume source.

In his further investigation, Morton (33) expanded his work on the turbulent, forced plumes which were generated by a steady release of mass, momentum, and buoyancy force from a source located in a uniform or stably stratified fluid. For the uniform environment, the plume was assumed to have a Gaussian profile of mean vertical velocity. By an integral method ODE's were developed for mass, momentum, and density deficiency. For a stably stratified environment, a "top hat" profile was assumed for mean vertical velocity, and integral technique was applied in the solution. The concept of a pointsource for generation of momentum and buoyancy was used. As the solution plume radius, vertical velocity, temperature excess, and in the case of stratified environment, height of rise were presented as functions of the vertical distance from the nozzle and density distribution in the ambient.

Experimental investigations of the buoyant air jets are presented in references (19), (25), (37) and (39). They were concerned with impact of the wind on the trajectory, effects of stratification and buoyancy.

Purely theoretical approach utilizing potential flow theory for a simple jet was presented by von J. Förste (16).

Problem of entrainment was extensively investigated by Morton, ref. (34). He proposes development of entrainment models for laminar axisymmetric flow in viscous jets, plumes, and wakes, and an application is made to the ascent of laminar plumes in a stably stratified environment. The entrainment flux scale is obtained using order of magnitude arguments, and in each case it is shown to be proportional to the kinematic viscosity ν with exception of thermal plumes at Prandtl numbers less than unity.

Further investigation of entrainment was carried out by other authors and is described in references (14), (15) and (37).

Horizontal buoyant jets form an important group of discharges. The magnitude of a densimetric Froude number and an interaction between momentum and buoyancy forces have impact on the shape of the jet trajectory. In this area Abraham (1) presents an analytical work and experimental results. His theory is set up in such a way that the solution matches the limits of either a simple plume or a simple jet. The resulting set of ordinary differential equations for mass, concentration, and momentum equations is solved numerically. In setting up the equations, Gaussian profiles for velocity and concentration distribution were assumed. From the experimental point of view, the investigation is restricted to measurements of concentration distribution of a tracer.

Similar approach is taken by Anwar (4) who extends investigation to discharge with angle of inclination of 30^{o}, and evaluates distribution of centerline dilution for various densimetric Froude numbers. Effect of thermal discharge on temperature distribution in river and also investigation of a radial, horizontal surface discharge were presented by Lawler, Ieporati and Lawler in references (28) and (29) respectively.

The buoyant discharge concept is applied to analysis of turbulent diffusion of a sewage field in an ocean current by Brooks (7). Two-dimensional PDE for diffusion with the assumptions of steady flow, and negligible vertical and horizontal mixing, describes the field of concentration.

A transformation is applied to reduce the governing equation to a form analogical to the heat conduction equation and an exact solution is obtained. The results show the dependence of concentration (decrease) on the distance from the jet nozzle.

Majority of earlier described papers dealt with the flow field of the jet itself. Sharp (40) extends investigation to the thermal spread. He works out an introduction for analytical investigation of the following physical process: when a jet of fresh water is discharged at depth into saline water, it rises to the surface and then spreads laterally as a horizontal current at the surface. The writer suggests the use of the method of synthesis and describes studies intended to provide a diagram solution method for the rate of spread. The concept of geometric and dynamic similarity is being used to set up the basic expressions. Experiments that were carried out provided data for relations between the nozzle diameter, volume of discharge, density differences versus the speed of spreading.

Effect of stratification was accounted in an experimental work by Fan (15). In his doctoral thesis Fan investigates a round buoyant jet in both uniform and stratified environments. The investigations, mostly experimental, are paralleled by analytical work based on integral method with assumption for similar Gaussian type profiles for velocity and concentration. In the experimental part the measurement of concentration of salt over the jet cross-section is taken for various nozzle diameters, angles of jet inclination, concentration,and initial velocity.

Tulin and Schwartz (44) presented a paper on investigations of hot discharge into a moving stratified environment. The first part is the case of hot gases from the chimney, entering a stratified atmosphere with uniform cross wind. The set of coupled ODE's describing the flow field is developed and solved exactly giving the plume trajectory and concentration distribution as a result. In the second part the authors investigate a hot discharge from the bottom of a stream. Conservation equations for excess mass, momentum balance, and turbulence decay are set up and the similarity concept is introduced.

Later Hirst (23) analyses round, turbulent, buoyant jets discharged to flowing stratified ambients. He applies the integral method which is based on an integration of the differential equations written in a "natural" system of coordinates. The paper includes extensive comparison of theoretical results with experiments.

Mahajan and John (30) present an experimental paper on a shallow, heated water jet discharged horizontally. Jet trajectories were recorded as functions of temperature and entrance velocity, and empirical correlations were obtained which yielded the locus of the point of maximum jet velocity as the jet moved toward the surface.

The papers reviewed provide an overview of the jet,or buoyant jet research. Several additional papers included into the references provide some variations or more detailed analysis of the problems discussed above. The references include also publications on theory of turbulence, and those, that were needed for a numerical investigation of the equations as well as the development of the computer code.

Applications

The solution presented in this dissertation has numerous applications. It may be used to handle a variety of thermal pollution problems or be extended to chemical, or sewage discharges.

Thermal pollution poses a serious environmental problem to the country's fresh waters and coastal sea areas. Its magnitude is directly related to increasing numbers of conventional and nuclear power plants. It is estimated that by 1980, one-sixth of the United States' fresh runoff will be used for cooling; one-third by the end of the century.

The efficiency of power plants varies from 30 to 40 percent, which means that for every three units of energy supplied, one unit produces electricity and approximately two units are discharged as waste. Eighty to one hundred percent of the waste energy is sent into the cooling water. In order to pick up an appropriate location and to assure the safe and efficient operation of a power plant, the detailed knowledge of the physical phenomena is necessary.

It should be mentioned that thermal pollution, when properly handled may even have beneficial, and not harmful effects.

The field of a thermal discharge may be subject to various external conditions. In addition to the parameters of discharge like rate of flow, temperature, size and orientation of the nozzle, the factors deciding the development of the flow include density stratification, current effects and the depth of the discharge. Density stratification depends either on a salt distribution, or on a temperature distribution in the reservoir, but in many cases on a combination of both.

In the case of a nonstratified reservoir a submerged thermal discharge reaches the surface and spreads horizontally; whereas, in the stratified case the discharge mixed with ambient reaches only a certain level and starts spreading in the lateral direction, often unable to reach the surface at all. This phenomenon is of serious importance in the operation of a sea or near-sea located power plant.

When discharging hot water to a river, large lake, or even to the ocean, current effects play the important role of introducing an extra velocity, changing the mixing pattern and significantly altering the motion of the fluid and its temperature distribution.

The flow and mixing pattern depend also on a design of discharge outlets, their location, depth of submersion, and orientation with respect to the stream or reservoir.

Major types of the flow fields are illustrated on the next page.

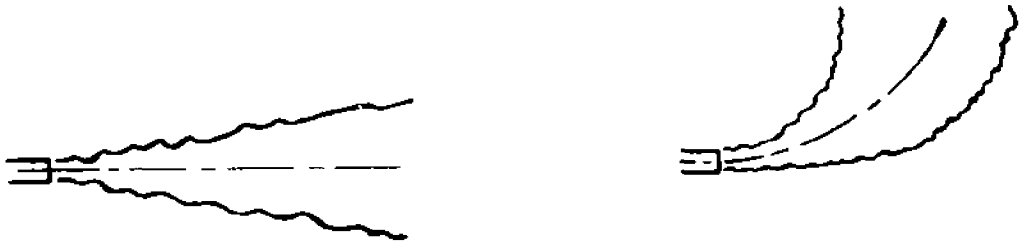

Simple jet

Hot jet

Buoyancy Effect

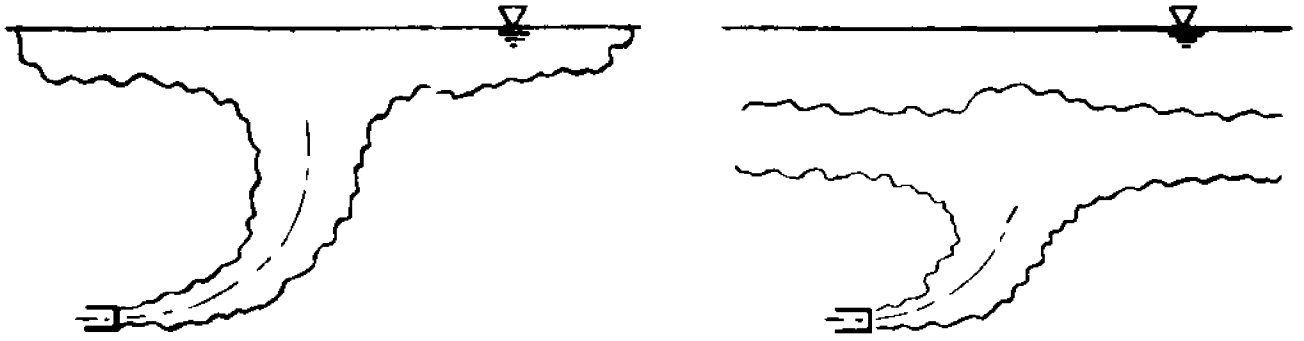

Uniform density reservoir

ρ_r = const

Density stratified reservoir

$\rho_r = \rho_r(\text{depth})$

Stratification Effect

Stagnant

$U_s = 0$

With current

$U_s = 0$

Current Effects

Fig. 2. JET BEHAVIOR IN VARIOUS EXTERNAL CONDITIONS

ρ_j - entrance density of a discharge

ρ_r - reservoir density

Summary

In brief, a summary of the thermal discharge research showed a large portion of prior theoretical investigation to be based on approximate integral techniques.

There was a limited amount of work done which would incorporate the impact of turbulence into the governing equations. Greater emphasis was put on the jet structure than on the analysis of the thermal spread.

On the experimental side there is large quantity of data on thermal plumes, that is, thermal discharges in air. In comparison much less work was performed on thermal water jets. In many cases the primary object of gathering data was the determination of the jet trajectories, jet boundaries, and concentration distribution. Little data is available on the velocity and temperature distribution of thermal water discharges. Again, investigations were most often limited to the jet area and there is not too much data available on the thermal layer. A significant contribution to the investigation of turbulent flows (not thermal) was made over the last few years by the Los Alamos group (Ref. (20)). Some concepts on turbulence introduced by that group were used in the development of the present investigation.

The contribution of the present work is that it synthesizes all the major aspects of the flow including the impact of the buoyancy force and turbulence. In the development of the governing equations no terms were neglected and thus the solution provides an accurate picture of thermal discharges and is thus applicable to a wide variety of problems.

Expressions relating eddy viscosity, turbulence intensity and mean square turbulent vorticity which were derived through the analysis of turbulent energy spectrum in the wave number space, introduce a new way of modeling turbulent viscosity. This significantly simplifies calculations and the evaluation of the turbulent quantities and yet closely satisfies the physical reality.

Experimental data that were gathered implement and also verify the theoretical results.

II. MATHEMATICAL FORMULATION

1. DEVELOPMENT OF ANALYTICAL SOLUTION

The analytical formulation was developed for an unsteady, three-dimensional flow of the thermal discharge.

It consists of two major parts. First, a simplified case where the flow is assumed laminar. Second, where the flow is considered to be turbulent.

This two-step development will permit a comparison of laminar and turbulent flow solutions with the experimental results.

Equations describing the flow field were formulated and then transformed to a form which is suitable for numerical integration.

Initial and boundary conditions which were applied are described later in this chapter.

Cartesian tensor, or subscript notation, with its principles, was used in the analytical part.

A. LAMINAR FLOW

Let us start with the formulation of the governing equations. Describing the flow field the following assumptions have been made:

a. Fluid flow is laminar.

b. Viscous dissipation terms in the energy equation are neglected.

c. Molecular viscosity and thermal diffusivity coefficients are assumed to be constant.

d. Fluid is everywhere incompressible with respect to pressure, but density is a function of temperature in buoyancy, which is known as the Boussinesq assumption.

Rayleigh dissipation, i.e. frictional heating, is neglected in the energy equation for the laminar flow since its effects are negligible at a small Eckert number.

Therefore, the equations will be in the following form:

Continuity equation:

$$\frac{\partial u_i}{\partial x_i} = 0 \tag{1}$$

Momentum equation:

$$\frac{\partial u_i}{\partial t} + u_k \frac{\partial u_i}{\partial x_k} = g_i - \frac{1}{\rho}\frac{\partial p}{\partial x_i} + \nu \frac{\partial^2 u_i}{\partial x_k^2} \tag{2}$$

Energy equation:

$$\frac{\partial T}{\partial t} + u_k \frac{\partial T}{\partial x_k} = \alpha \frac{\partial^2 T}{\partial x_k^2} \tag{3}$$

It can be proved that if the fluid velocity is small compared with the velocity of sound the pressure variations occurring as a result of the density changes are so small that they can be neglected. The relation between density and temperature of water can be assumed linear, with sufficient degree of accuracy in the investigated temperature region, and this justifies dropping the pressure term from the energy equation.

To incorporate the buoyancy effects into the momentum equation, the variable temperature $T(x_i,t)$ is written in the following form:

$$T(x_i,t) = T_r + \tilde{T}(x_i,t) \tag{4a}$$

where T_r is a constant ambient temperature from which the variation $T(x_i,t)$ is computed.

The fluid density is a function of temperature and can be expressed in a similar form:

$$\rho(T) = \rho_r + \tilde{\rho}(T) \tag{4b}$$

where ρ_r is a constant reference density and $\tilde{\rho}(T)$ represents density changes due to temperature variations.

Density variations are given by the following expression:

$$\tilde{\rho}(T) = -\rho_r \beta \tilde{T} \tag{4c}$$

Here $\beta = -\frac{1}{\rho}\frac{\partial \rho}{\partial T}$ is the thermal expansion coefficient of the fluid. For the temperature range that we are concerned with density changes linearly with temperature and value of β can be assumed constant.

To represent pressure in the fluid we write:

$$p = p_r + \tilde{p} \tag{4d}$$

p_r is not a constant, it varies with height according to hydrostatic equation and therefore:

$$p_r = \rho_r \, \bar{g} \cdot \bar{x} + \text{const.} \tag{4e}$$

where $\bar{x}$ represents depth and g gravity.

With the expressions for pressure and density defined above we can now transform the pressure term from the momentum equation. Using (4b) and (4d) we get:

$$\frac{1}{\rho} \frac{\partial p}{\partial x_i} = \frac{1}{\rho_r + \tilde{\rho}} \frac{\partial}{\partial x_i} (p_r + \tilde{p}) \tag{4f}$$

Let us expand $(\rho_r + \tilde{\rho})^{-1}$ by binomial expansion and neglect second and higher order terms on the right hand side of (4f). We have:

$$\frac{1}{\rho} \frac{\partial p}{\partial x_i} = \frac{1}{\rho_r} \frac{\partial p}{\partial x_i} + \frac{1}{\rho_r} \frac{\partial p_r}{\partial x_i} - \frac{\tilde{\rho}}{\rho_r^2} \frac{\partial p_r}{\partial x_i} \tag{4g}$$

By definition:

$$\frac{1}{\rho_r} \frac{\partial p_r}{\partial x_i} = g_i \tag{4h}$$

and

$$\frac{\tilde{\rho}}{\rho_r} \frac{\partial p_r}{\partial x_i} = g_i \tilde{T} \tag{4i}$$

Substitution of (4h) and (4i) into (4g) gives us an expression for the pressure term:

$$\frac{1}{\rho}\frac{\partial p}{\partial x_i} = g_i + \frac{1}{\rho_r}\frac{\partial \tilde{p}}{\partial x_i} + g_i \beta \tilde{T} \qquad (5)$$

Since ρ is constant except in the buoyancy, we can also write:

$$\frac{1}{\rho}\frac{\partial p}{\partial x_i} = \frac{\partial}{\partial x_i}\left(\frac{\tilde{p}}{\rho_r}\right) \equiv \frac{\partial \psi}{\partial x_i} \qquad (6)$$

The concept introduced by (4i) thru (6) is known as Boussinesq assumption.

In a case of a temperature stratified reservoir ambient temperature (and density) will be a function of depth. Therefore, for that particular set of problems we assume: $T_r = T(x)$, where x represents depth.

Including the developed pressure gradient term into the momentum equation, the following set of equations is presented:

Continuity equation:

$$\frac{\partial u_k}{\partial x_k} = 0 \qquad (1a)$$

Momentum equation:

$$\frac{\partial u_i}{\partial \tau} + u_k \frac{\partial u_i}{\partial x_k} = -\frac{\partial \psi}{\partial x_i} - \beta g_i \tilde{T} + \nu \frac{\partial^2 u_i}{\partial x_k^2} \qquad (2a)$$

Energy equation:

$$\frac{\partial T}{\partial \tau} + u_k \frac{\partial T}{\partial x_k} = \alpha \frac{\partial^2 T}{\partial x_k^2} \qquad (3a)$$

The equations (1a) through (3a) form a closed set of five equations (in expanded form) with five unknowns. The solutions will be worked out together with various sets of initial and boundary conditions that will be described later in this chapter.

B. TURBULENT FLOW

From the experimental observation it is known that the field of the thermal discharge, or at least its initial portion, is turbulent. Consequently, in the next stage we shall develop the investigation which will more closely resemble the actual physical process rather than the laminar approximation.

To describe the physical phenomena the equations of continuity, momentum and energy for the unsteady, nonhomogeneous turbulent flow will be developed. In addition to that, two equations, namely, the equation for transport of the turbulent energy and the equation for turbulent viscosity will be derived.

The experimental research has been carried out parallel to the theoretical investigation and the phenomenological theory of turbulence will be used to evaluate the correlations of fluctuating quantities and the closure problem. This was done in order to assure close interrelation between the theoretical structure of the model and the experimental results.

A simplifying assumption of isotropic turbulence was applied. Justification for it comes from the fact that it is known from experimental evidence that the fine structure of most nonisotropic flows is nearly isotropic, and that the differences between the actual experimental results and the isotropic assumptions are negligibly small and may even be smaller than the spread in the experimental data.

We again start with basic equations (1a), (2a) and (3a) for continuity, momentum and energy conservation, with the addition that viscous dissipation terms are included into the energy equation.

Introducing mean and fluctuating parts of turbulent flow we write:

$$u_i = \bar{u}_i + u_i' \tag{7a}$$

$$\varphi = \bar{\varphi} + \varphi' \tag{7b}$$

$$T = \bar{T} + T' \tag{7c}$$

where bars denote an average and primes, a fluctuating quantity. By definition:

$$\overline{u_i'} = 0, \quad \overline{\varphi'} = 0, \quad \text{and} \quad \overline{T'} = 0$$

The substitution of the expressions (7a), (7b) and (7c) into the continuity, momentum and energy equations will yield after time averaging and simplifications the following set of equations:

Continuity:

$$\frac{\partial \bar{u}_i}{\partial x_i} = 0 \tag{8}$$

Momentum equation for the mean flow:

$$\frac{\partial \bar{u}_i}{\partial t} + \bar{u}_k \frac{\partial \bar{u}_i}{\partial x_k} = -\beta g_i \bar{T} - \frac{\partial \bar{\varphi}}{\partial x_i} + \frac{\partial}{\partial x_k}\left(\nu \frac{\partial \bar{u}_i}{\partial x_k} - \overline{u_i' u_k'}\right) \tag{9}$$

Momentum equation for the fluctuating flow:

$$\frac{\partial u_i'}{\partial t} + u_k' \frac{\partial \bar{u}_i}{\partial x_k} + \bar{u}_k \frac{\partial u_i'}{\partial x_k} + u_k' \frac{\partial u_i'}{\partial x_k} = \beta g_i T' - \frac{\partial \varphi'}{\partial x_i} + \frac{\partial}{\partial x_k}\left(\nu \frac{\partial u_i'}{\partial x_k} + \overline{u_i' u_k'}\right) \tag{10}$$

Energy equation:

$$\frac{\partial \bar{T}}{\partial t} + \bar{u}_k \frac{\partial \bar{T}}{\partial x_k} + \overline{u'_k \frac{\partial T'}{\partial x_k}} = \frac{\partial}{\partial x_k}\left(\alpha \frac{\partial \bar{T}}{\partial x_k}\right) + \frac{\nu}{2c_p}\left[\left(\frac{\partial \bar{u}_i}{\partial x_k} + \frac{\partial \bar{u}_k}{\partial x_i}\right)^2 + \overline{\left(\frac{\partial u'_i}{\partial x} + \frac{\partial u'_k}{\partial x}\right)^2}\right] \qquad (11)$$

The frictional heating terms are included this time in the energy equation, for the reason that the magnitude of the velocity gradients is larger and therefore we can expect a greater amount of heat to be generated in the turbulent flow.

For an incompressible fluid:

$$\overline{u'_i \frac{\partial T'}{\partial x_i}} = \frac{\partial}{\partial x_i} \overline{u'_i T'}$$

therefore the energy equation will have the form:

$$\frac{\partial \bar{T}}{\partial t} + \bar{u}_k \frac{\partial \bar{T}}{\partial x_k} = \frac{\partial}{\partial x_k}\left(\alpha \frac{\partial \bar{T}}{\partial x_k} - \overline{u'_k T'}\right) + \frac{\nu}{2c_p}\left[\left(\frac{\partial \bar{u}_i}{\partial x_k} + \frac{\partial \bar{u}_k}{\partial x}\right)^2 + \overline{\left(\frac{\partial u'_i}{\partial x_k} + \frac{\partial u'_k}{\partial x_i}\right)^2}\right] \qquad (11a)$$

Equations (8), (9), (10) and (11a) fully describe the turbulent process. There are however , the time averaged correlations of fluctuating quantities which must be evaluated in terms of easier to handle relations.

As a next step, we shall develop an equation for the Reynolds stress transport. To achieve this let us multiply the equation for fluctuating flow by u'_j, time average it, and then make appropriate simplifications.

The result is:

$$\frac{\partial \overline{u_i' u_j'}}{\partial t} + \bar{u}_k \frac{\partial \overline{u_i' u_j'}}{\partial x_k} + \overline{u_i' u_k'} \frac{\partial \bar{u}_j}{\partial x_k} + \overline{u_j' u_k'} \frac{\partial \bar{u}_i}{\partial x_k} +$$

$$\frac{\partial \overline{u_i' u_j' u_k'}}{\partial x_k} = -\left(\overline{u_i' \frac{\partial \varphi'}{\partial x_j}} + \overline{u_j' \frac{\partial \varphi'}{\partial x_k}}\right) + \nu \left(\overline{u_i' \frac{\partial^2 u_j'}{\partial x_k^2}} + \overline{u_j' \frac{\partial^2 u_i'}{\partial x_k^2}}\right)$$

$$- \beta \left(g_j \overline{u_i' T'} + g_i \overline{u_j' T'}\right) \tag{12}$$

Equation (12) developed by Reynolds is known as Reynolds stress equation

Where the Reynolds stress:

$$R_{ij} = -\rho \overline{u_j' u_i'} \tag{13}$$

For future convenience let us transform some terms of the Reynolds stress equation. As a result we have:

$$\frac{\partial \overline{u_i' u_j'}}{\partial t} + \bar{u}_k \frac{\partial \overline{u_i' u_j'}}{\partial x_k} + \overline{u_i' u_k'} \frac{\partial \bar{u}_j}{\partial x_k} + \overline{u_j' u_k'} \frac{\partial \bar{u}_i}{\partial x_k} + \tag{12a}$$

$$\frac{\partial \overline{u_i' u_j' u_k'}}{\partial x_k} = -\left(\frac{\partial \overline{u_i' \varphi'}}{\partial x_j} + \frac{\partial \overline{u_j' \varphi'}}{\partial x_i}\right) + \overline{\varphi' \left(\frac{\partial u_j'}{\partial x_i} + \frac{\partial u_i'}{\partial x_j}\right)}$$

$$+ \nu \left(\frac{\partial^2 \overline{u_i' u_j'}}{\partial x_k^2} - 2 \frac{\partial \overline{u_i'}}{\partial x_k} \frac{\partial \overline{u_j'}}{\partial x_k}\right) - \beta \left(g_i \overline{u_j' T'} + g_j \overline{u_i' T'}\right)$$

The equation of Reynolds stress, as well as all other equations involve several unknown correlations of fluctuating quantities. For isotropic turbulence we can express the Reynolds stress in terms of mean flow quantities in a following way:

$$\overline{u_i' u_j'} = \frac{2}{3}\bar{q}\,\delta_{ij} - \epsilon_m\left(\frac{\partial \bar{u}_i}{\partial x_j} + \frac{\partial \bar{u}_j}{\partial x_i}\right) \tag{14}$$

where q is the mean kinetic energy of turbulent fluctuations:

$$\bar{q} \equiv \frac{1}{2}\overline{(u_i)^2} \tag{15}$$

and ϵ_m is the eddy viscosity.

Reynolds stress is thus expressed by two functions q and ϵ_m. For i = j mean flow velocity gradients in the expression (14) vanish and Reynolds stress is reduced to the turbulent energy carried by the flow.

In that case, substitution of (14) into (12a) yields:

$$\frac{\partial \bar{q}}{\partial t} + \bar{u}_k \frac{\partial \bar{q}}{\partial x_k} = \epsilon_m \left(\frac{\partial \bar{u}_i}{\partial x_k} + \frac{\partial \bar{u}_k}{\partial x_i} \right) \frac{\partial \bar{u}_i}{\partial x_k} - \frac{\partial}{\partial x_k} \left(\overline{u'_k \, \tfrac{1}{2} u'_i u'_i} \right) \tag{16}$$

$$- \frac{\partial \overline{u'_k p'}}{\partial x_k} + \nu \frac{\partial^2 \bar{q}}{\partial x_k^2} - \nu \overline{\left(\frac{\partial u'_i}{\partial x_k} \right)^2} - \beta g_i \overline{u'_i T'}$$

The above equation was obtained with the assumption that for i = j we have:

$$\frac{\partial \bar{u}_i}{\partial x_i} = 0$$

Equation (16), which is the turbulent kinetic energy transport equation includes several terms containing correlations of fluctuating quantities that need to be evaluated.

In the first step we shall evaluate triple velocity correlation and pressure-velocity correlation.

The diffusion of turbulent energy q , which is a scalar quantity, can be approximated by the flux (Ref.(20),(21)):

$$\frac{\partial \overline{u'_k u'_i u'_i}}{\partial x_k} = - \frac{\partial \overline{u'_k q'}}{\partial x_k} = - c_1 \frac{\partial}{\partial x_k} \left(\epsilon_m \frac{\partial \bar{q}}{\partial x_k} \right) \tag{17}$$

similarly:

$$\frac{\partial \overline{u'_k p'}}{\partial x_k} = - c_2 \frac{\partial}{\partial x_k} \left(\epsilon_m \frac{\partial \bar{q}}{\partial x_k} \right) \tag{18}$$

where $\mathcal{X}_1$ and $\mathcal{Y}_2$ are dimensionless constants. Values of $\mathcal{X}_1$ and $\mathcal{X}_2$ were found to be close to unity.

The temperature-velocity correlation can be expressed by the eddy diffusivity concept:

$$\overline{u_i' T'} = -\epsilon_h \frac{\partial \bar{T}}{\partial x_i} \tag{19}$$

where ϵ_h is the thermal eddy diffusivity.

To evaluate ϵ_h we will introduce the experimental results obtained by Fage and Falkner (12). They conclude, that the turbulent mechanism for momentum transfer and for heat transfer, although similar, are not identical. It was found that heat diffuses faster than momentum and the conclusion of their results is presented below:

$$\epsilon_h = \sigma \epsilon_m \qquad \sigma_{experiment} = 2.0$$

thus: (See also page 147)

$$-\overline{u_i' T'} = \sigma \epsilon_m \frac{\partial \bar{T}}{\partial x_i} \tag{19a}$$

The last term that we need to evaluate is: $\overline{\left(\frac{\partial u_i'}{\partial x_k}\right)^2}$
Let us start with an expression for a fluctuating vorticity:

$$\eta_i' = \epsilon_{ikl} \frac{\partial u_l'}{\partial x_k} \tag{20}$$

where η_i' is the fluctuating vorticity.

ϵ_{ijk} is a third order tensor defined by the condition that if any two values of l,i,j are equal, then the corresponding component is zero.

If l, i, j are all unequal and in cyclic order the component is +1 and if the order of l, i, j is not cyclic the component is -1. ϵ_{lij} is called the alternating tensor.

Let us square and average both sides of expression (20).That results in:

$$\overline{r_l' r_l'} = \epsilon_{ikl}\epsilon_{pql}\overline{\frac{\partial u_i'}{\partial x_k}\frac{\partial u_p'}{\partial x_q}} \tag{21}$$

or:

$$\overline{r_l' r_l'} = \left(\delta_{ip}\delta_{kq} - \delta_{iq}\delta_{kp}\right)\overline{\frac{\partial u_i'}{\partial x_k}\frac{\partial u_p'}{\partial x_q}} \tag{21a}$$

Performing multiplications gives us:

$$\overline{r_l' r_l'} = \overline{\frac{\partial u_i'}{\partial x_k}\frac{\partial u_i'}{\partial x_k}} - \overline{\frac{\partial u_i'}{\partial x_k}\frac{\partial u_k'}{\partial x_i}} \tag{21b}$$

Thus, we get:

$$\overline{\left(\frac{\partial u_i'}{\partial x_k}\right)^2} = \overline{\left(r_l'\right)^2} + \overline{\frac{\partial u_i'}{\partial x_k}\frac{\partial u_k'}{\partial x_i}} \tag{22}$$

Applying the continuity equation for an incompressible fluid we can prove that:

$$\overline{\frac{\partial u_i'}{\partial x_k}\frac{\partial u_k'}{\partial x_i}} = \frac{\partial^2 \overline{u_i' u_k'}}{\partial x_i \partial x_k} \tag{23}$$

Substitute expression (14) for correlation $\overline{u_i' u_k'}$.

Therefore:

$$\overline{\frac{\partial u_i'}{\partial x_k}\frac{\partial u_k'}{\partial x_i}} = \frac{\partial^2}{\partial x_i \partial x_k}\left[\frac{2}{3}\bar{q}\delta_{ik} - \epsilon_m\left(\frac{\partial \bar{u}_i}{\partial x_k} + \frac{\partial \bar{u}_k}{\partial x_i}\right)\right] \quad (23a)$$

Finally:

$$\overline{\left(\frac{\partial u_i'}{\partial x_k}\right)^2} = \overline{\eta_i'^2} + \frac{2}{3}\frac{\partial^2 \bar{q}}{\partial x_i^2} - \frac{\partial^2}{\partial x_i \partial x_k}\left[\epsilon_m\left(\frac{\partial \bar{u}_i}{\partial x_k} + \frac{\partial \bar{u}_k}{\partial x_i}\right)\right] \quad (24)$$

Gathering together expressions (17), (18), (19) and (20) and substituting them into equation (16a) gives us the final form of the turbulent, kinetic transport equation:

$$\frac{\partial \bar{q}}{\partial t} + \bar{u}_k\frac{\partial \bar{q}}{\partial x_k} = \epsilon_m\left(\frac{\partial \bar{u}_i}{\partial x_k} + \frac{\partial \bar{u}_i}{\partial x_i}\right)\frac{\partial \bar{u}_i}{\partial x_k} + \beta g \epsilon_m \frac{\partial \bar{T}}{\partial x_i}$$

$$+ \frac{\nu}{3}\frac{\partial \bar{q}}{\partial x_k^2} - \nu\overline{\eta_i'^2} + \nu\frac{\partial^2}{\partial x_i \partial x_k}\left[\epsilon_m\left(\frac{\partial \bar{u}_i}{\partial x_k} + \frac{\partial \bar{u}_k}{\partial x_i}\right)\right]$$

$$- \alpha_1\frac{\partial}{\partial x_k}\left(\epsilon_m\frac{\partial \bar{q}}{\partial x_k}\right) - \alpha_2\frac{\partial}{\partial x_k}\left(\epsilon_m\frac{\partial \varphi}{\partial x_k}\right) \quad (25)$$

The energy equation (11a) can be presented in an expanded form:

$$\frac{\partial \bar{T}}{\partial t} + \bar{u}_k \frac{\partial \bar{T}}{\partial x_k} = \frac{\partial}{\partial x_k}\left(\alpha \frac{\partial \bar{T}}{\partial x_k} - \overline{u_k' T'}\right) + \frac{\nu}{2C_p}\left[\left(\frac{\partial \bar{u}_i}{\partial x_k} + \frac{\partial \bar{u}_k}{\partial x_i}\right)^2 + \overline{\left(\frac{\partial u_i'}{\partial x_k}\right)^2} + 2\,\overline{\frac{\partial u_i'}{\partial x_k}\frac{\partial u_k'}{\partial x}} + \overline{\left(\frac{\partial u_k'}{\partial x_i}\right)^2}\right] \quad (11b)$$

In the temperature range that we are dealing with we can assume thermal diffusion coefficient α to be a constant. Term $\overline{u_k' T'}$ and the last three terms on the right hand side of equation (11b) are already evaluated by expressions (19), (22), and (23).

Thus, the final form of an energy equation will be as follows:

$$\frac{\partial \bar{T}}{\partial t} + \bar{u}_k \frac{\partial \bar{T}}{\partial x_k} = \frac{\partial}{\partial x_k}\left(\alpha \frac{\partial \bar{T}}{\partial x_k}\right) + \frac{\partial}{\partial x_k}\left(- n \frac{\partial \bar{T}}{\partial x_k}\right) + \frac{\nu}{2C_p}\left(\frac{\partial \bar{u}_i}{\partial x_k} + \frac{\partial \bar{u}_k}{\partial x_i}\right)^2 + \frac{2}{C_p}\overline{T_L'^2} + \frac{4}{3}\frac{\nu}{C_p}\frac{\partial^2 \bar{q}}{\partial x^2} - \frac{2\nu}{C_p}\frac{\partial^2}{\partial x\,\partial x_k}\left[\epsilon_r\left(\frac{\partial \bar{u}_i}{\partial x_k} + \frac{\partial \bar{u}_k}{\partial x_i}\right)\right] \quad (11c)$$

To derive expressions for the eddy viscosity and the mean square turbulent vorticity, it will be necessary to transfer the derivation from the physical space into the wave number space. Thus, the new set of variables will be introduced that will apply to the wave number space:

k	-	wave number
k_e	-	wave number at which the energy-spectrum function $E(k,t)$ has its maximum
$E(k,t)$	-	three-dimensional energy-spectrum function averaged over a spherical surface in the wave number space
$F(k,t)$	-	three-dimensional transfer-spectrum function averaged over a spherical surface in the wav wave number space
W_k	-	transfer function
Ψ_k	-	production function
K_k	-	diffusion by inhomogeneity
$\gamma', \gamma'', \gamma'''$	-	numerical constants
$\zeta_1, \zeta_2, \zeta_3, \zeta_4$	-	numerical constants

First, the turbulent energy spectrum function will be analyzed and the eddy viscosity, ϵ_m, will be evaluated.

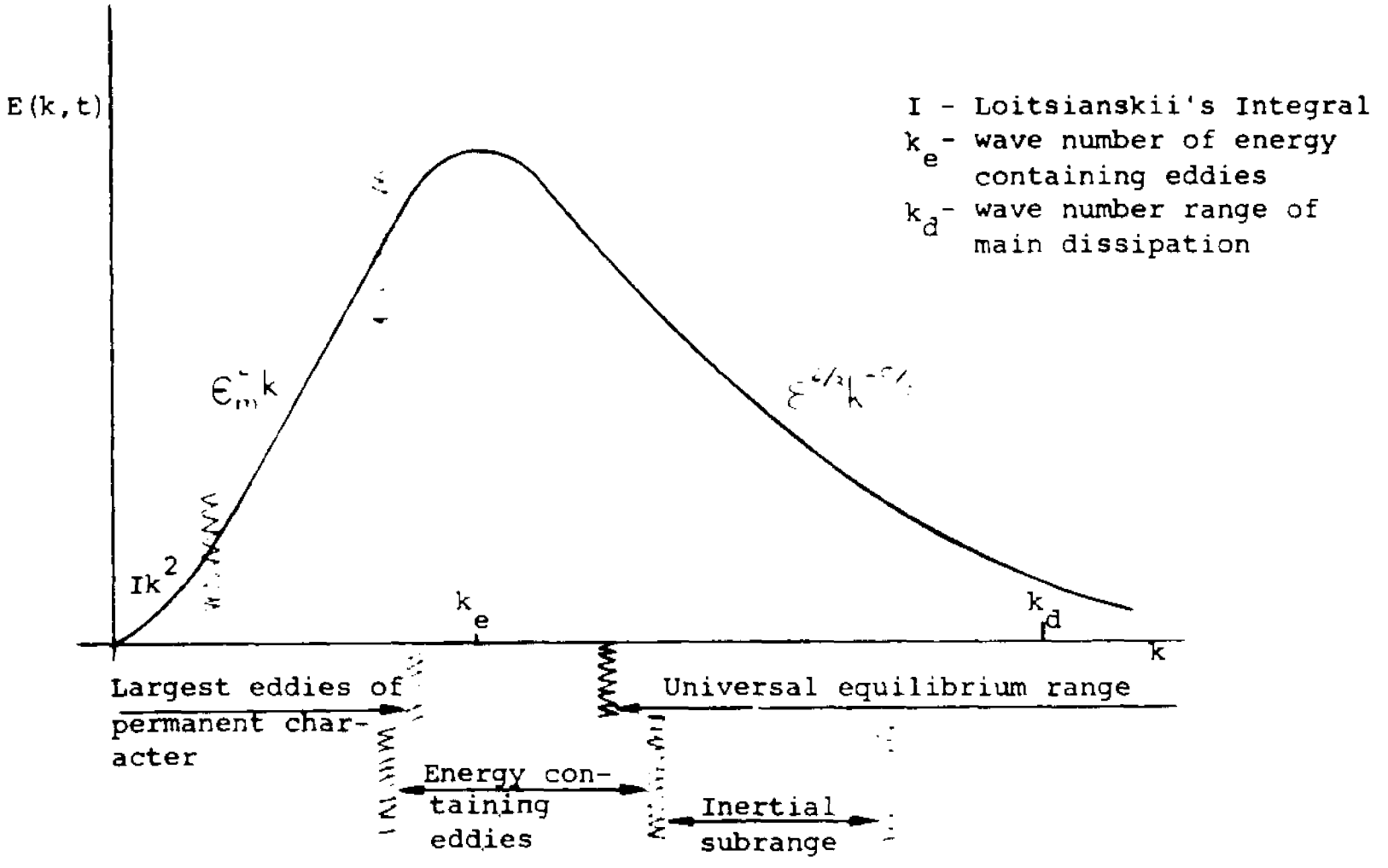

FIG.3. FORM OF ENERGY SPECTRUM FUNCTION E(k,t) IN THE VARIOUS WAVE NUMBER RANGES

As indicated, the turbulent energy of the eddies is distributed over various wave number k ranges depending on their character. And thus, in the lowest range there are the largest eddies of permanent character, then a range of energy containing eddies and a range of universal equilibrium. The last one with an inertial subrange and viscous dissipation range. The energy of the eddies is balanced in a sense that the source of energy must be equal to the dissipation.

A characteristic feature of the large eddies in the lower range is that the diffusive action of turbulence is determined mainly by the large eddies. Von Karman and Lin (45), therefore, assumed that the eddy viscosity ϵ_m may be regarded as a parameter determining the character of the turbulence in the lower wave number range. That is:

$$E(k,t)_{\substack{\text{lower} \\ \text{wave number} \\ \text{range}}} = \zeta_1 \epsilon_m^2 k \qquad (26a)$$

where ζ_1 is a constant.

Turbulence energy gets dissipated with the passage of time and different periods of decay may be distinguished i.e., an initial period, transition period and final period. This consideration was taken with respect to time, but for turbulence in the jet problem it applies to consecutive regions away from the jet nozzle.

In the initial period (or, close to the jet nozzle) the decay is determined predominantly by the decay of the energy-containing eddies. Far away from the nozzle the viscous effects predominate over the inertial effects. The turbulent energy spectra for various distances from the jet nozzle are illustrated on Fig.(4). Ref. (21).

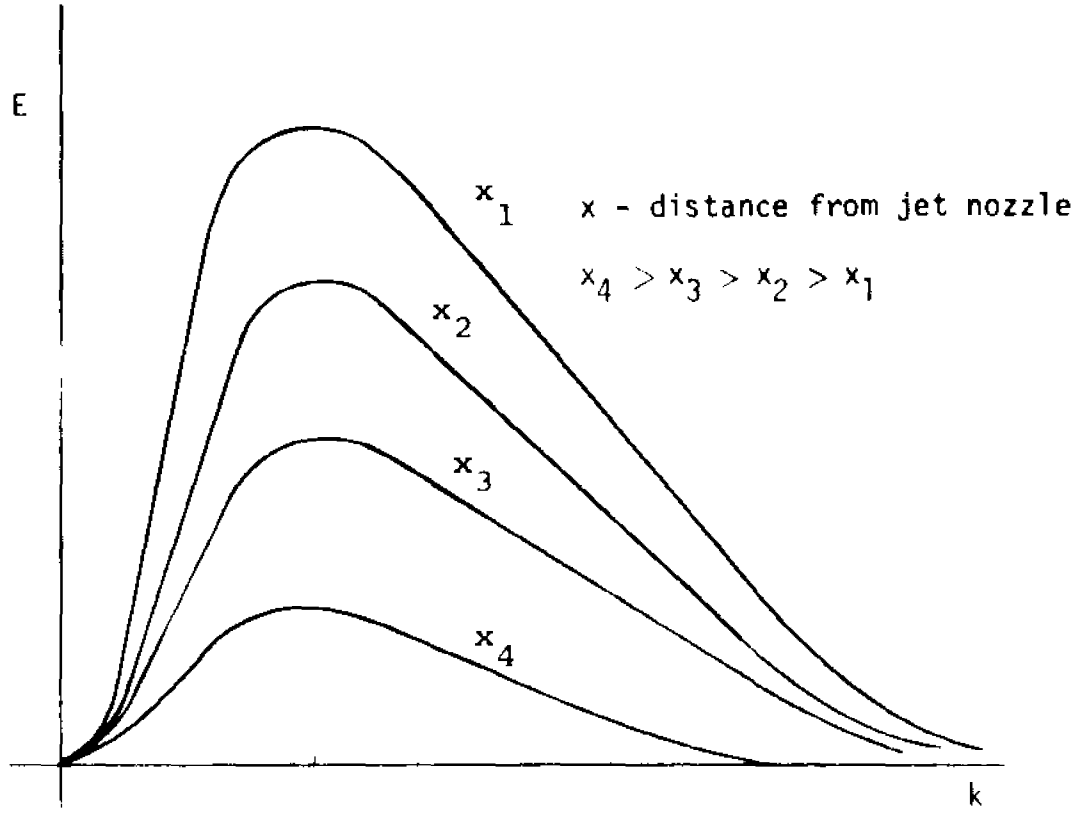

Fig. 4. Change of the Energy Spectrum in Space

First the turbulent energy spectrum and expression (26a) were investigated. The turbulent viscosity ϵ_m could have been evaluated from (26a) provided $E(k,t)$ and the corresponding values of k were specified as limits in the lower wave number range where there is a straight line relation between $E(k,t)$ and k.

It is proposed here that the value of turbulent viscosity ϵ_m be derived from the range of the permanent eddies, that is, the straight line part of the spectrum. The method is described below and it is illustrated on Fig. (5).

Although the discussed portion of the spectrum is represented by a straight line, its precise limits are not defined. This makes it difficult to use equation (26a) directly to find ϵ_m.

Instead, let the turbulent energy spectrum over the entire lower wave number range be approximated by a straight line. This is done only for the purpose of specifying two points on E,k-plane so that the equation of the straight line could be written, and not to change the actual E(k,t) profile. To define that line precisely the origin of the system and the maximum value of E(k,t) are connected. This process is illustrated on Fig. (5).

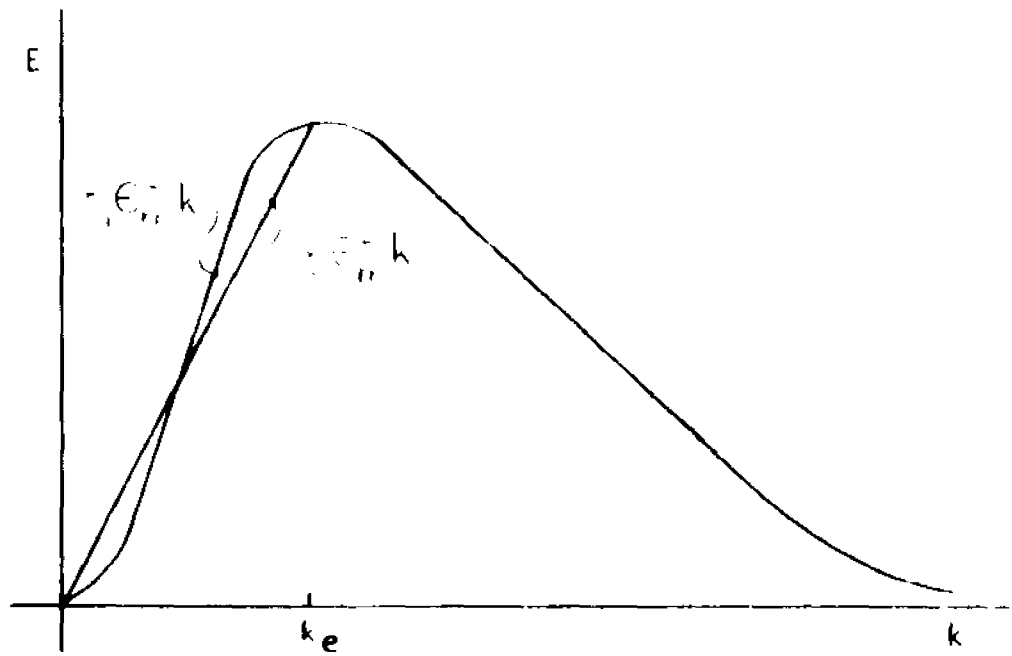

Fig. 5. Turbulent Energy Spectrum - Straight Line Relations

Now it is possible to write the equation of the straight line and to evaluate the angle of its inclination. The new line will be represented by the following:

$$E(k_e,t) = \zeta_2 \epsilon_m^{\frac{2}{3}} k_e \qquad (26b)$$

where ζ_2 is a constant.

Thus, equations (26a) and (26b) both representing a straight line can be related to each other by a certain constant. From the combination of (26a) and (26b), ϵ_m can be evaluated. The expression for $E(k_e,t)$ will now be determined. Following Hinze (pp.198,199) where the value of $E(k_e,t)$ is found, the following can be written:

$$E(k_e,t) = 0.2\ q/k_e \qquad (26c)$$

It remains now to find the value of k_e, that is, the wave number at which $E(k,t)$ has its maximum. That is again discussed in Hinze in chapter 3 on "The Decay of Isotropic Turbulence" (pp. 204-19). The maximum value of $E(k,t)$ is obtained at $k^2 \nu t = 1$, or:

$$k = \frac{1}{\sqrt{\nu t}} \qquad (26d)$$

Further:

$$u'^2 (\sqrt{\nu t})^5 = \zeta_1 \qquad (26e)$$

where ζ_1 is a constant.

Equation (26e) is the decay law.

Expressions (26d) and (26e) combined together yield:

$$q\,(k_e)^{-5} = \zeta_3$$

or

$$k_e = (\zeta_3^{-1} q)^{1/5} \tag{26f}$$

Now, all the necessary expressions have been derived and (26c) can be substituted into (26b):

$$0.2\ q/k_e = \zeta_2 \epsilon_m k_e \tag{26g}$$

Then, transforming and substituting (26f) into (26g):

$$\epsilon_m = \frac{0.2\ \zeta_3^{2/5}}{\zeta_2}\, q^{3/5} \tag{27a}$$

Constants on the right hand side can be combined into one and thus, the expression for ϵ_m is as follows:

$$\epsilon_m = \zeta_4\, q^{3/10} \tag{27b}$$

The constant ζ_4 can be evaluated experimentally or investigated numerically. It will be assumed that the transformation from the straight line described by equation (26e) and the straight line described by equation (26b) is reflected in the value of this constant.

Application of the just proposed theory on the evaluation of eddy viscosity is of serious importance. It has the advantage over the Prandtl mixing length theory since it is applicable also in the regions where the mean flow velocity gradient is negligible, or equal to zero. Its simplicity is also important. Various sophisticated methods of evaluation of eddy viscosity involve complex equations and many universal constants while this expression is extremely simple. This cuts down the computation time and also eliminates the necessity of evaluation of several universal constants.

To close the system of equations a relation between the mean square turbulent vorticity and the other variables is necessary. In the development of this relationship we shall use Tchen's work which investigated the interaction between the vorticity of a mean motion and the turbulent vorticity. See ref.(42) and (43).

First, the possible cases with respect to their application to the jet problem will be examined. Altogether, four relations may take place:

1.	high	$\frac{\partial \bar{u}_i}{\partial x_j}$	low	$\sqrt{\overline{\eta_i'^2}}$
2.	high	$\frac{\partial \bar{u}_i}{\partial x_j}$	high	$\sqrt{\overline{\eta_i'^2}}$
3.	low	$\frac{\partial \bar{u}_i}{\partial x_j}$	low	$\sqrt{\overline{\eta_i'^2}}$
4.	low	$\frac{\partial \bar{u}_i}{\partial x_j}$	high	$\sqrt{\overline{\eta_i'^2}}$

Without going into a detailed analysis (which can be found in references (42) and (43)) the total dissipation will be expressed by the following relation:

$$\varepsilon = 2\nu \int_0^\infty dk\, k^2 E(k) \tag{28}$$

Case (2) and (3) will be of a principal interest since from the physical reality point of view relations (1) and (4) will have little, if any, impact on the jet structure. The only possibility where case (1) could take place would be in the flow area immediate to the jet nozzle. Here, however, the high velocity gradient results in the development of high turbulent vorticity almost instantly.

It is also reasonable to assume that in the far field where mean flow vorticity is low, the turbulent vorticity is also of a rather small magnitude. At any rate these assumptions should not be too far off from the actual physical process.

In his papers on the spectrum of energy in turbulent shear flow Tchen (Ref. (42) and (43)) considers two cases:

1). Vorticity $\frac{\partial \bar{u}_i}{\partial x_j}$ of the main motion is small compared with the vorticity of the turbulence in the wave number range under consideration (no resonance).

2). The vorticity of the main motion is comparable to the vorticity of the turbulence in the wave number under consideration (strong interaction between vortices and the resonance may occur), and then the square vorticity of the mean motion is replaced with a product of mean flow vorticity and turbulent vorticity.

In accordance with our earlier analysis we shall use case (2) to develop the desired relationship.

Now we can expand total dissipation into several terms and analyze its structure:

$$\varepsilon = 2\nu\int_0^k dk'\,k'^2 E(k') + \gamma'\int_k^\infty dk''\sqrt{\frac{E(k'')}{k''}}\left(\frac{\partial\bar{u}_i}{\partial x_j}\right)^2\zeta$$
$$-\int_0^k F(k')dk' + \frac{\partial}{\partial x_2}\left[\gamma'''\int_k^\infty dk''\sqrt{\frac{E(k')}{k''}}\,\frac{\partial}{\partial x_2}\left(\frac{1}{2}\overline{u_i'^2}\right)\right] \qquad (29)$$

$$\zeta = \begin{cases} 1 & \text{,no resonance} \\ \dfrac{\gamma''}{\gamma'}\left[\dfrac{2\int_0^k dk'\,k'^2 E(k')}{\left(\frac{\partial\bar{u}_i}{\partial x_j}\right)^2}\right]^{1/2} & \text{,resonance} \end{cases}$$

with:

where:

$$2\int_0^k dk'\,k'^2 E(k') = \overline{\eta_i'^2} \qquad (30)$$

The last expression is the mean square turbulent vorticity.

The first term in equation (29) represents viscous dissipation of turbulence in the wave number range from 0 to k, the second term represents the production of turbulence in the range from k to ∞, the third term represents transfer of turbulent energy in the range 0 to k to turbulence of higher wave numbers, and the fourth term represents diffusion by inhomogeneity of the field.

Using the variables that were already introduced we can present total dissipation as:

$$\varepsilon = 2\nu\int_0^k dk'\,k'^2 E(k') + W_k(k,\infty) + \Psi_k(k,\infty) + K_k(k,\infty) \tag{29a}$$

Applying Heisenberg's assumption (Ref. (21) eq.(3-121)) to the transfer spectrum function we can present W_k as:

$$W_k = \int_0^k dk' F(k') = -\int_k^\infty dk' F(k') = -2\gamma''\int_k^\infty dk''\sqrt{\frac{E(k'')}{k''^3}}\int_0^k dk'\,k'^2 E(k') \tag{31}$$

Relation (31) above is valid for an isotropic flow.

From Heisenberg's concept:

$$\epsilon_{rm}(k) = \gamma''\int_k^\infty dk'\sqrt{\frac{E(k')}{k'^3}} \tag{32}$$

For the case with a resonance between the two vorticities and introducing equations (30), (31) and (32) into Eqn.(29) we may write expression for total dissipation as follows:

$$\varepsilon = 2\nu\int_0^k dk'\,k'^2 E(k') + \epsilon_{rm}(k)\left(\frac{\partial\overline{u_i}}{\partial x_j}\right)\sqrt{\overline{\eta_i^2}}$$

$$+ 2\epsilon_{rm}\int_0^k dk' k'^2 E(k') + \frac{\partial}{\partial x_2}\left[\epsilon_{rm}\frac{\partial}{\partial x_2}\left(\frac{1}{2}\overline{u_i'^2}\right)\right] \tag{29b}$$

For the investigated case, that is, a resonance between vorticity of the turbulent motion and the mean motion, if $\left(\frac{\partial \bar{u}_i}{\partial x_j}\right)$ is large and wave number k is sufficiently small, we have:

$$2\int_0^k dk' k'^2 E(k') \ll \left(\frac{\partial \bar{u}_i}{\partial x_j}\right)^2 \tag{33}$$

Thus, the production function is predominant, and all other functions become negligible.

Therefore:

$$\varepsilon = \Psi_k \tag{34}$$

Total dissipation for a steady state can be written as:

$$\varepsilon = \overline{u_i' u_j'} \frac{\partial \bar{u}_i}{\partial x_j} \tag{35}$$

The production of turbulence in the range k to ∞, or the dissipation by turbulence of the main motion in this range (Eqn. (34) and Eqn. (35)) may be presented as:

$$\varepsilon = \Psi_k = \epsilon_m(k) \left(\frac{\partial \bar{u}_i}{\partial x_j}\right) \sqrt{\overline{u_i'^2}}$$

or:

$$\overline{u_i' u_j'} \frac{\partial \bar{u}_i}{\partial x_j} = \epsilon_m \sqrt{\overline{u_i'^2}} \left(\frac{\partial \bar{u}_i}{\partial x_j}\right) \tag{36}$$

ϵ_m and root mean square turbulent vorticity are the scalar expressions on the right hand side of the equation. To balance that on the left hand side, we may present this equality in the form:

$$\tau_{ij}\bar{q}\,\frac{\partial \bar{u}_i}{\partial x_j} = \epsilon_m\sqrt{\overline{u'^2}}\left(\frac{\partial \bar{u}_i}{\partial x_j}\right) \tag{36a}$$

or, simply:

$$l_3\bar{q} = \epsilon_m\sqrt{\overline{u'^2}} \tag{37}$$

where l_3 is a numerical constant.

This final relation agrees with that of Saffman (38) who came to his expression by dimensional considerations.

The constant l_3 may vary between 0 and 2, or defining it more closely, it should be greater than 0 and smaller than 2. A value of 1.0 was found to satisfy most closely the numerical solution. See also Saffman (38).

The last expression closes the system and thus, we can present the final set of equations:

Continuity Equation:

$$\frac{\partial \bar{u}_k}{\partial x_k} = 0 \tag{38}$$

Momentum Equation:

$$\frac{\partial \bar{u}_i}{\partial t} + \bar{u}_k \frac{\partial \bar{u}_i}{\partial x} = -\beta g_i \bar{T} - \frac{\partial \bar{p}}{\partial x_i} - \frac{2}{3}\frac{\partial \bar{q}}{\partial x_i}$$

$$+ \frac{\partial}{\partial x_k}\left[(\nu + \epsilon_m)\left(\frac{\partial \bar{u}_i}{\partial x_k} + \frac{\partial \bar{u}_k}{\partial x_i}\right)\right] \tag{39}$$

Energy Equation:

$$\frac{\partial \bar{T}}{\partial t} + \bar{u}_k \frac{\partial \bar{T}}{\partial x} = \frac{\partial}{\partial x_k}\left[\left(\alpha + \frac{\nu}{Pr}\epsilon_m\right)\frac{\partial \bar{T}}{\partial x}\right] + \frac{\nu}{2c_p}\left(\frac{\partial \bar{u}_i}{\partial x_k} + \frac{\partial \bar{u}_k}{\partial x_i}\right)^2 \tag{40}$$

$$+ \frac{\nu}{c_p}\overline{(T_i')^2} + \frac{4\nu}{3c_p}\frac{\partial \bar{q}}{\partial x_i} - \frac{2\nu}{c_p}\frac{\partial^2}{\partial x_i \partial x_k}\left[\epsilon_m\left(\frac{\partial \bar{u}_i}{\partial x_k} + \frac{\partial \bar{u}_k}{\partial x_i}\right)\right]$$

Turbulent Energy Transport Equation:

$$\frac{\partial \bar{q}}{\partial t} + \bar{u}_k \frac{\partial \bar{q}}{\partial x_k} = \epsilon_m\left(\frac{\partial \bar{u}_i}{\partial x_k} + \frac{\partial \bar{u}_k}{\partial x_i}\right)\frac{\partial \bar{u}_i}{\partial x_k} + g_i \epsilon_m \frac{\partial \bar{T}}{\partial x_i} + \frac{\nu}{3}\frac{\partial^2 \bar{q}}{\partial x_k^2}$$

$$- \frac{\nu}{2}\overline{(T_i')^2} - \nu \frac{\partial^2}{\partial x_i \partial x_k}\left[\epsilon_m\left(\frac{\partial \bar{u}_i}{\partial x_k} + \frac{\partial \bar{u}_k}{\partial x_i}\right)\right]$$

$$- \alpha_1 \frac{\partial}{\partial x_k}\left(\epsilon_m \frac{\partial \bar{q}}{\partial x_k}\right) - \alpha_2 \frac{\partial}{\partial x_k}\left(\epsilon_m \frac{\partial \varphi}{\partial x_k}\right) \tag{41}$$

Eddy Viscosity:

$$\epsilon_{rn} = \tilde{\chi}_4 q^{3/10} \tag{42}$$

Mean Square Turbulent Vorticity:

$$\sqrt{\overline{r_{ij}'^2}} = \chi_3 \frac{q}{\epsilon_{rn}} \tag{43}$$

The equations (38) to (43) form a closed set with the addition of the desired boundary conditions. The quations can now be written in a finite difference form and solved numerically. The numerical solution will provide us with initial jet development, as well as, with a steady case when enough time for a flow field formation is allowed.

Equations (38) and (39) are in a standard form assumed for incompressible turbulent flow with the inclusion of Boussinesq assumption for buoyancy. The development of equations (40) and (41) to the present form includes the contribution of several authors to the theory of turbulence. The last two expressions (42) and (43) represent the contribution of the present work to the theory of the thermal turbulent flows.

C. INITIAL AND BOUNDARY CONDITIONS

The equations for the flow field developed earlier were solved together with initial and boundary conditions that are described in this section.

A variety of problems were investigated. Conditions describing them are divided into two major groups of vertical and horizontal jets. Flow field is assumed two dimensional.

a). Vertical Jets

The drawing below illustrates boundary dimensions that will be used in the specification of the boundary conditions in the x-y coordinate system for a vertical jet.

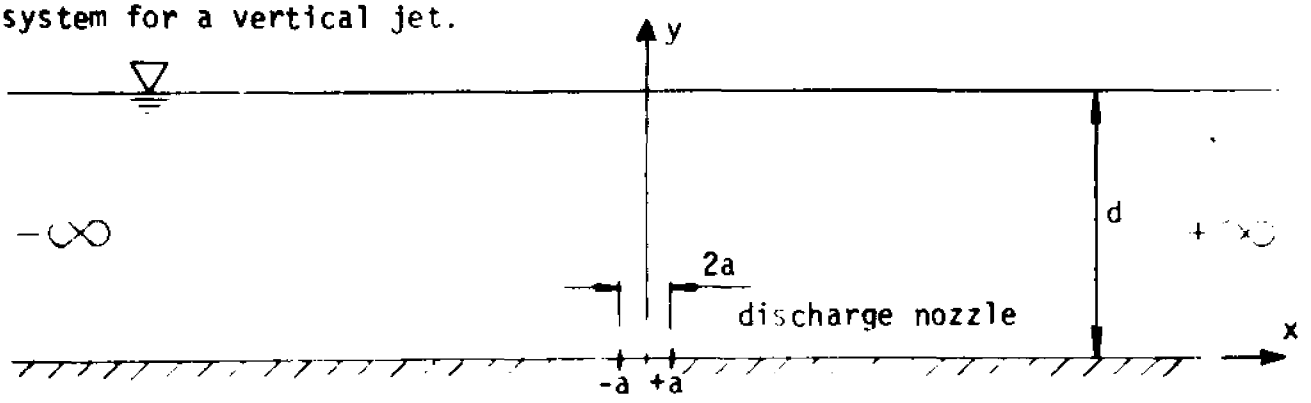

Fig.6. Two-dimensional cross-section of the flow field
Vertical Jet

where: d - depth

2a - size of the jet entrance

We should note here that although the drawing shows the region spreading from $-\infty$ to $+\infty$, cases with vertical jet and stationary reservoir were solved for a region $(0,+\infty)$, since the left hand side would be a mirror image of the right hand side. Savings on computer time were considerable. The analytical concept of infinity cannot be applied on the computer since the evaluated field must be finite in size. Thus, by symbols $-\infty$, or $+\infty$ we mean the left-most, or right-most boundary, respectively.

Let us describe the initial and boundary conditions for the investigated problems, noting that they will apply equally for either laminar, or turbulent cases with the exclusion of turbulent terms for laminar flows.

1. Vertical Jet, Stationary Reservoir, no Temperature Variations.

Initial Conditions:

I.C.(1a). $u(-\infty < x < +\infty,\ 0 < y < d) = 0$

I.C.(1b). $v(-a < x < +a,\ 0) = V_{entrance}$

I.C.(1c) $v(-\infty < x < +\infty,\ 0 < y < d) = 0$

Turbulent variables are equal to zero everywhere.

Boundary Conditions:

B.C.(1a). $\frac{\partial}{\partial x} u(0,y) = 0$

B.C.(1b). $\frac{\partial}{\partial x} v(0,y) = 0$

B.C.(1c). $\frac{\partial}{\partial x} \Phi(0,y) = 0$

B.C.(1d). $\frac{\partial}{\partial x} \eta(0,y) = 0$

B.C.(1e). $\frac{\partial}{\partial x} \epsilon(0,y) = 0$

B.C.(1f). $\frac{\partial}{\partial x} q(0,y) = 0$

B.C.(1g). $u(-\infty < x < +\infty,\ 0) = 0$ velocity at the bottom

B.C.(1h). $v(-\infty < x < -a,\ 0) = 0$ and $v(+a < x < +\infty,\ 0) = 0$

B.C.(1i). $v(-a < x < +a,\ 0) = V_{entrance}$

B.C.(1j). $v(x,d) = 0$ surface condition

Note, that B.C's (1d), (1e), (1f) apply to turbulent flow only.

For the output boundary we assume no gradient for any of the investigated variables and therefore:

B.C.(1k). $u_{i-1/2,j} = u_{i+1/2,j}$

B.C.(1l). $v_{i-1/2,j} = v_{i+1/2,j}$

B.C.(1m). $\varphi_{i-1/2,j} = \varphi_{i+1/2,j}$

B.C.(1n). $\eta_{i-1/2,j} = \eta_{i+1/2,j}$

B.C.(1o). $\epsilon_{m_{i-1/2,j}} = \epsilon_{m_{i+1/2,j}}$

B.C.(1p). $q_{i-1/2,j} = q_{i+1/2,j}$

B.C.(1q). $T_{i-1/2,j} = T_{i+1/2,j}$

Finite difference notation was used here for convenience and the temperature condition was listed to specify all output boundary conditions at one place.

Note: The conditions for the output boundary will apply to all problems.

2. Heated Vertical Jet Enters Reservoir of Uniform Temperature.

Initial Conditions:

All Initial Conditions from problem no.1. apply here, namely, IC(1a), IC(1b), IC(1c); with the following additions:

I.C.(2d). $T(-\infty < x < +\infty,\ 0 < y < d) = T_{reservoir}(\text{constant})$

I.C.(2e). $T(-a < x < +a,\ 0) = T_{entrance}$

We assume that air temperature above the water surface is close to the water temperature and thus no heat loss to the atmosphere is taken under consideration. In the case of a large difference of temperatures between air and water, terms evaluating heat loss (or gain) due to radiation, convection, or evaporation can be added to the program without any difficulty.

Boundary Conditions:

All the Boundary Conditions from problem no.1. i.e.(BC(1a) through BC(1q)) apply here, with the following additions:

B.C.(2r) $T(0,y) = 0$ symmetry condition

B.C.(2s) $\frac{\partial T}{\partial y}(-\infty < x < +\infty, d) = 0$ no heat exchange with [atmosphere

B.C.(2t) $\frac{\partial T}{\partial y}(-\infty < x < +\infty, 0) = 0$ no heat exchange with [the bottom

3. Heated Jet Enters Temperature (and therefore density) Stratified Reservoir.

Initial Conditions:

All Initial Conditions (IC(1a) through IC(1e)) apply here, with an exception of IC(2d) which will be replaced by:

I.C.(2f) $T(-\infty < x < +\infty, 0 < y < d) = T(y)_{reservoir}$

where $T(y)_{reservoir}$ is specified.

Boundary Conditions:

All Boundary Conditions developed ealier (i.e. BC(1a) through BC(2m)) apply here.

4. Heated Jet Enters Stream of Uniform Temperature.

Initial Conditions:

I.C.(4a) $u(-\infty < x < +\infty, 0 < y < d) = U(y)$ where U(y) is [specified stream velocity

I.C.(4b) $v(-a < x < +a, 0) = V_{entrance}$

I.C.(4c) $v(-\infty < x < +\infty, 0 < y < d) = 0$

I.C.(4d) $T(-\infty < x < +\infty, 0 < y < d) = T_{stream}$

I.C.(4e) $T(-a < x < +a, 0) = T_{entrance}$

Boundary Conditions:

B.C.(4a). $u(-\infty < x < +\infty, 0) = 0$

B.C.(4b). $v(-\infty < x < -a, 0) = 0$ and $v(a < x < +\infty, 0) = 0$

B.C.(4c). $v(-a < x < +a, 0) = V_{entrance}$

B.C.(4d). $v(-\infty < x < +\infty, d) = 0$

B.C.(4e). $u(-\infty < x < +\infty, y) = U(y)$ where U(y) is specified

The case of a temperature stratified stream was not considered. It is unlikely to expect significant change of temperature across stream depth.

b). Horizontal Jets

The dimensions describing flow field boundaries are shown below.

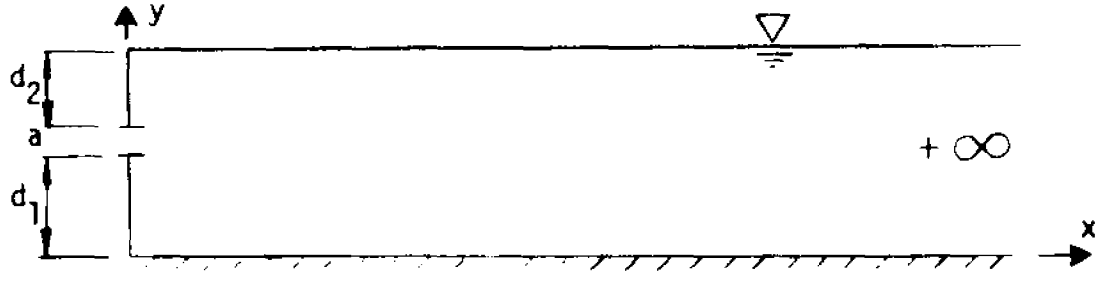

Fig. 7. Two-dimensional cross-section of the flow field Horizontal Jet

We will not go into a detailed listing of initial and boundary conditions since they are in nature identical with those for the vertical jet.

Investigated cases of a horizontal jet included:

1. Horizontal jet entering a stationary reservoir with no temperature variations.

2. Horizontal heated jet is discharged to a reservoir of uniform temperature.

3. Heated jet is discharged to a temperature stratified reservoir.

4. Heated jet entering a co-flowing, or counter-flowing stream.

For the cases listed above it was necessary to specify discharge nozzle size and its location, depth of a reservoir, initial velocity, and temperature of the jet, and a reservoir temperature.

All these conditions have been incorporated into the computer program in conjunction with the equations of the flow.

2. FINITE DIFFERENCE EQUATIONS AND NUMERICAL STABILITY ANALYSIS

The equations developed in the previous section will now be presented in a finite difference scheme.

As previously, we will develop a two stage system. First, we shall write equations for a laminar flow and then expand them further into turbulent case.

As we mentioned already the numerical analysis will be developed for a two-dimensional flow, and so all analytical equations that were originally written in a shorthand subscript notation will now have to be expanded for both x and y directions of flow.

A. LAMINAR FLOW

We now rewrite equations (1a), (2a) and (3a) in the x-y coordinate system.

Continuity Equation:

$$\frac{\partial u}{\partial x} + \frac{\partial v}{\partial y} = 0 \tag{101}$$

Momentum Equation x-direction:

$$\frac{\partial u}{\partial t} + \frac{\partial u^2}{\partial x} + \frac{\partial uv}{\partial y} = -\frac{\partial \varphi}{\partial x} - \beta g_x T + \nu\left(\frac{\partial^2 u}{\partial x^2} + \frac{\partial^2 u}{\partial y^2}\right) \tag{102}$$

Momentum Equation y-direction:

$$\frac{\partial v}{\partial t} + \frac{\partial uv}{\partial x} + \frac{\partial v^2}{\partial y} = -\frac{\partial \varphi}{\partial y} - \beta g_y T + \nu\left(\frac{\partial^2 v}{\partial x^2} + \frac{\partial^2 v}{\partial y^2}\right) \tag{103}$$

Energy Equation:

$$\frac{\partial T}{\partial t} + u\frac{\partial T}{\partial x} + v\frac{\partial T}{\partial y} = \alpha\left(\frac{\partial^2 T}{\partial x^2} + \frac{\partial^2 T}{\partial y^2}\right) \qquad (104)$$

Using a Taylor series expansion for each term we will write the above equations in finite difference form using the explicit scheme which will be explained in detail below.

Continuity:

$$\frac{U^{n+1}_{i+\frac{1}{2},j} - U^{n+1}_{i-\frac{1}{2},j}}{dx} + \frac{V^{n+1}_{i,j+\frac{1}{2}} - V^{n+1}_{i,j-\frac{1}{2}}}{dy} = 0 \qquad (105)$$

Momentum x-direction:

$$\frac{U^{n+1}_{i+\frac{1}{2},j} - U^{n}_{i+\frac{1}{2},j}}{dt} = \frac{U_{i+\frac{1}{2},j}\,U_{i-\frac{1}{2},j} - U_{i+\frac{1}{2},j}\,U_{i+\frac{1}{2},j}}{dx} +$$

$$\frac{U_{i+\frac{1}{2},j-\frac{1}{2}}\,V_{i+\frac{1}{2},j-\frac{1}{2}} - U_{i+\frac{1}{2},j+\frac{1}{2}}\,V_{i+\frac{1}{2},j+\frac{1}{2}}}{dy}$$

$$+ \frac{\rho_{i,j} - \rho_{i+1,j}}{dx} + \beta g_x (T_{i,j} - T_r)$$

$$+ \nu\left\{\frac{U_{i+\frac{1}{2},j} + U_{i-\frac{1}{2},j} - 2U_{i+\frac{1}{2},j}}{(dx)^2}\right.$$

$$\left. + \frac{U_{i+\frac{1}{2},j+1} + U_{i+\frac{1}{2},j-1} - 2U_{i+\frac{1}{2},j}}{(dy)^2}\right\} \qquad (106)$$

Momentum y-direction:

$$\frac{V_{i,j+\frac{1}{2}}^{n+1} - V_{i,j+\frac{1}{2}}^{n}}{dt} = \frac{U_{i-\frac{1}{2},j+\frac{1}{2}} V_{i-\frac{1}{2},j+\frac{1}{2}} - U_{i+\frac{1}{2},j+\frac{1}{2}} V_{i+\frac{1}{2},j+\frac{1}{2}}}{dx}$$

$$+ \frac{V_{i,j+\frac{1}{2}} V_{i,j-\frac{1}{2}} - V_{i,j+\frac{1}{2}} V_{i,j+\frac{1}{2}}}{dy}$$

$$+ \frac{\varphi_{i,j} - \varphi_{i,j+1}}{dy} + \beta g_y (T_{i,j} - T_r)$$

$$+ \nu \left\{ \frac{V_{i+1,j+\frac{1}{2}} + V_{i-1,j+\frac{1}{2}} - 2 V_{i,j+\frac{1}{2}}}{(dx)^2} \right.$$

$$\left. + \frac{V_{i,j+\frac{1}{2}} + V_{i,j-\frac{1}{2}} - 2 V_{i,j+\frac{1}{2}}}{(dy)^2} \right\} \qquad (107)$$

Energy:

$$\frac{T_{i,j}^{n+1} - T_{i,j}^{n}}{dt} = (U_{i\ \frac{1}{2},j} + U_{i+\frac{1}{2},j}) \frac{T_{i-1,j} - T_{i+1,j}}{2dx}$$

$$+ (V_{i,j-\frac{1}{2}} + V_{i,j+\frac{1}{2}}) \frac{T_{i,j-1} - T_{i,j+1}}{2dy}$$

$$+ \alpha \left\{ \frac{T_{i+1,j} - 2T_{i,j} + T_{i-1,j}}{(dx)^2} \right.$$

$$\left. + \frac{T_{i,j+1} - 2T_{i,j} + T_{i,j-1}}{(dy)^2} \right\} \qquad (108)$$

Superscript n refers to a time step (in all places where not shown it is assumed to be n).

Subscripts i and j refer to x and y direction steps, respectively. The finite difference scheme is explicit since e.g. if all the $v_{i,j}^{n}$ are known at any time level t_n, any one of the above finite difference equations enables $v_{i,j}^{n+1}$ to be calculated directly at the time level t_{n+1}.

The differencing is set up in such a way that the quantity that is to be fluxed is located at the same mesh position as the fluxing velocity.

Examples below illustrate differencing technique:

$$(UF)_{i+\frac{1}{2},j} = 0.5\ (U_{i+1,j}F_{i,j} + U_{i,j}F_{i+1,j})$$

$$(U_{i,j})^2 = U_{i-\frac{1}{2},j}U_{i+\frac{1}{2},j} \qquad \text{(dx - step)}$$

It will be shown later that an application of the above scheme for finite difference equations will give us truncation errors connected with diffusion-like terms dependent on time step Δt only and free from space step terms.

Fig. 8. below defines dependent variables for an individual cell.

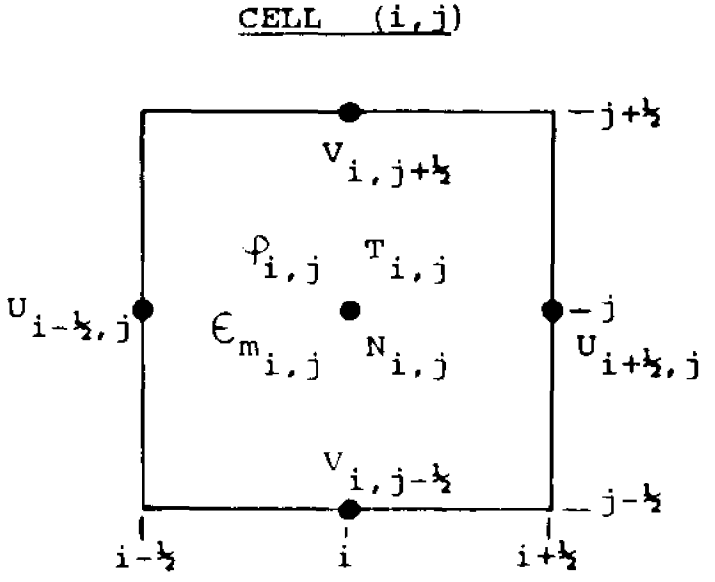

FIG. 8. THE LOCATION OF CELL VARIABLES

Since the partial differential equations, we are dealing with, are nonlinear, the Fourier method for investigation of stability cannot be applied.

Instead we shall try to examine the truncation errors and from that analysis come out with stability conditions.

A leading point used in the investigation is the fact that viscous terms should be of the same order of magnitude as inertia terms. This prevents an exponential blow up of the equations. The major cause of instability comes from the approximation of PDEs by terms from the Taylor expansion where only the lowest order terms are retained and those of higher order are dropped.

We shall start with analyzing the higher order terms of the Taylor expansion which were neglected when writing the simplified difference equations.

Expanding each term of the difference equations in a Taylor series and dropping all nondiffusionlike terms leaves us with the following equation of momentum:

$$\frac{\partial u}{\partial t} + \frac{\delta t}{2}\frac{\partial^2 u}{\partial t^2} + o\left[(\delta t)^2\right] + u\frac{\partial u}{\partial x} + v\frac{\partial u}{\partial y} =$$

$$-\frac{\partial \psi}{\partial x} - \beta g_x \bar{T} + \nu\left(\frac{\partial^2 u}{\partial x^2} + \frac{\partial^2 u}{\partial y^2}\right) \qquad (109)$$

Equation for y-direction has the same structure.

Evaluation of $\frac{\partial^2 u}{\partial t^2}$ after dropping all nondiffusionlike terms leaves us with:

$$\frac{\partial^2 u}{\partial t^2} = u^2\frac{\partial^2 u}{\partial x^2} + v^2\frac{\partial^2 u}{\partial y^2} + o\left[(\delta t)^2\right] \qquad (110)$$

If we substitute this result to equation (109) we have:

$$\frac{\partial u}{\partial t} + u\frac{\partial u}{\partial x} + v\frac{\partial u}{\partial y} = -\frac{\partial \varphi}{\partial x} - \beta g_x T + \tag{111}$$

$$\left[\nu - \frac{\delta t}{2}u^2 + \sigma\left[(\delta t)^2\right]\right]\frac{\partial^2 u}{\partial x^2} + \left[\nu - \frac{\delta t}{2}v^2 + \sigma\left[(\delta t)^2\right]\right]\frac{\partial^2 u}{\partial y^2}$$

By analogy the momentum equation in the y-direction:

$$\frac{\partial v}{\partial t} + u\frac{\partial v}{\partial x} + v\frac{\partial v}{\partial y} = -\frac{\partial \varphi}{\partial y} - \beta g_y T + \tag{112}$$

$$\left[\nu - \frac{\delta t}{2}u^2 + \sigma\left[(\delta t)^2\right]\right]\frac{\partial^2 v}{\partial x^2} + \left[\nu - \frac{\delta t}{2}v^2 + \sigma\left[(\delta t)^2\right]\right]\frac{\partial^2 v}{\partial y^2}$$

It is apparent that negative coefficients of viscous terms could cause instability. The necessary conditions that must be met are:

$$\left[\nu - \frac{\delta t}{2}u^2\right] > 0 \quad , \quad \left[\nu - \frac{\delta t}{2}v^2\right] > 0$$

It is of importance that there are no diffusionlike truncation errors involving powers of space steps x or y.

Stability conditions are then satisfied if $\nu > \frac{\delta t}{2}u^2$ and $\nu > \frac{\delta t}{2}v^2$ so by keeping the δt sufficiently small we can keep the solution stable.

As another possibility, we can introduce such an expression into the computer scheme that would exactly balance and nullify the effect of $\delta t/2\ U^2$ or $\delta t/2\ V^2$. A finite difference approximation accurate to second order in δt could also be develoned.

B. TURBULENT FLOW

Similarly to the procedure applied to the laminar set of equations we shall rewrite equations (38) through (43) in the x-y coordinate system.

Continuity:

$$\frac{\partial u}{\partial x} + \frac{\partial v}{\partial y} = 0 \tag{138}$$

Momentum x-direction:

$$\frac{\partial u}{\partial t} + \frac{\partial u^2}{\partial x} + \frac{\partial uv}{\partial y} = -\frac{\partial \varphi}{\partial x} - \frac{2}{3}\frac{\partial q}{\partial x} - \beta g_x \tilde{T}$$

$$+2\frac{\partial}{\partial x}\left[(\nu + \epsilon_m)\left(\frac{\partial u}{\partial x}\right)\right] \tag{139}$$

$$+\frac{\partial}{\partial y}\left[(\nu + \epsilon_m)\left(\frac{\partial u}{\partial y} + \frac{\partial v}{\partial x}\right)\right]$$

Momentum y-direction:

$$\frac{\partial v}{\partial t} + \frac{\partial v}{\partial y} + \frac{\partial uv}{\partial x} = -\frac{\partial \varphi}{\partial y} - \frac{2}{3}\frac{\partial q}{\partial y} - \beta g_y \tilde{T}$$

$$+2\frac{\partial}{\partial y}\left[(\nu + \epsilon_m)\left(\frac{\partial v}{\partial y}\right)\right] \tag{140}$$

$$+\frac{\partial}{\partial x}\left[(\nu + \epsilon_m)\left(\frac{\partial u}{\partial y} + \frac{\partial v}{\partial x}\right)\right]$$

Energy:

$$\frac{\partial T}{\partial t}+\frac{\partial uT}{\partial x}+\frac{\partial vT}{\partial y}=\frac{\partial}{\partial x}\left[(\alpha+\sigma\epsilon_m)\frac{\partial T}{\partial x}\right]$$

$$+\frac{\partial}{\partial y}\left[(\alpha+\sigma\epsilon_m)\frac{\partial T}{\partial y}\right]+\frac{2\nu}{c_p}\left(\frac{\partial u}{\partial x}+\frac{\partial u}{\partial y}+\frac{\partial v}{\partial x}+\frac{\partial v}{\partial y}\right)^2$$

$$+\frac{\nu}{c_p}\left\{\overline{\eta_l'^2}+\frac{\partial^2 q}{\partial x^2}+\frac{\partial^2 q}{\partial y^2}-4\frac{\partial^2}{\partial x^2}\left[\epsilon_m\left(\frac{\partial u}{\partial x}\right)\right]\right.$$

$$\left.-4\frac{\partial^2}{\partial x\,\partial y}\left[\epsilon_m\left(\frac{\partial u}{\partial y}+\frac{\partial v}{\partial x}\right)\right]-4\frac{\partial^2}{\partial y^2}\left[\epsilon_m\left(\frac{\partial v}{\partial y}\right)\right]\right\} \quad (141)$$

Turbulent Kinetic Energy:

$$\frac{\partial q}{\partial t}+\frac{\partial uq}{\partial x}+\frac{\partial vq}{\partial y}=2\epsilon_m\left(\frac{\partial u}{\partial x}\right)^2+\epsilon_m\left(\frac{\partial u}{\partial y}+\frac{\partial v}{\partial x}\right)^2$$

$$+2\epsilon_m\left(\frac{\partial v}{\partial y}\right)^2+\beta\sigma g_x\epsilon_m\frac{\partial T}{\partial x}+\beta\sigma g_y\epsilon_m\frac{\partial T}{\partial y}$$

$$+\frac{\nu}{3}\left(\frac{\partial^2 q}{\partial x^2}+\frac{\partial^2 q}{\partial y^2}\right)-\nu\left\{\frac{1}{2}\overline{\eta_l'^2}-2\frac{\partial^2}{\partial x^2}\left[\epsilon_m\left(\frac{\partial u}{\partial x}\right)\right]\right.$$

$$\left.-2\frac{\partial^2}{\partial x\,\partial y}\left[\epsilon_m\left(\frac{\partial u}{\partial y}+\frac{\partial v}{\partial x}\right)\right]-2\frac{\partial^2}{\partial y^2}\left[\epsilon_m\left(\frac{\partial v}{\partial y}\right)\right]\right\} \quad (142)$$

$$-\ell_1\left[\frac{\partial\epsilon_m}{\partial x}\frac{\partial q}{\partial x}+\frac{\partial\epsilon_m}{\partial y}\frac{\partial q}{\partial y}+\epsilon_m\left(\frac{\partial^2 q}{\partial x^2}+\frac{\partial^2 q}{\partial y^2}\right)\right]$$

continued on the next page.

Turbulent Kinetic Energy (continued from previous page):

$$-\mathcal{K}_2\left[\frac{\partial \epsilon_m}{\partial x}\frac{\partial \varphi}{\partial x}+\frac{\partial \epsilon_m}{\partial y}\frac{\partial \varphi}{\partial y}+\epsilon_m\left(\frac{\partial^2 \varphi}{\partial x^2}+\frac{\partial^2 \varphi}{\partial y^2}\right)\right] \quad (142)$$

Eddy Viscosity:

$$\epsilon_m = \zeta_4 q^{3/10} \quad (143)$$

Mean Square Turbulent Vorticity:

$$\sqrt{\overline{\eta_t'^2}} = \mathcal{K}_3 \frac{q}{\epsilon_m} \quad (144)$$

Subsequently equations (138) through (144) will be written in finite difference form using the explicit scheme.

Continuity Equation:

$$\frac{U^{n+1}_{i+\frac{1}{2},j} - U^{n+1}_{i-\frac{1}{2},j}}{dx} + \frac{V^{n+1}_{i,j+\frac{1}{2}} - V^{n+1}_{i,j-\frac{1}{2}}}{dy} = 0 \qquad (145)$$

Momentum Equation x - direction:

$$U^{n+1}_{i-\frac{1}{2},j} = U^{n}_{i-\frac{1}{2},j} + dt\left\{\frac{(U_{i-1,j})^2 - (U_{i,j})^2}{dx} + \frac{(UV)_{i-\frac{1}{2},j-\frac{1}{2}} + (UV)_{i-\frac{1}{2},j+\frac{1}{2}}}{dy}\right.$$

$$+ \frac{F_{i-1,j} - F_{i,j}}{dx} - \beta g_x (T_{i,j} - T_r)$$

$$- \frac{2}{dx\,dy}\left[(\nu + \epsilon_{m_{i,j}})\,(V_{i,j+\frac{1}{2}} - V_{i,j-\frac{1}{2}})\right.$$

$$\left. - (\nu + \epsilon_{m_{i-1,j}})\,(V_{i-1,j+\frac{1}{2}} - V_{i-1,j-\frac{1}{2}})\right]$$

$$+ \frac{1}{dy}\left\{(\nu + \epsilon_{m_{i-\frac{1}{2},j+\frac{1}{2}}})\left[\frac{U_{i-\frac{1}{2},j+1} - U_{i-\frac{1}{2},j}}{dy}\right.\right.$$

$$\left. + \frac{V_{i,j+\frac{1}{2}} - V_{i-1,j+\frac{1}{2}}}{dx}\right] - (\nu + \epsilon_{m_{i-\frac{1}{2},j-\frac{1}{2}}})\left[\frac{U_{i-\frac{1}{2},j} - U_{i-\frac{1}{2},j-1}}{dy}\right.$$

$$\left.\left.\left. + \frac{V_{i,j-\frac{1}{2}} - V_{i-1,j-\frac{1}{2}}}{dx}\right]\right]\right\} \qquad (146)$$

Momentum Equation y-direction:

$$V^{n+1}_{i,j-\frac{1}{2}} = V^{n}_{i,j-\frac{1}{2}} + dt\left\{\frac{(V_{i,j-1})^2 - (V_{i,j})^2}{dy} + \frac{(UV)_{i-\frac{1}{2},j-\frac{1}{2}} - (UV)_{i+\frac{1}{2},j-\frac{1}{2}}}{dx}\right.$$

$$+ \frac{F_{i,j-1} - F_{i,j}}{dy} - \beta g_y (T_{i,j} - T_r)$$

$$- \frac{2}{dx\ dy}\left[(\nu + \epsilon_{m_{i,j}})\ (U_{i+\frac{1}{2},j} - U_{i-\frac{1}{2},j})\right.$$

$$\left. - (\nu + \epsilon_{m_{i,j-1}})\ (U_{i+\frac{1}{2},j-1} - U_{i-\frac{1}{2},j-1})\right]$$

$$+ \frac{1}{dx}\left\{(\nu + \epsilon_{m_{i+\frac{1}{2},j-\frac{1}{2}}})\left[\frac{U_{i+\frac{1}{2},j} - U_{i+\frac{1}{2},j-1}}{dy}\right.\right.$$

$$\left. + \frac{V_{i+1,j-\frac{1}{2}} - V_{i,j-\frac{1}{2}}}{dx}\right] - (\nu + \epsilon_{m_{i-\frac{1}{2},j-\frac{1}{2}}})\left[\frac{U_{i-\frac{1}{2},j} - U_{i-\frac{1}{2},j-1}}{dy}\right.$$

$$\left.\left.\left. + \frac{V_{i,j-\frac{1}{2}} - V_{i-1,j-\frac{1}{2}}}{dx}\right]\right]\right\} \qquad (147)$$

where:

$$F_{i,j} = p_{i,j} + 2/3\ q_{i,j}$$

Energy Equation:

$$T^{n+1}_{i,j} = T^{n}_{i,j} + dt\left\{\frac{(UT)_{i-\frac{1}{2},j} - (UT)_{i+\frac{1}{2},j}}{dx} + \frac{(VT)_{i,j-\frac{1}{2}} - (VT)_{i,j+\frac{1}{2}}}{dy}\right. \qquad (148)$$

continued on the next page.

Energy Equation (continued from previous page):

$$+ \frac{1}{dx^2} \left[(\alpha + \sigma \epsilon_{m_{i+\frac{1}{2},j}}) (T_{i+1,j} - T_{i,j}) \right.$$

$$\left. - (\alpha + \sigma \epsilon_{m_{i-\frac{1}{2},j}}) (T_{i,j} - T_{i-1,j}) \right]$$

$$+ \frac{1}{dy^2} \left[(\alpha + \sigma \epsilon_{m_{i,j+\frac{1}{2}}}) (T_{i,j+1} - T_{i,j}) \right.$$

$$\left. - (\alpha + \sigma \epsilon_{m_{i,j-\frac{1}{2}}}) (T_{i,j} - T_{i,j-1}) \right]$$

$$+ \frac{2\nu}{c_p} \left(\frac{U_{i+\frac{1}{2},j} - U_{i-\frac{1}{2},j}}{dx} + \frac{U_{i,j+\frac{1}{2}} - U_{i,j-\frac{1}{2}}}{dy} \right.$$

$$\left. + \frac{V_{i+\frac{1}{2},j} - V_{i-\frac{1}{2},j}}{dx} + \frac{V_{i,j+\frac{1}{2}} - V_{i,j-\frac{1}{2}}}{dy} \right)^2$$

$$+ \frac{\nu}{c_p} \left\{ N_{i,j} + \frac{q_{i+1,j} - 2q_{i,j} + q_{i-1,j}}{(dx)^2} \right.$$

$$\left. + \frac{q_{i,j+1} - 2q_{i,j} + q_{i,j-1}}{(dy)^2} - \frac{4}{dx^2} \left[\epsilon_{m_{i+1,j}} \frac{U_{i+\frac{3}{2},j} - U_{i+\frac{1}{2},j}}{dx} \right. \right.$$

$$\left. \left. - 2 \epsilon_{m_{i,j}} \frac{U_{i+\frac{1}{2},j} - U_{i-\frac{1}{2},j}}{dx} + \epsilon_{m_{i-1,j}} \frac{U_{i-\frac{1}{2},j} - U_{i-\frac{3}{2},j}}{dx} \right] \right.$$

(148)

continued on the next page.

Energy Equation (continued from previous page):

$$- \frac{1}{dxdy}\left[\epsilon_{m_{i+1,j+1}}\left(\frac{U_{i+\frac{1}{2},j+1} - U_{i+\frac{1}{2},j}}{dy} + \frac{V_{i+1,j+\frac{1}{2}} - V_{i,j+\frac{1}{2}}}{dx}\right) - \epsilon_{m_{i-1,j+1}}\left(\frac{U_{i-\frac{1}{2},j+1} - U_{i-\frac{1}{2},j}}{dy} + \frac{V_{i,j+\frac{1}{2}} - V_{i-1,j+\frac{1}{2}}}{dx}\right) - \epsilon_{m_{i+1,j-1}}\left(\frac{U_{i+\frac{1}{2},j} - U_{i+\frac{1}{2},j-1}}{dy} + \frac{V_{i+1,j-\frac{1}{2}} - V_{i,j-\frac{1}{2}}}{dx}\right) + \epsilon_{m_{i-1,j-1}}\left(\frac{U_{i-\frac{1}{2},j} - U_{i-\frac{1}{2},j-1}}{dy} + \frac{V_{i,j-\frac{1}{2}} - V_{i-1,j-\frac{1}{2}}}{dx}\right)\right] - \frac{4}{dy^2}\left[\epsilon_{m_{i,j+1}}\left(\frac{V_{i,j+\frac{3}{2}} - V_{i,j+\frac{1}{2}}}{dy}\right) - 2\,\epsilon_{m_{i,j}}\left(\frac{V_{i,j+\frac{1}{2}} - V_{i,j-\frac{1}{2}}}{dy}\right) + \epsilon_{m_{i,j-1}}\left(\frac{V_{i,j-\frac{1}{2}} - V_{i,j-\frac{3}{2}}}{dy}\right)\right]\right\} \tag{148}$$

where:

$$N_{i,j} = \overline{\Pi'^2_1}_{i,j}$$

Turbulent Kinetic Energy Transport Equation:

$$q^{n+1}_{i,j} = q^{n}_{i,j} + dt\left\{\frac{(Uq)_{i-\frac{1}{2},j} - (Uq)_{i+\frac{1}{2},j}}{dx} + \right. \tag{149}$$

continued on the next page.

Turbulent Kinetic Energy Transport Equation (continued from previous page):

$$+ \frac{(Vq)_{i,j-\frac{1}{2}} - (Vq)_{i,j+\frac{1}{2}}}{dy} + 2\epsilon_{m_{i,j}}\left(\frac{U_{i+\frac{1}{2},j} - U_{i-\frac{1}{2},j}}{dx}\right)^2$$

$$+ 2\epsilon_{m_{i,j}}\left(\frac{V_{i,j+\frac{1}{2}} - V_{i,j-\frac{1}{2}}}{dy}\right)^2 + \epsilon_{m_{i,j}}\left(\frac{U_{i,j+\frac{1}{2}} - U_{i,j-\frac{1}{2}}}{dy}\right.$$

$$\left. + \frac{V_{i+\frac{1}{2},j} - V_{i-\frac{1}{2},j}}{dx}\right)^2 + \beta g_x \epsilon_{m_{i,j}} \frac{T_{i+\frac{1}{2},j} - T_{i-\frac{1}{2},j}}{dx}$$

$$+ \beta g_y \epsilon_{m_{i,j}} \frac{T_{i,j+\frac{1}{2}} - T_{i,j-\frac{1}{2}}}{dy}$$

$$+ \frac{\nu}{3}\left(\frac{q_{i+1,j} - 2q_{i,j} + q_{i-1,j}}{dx^2} + \frac{q_{i,j+1} - 2q_{i,j} + q_{i,j-1}}{dy^2}\right)$$

$$- \nu\left\{0.5\, N_{i,j} - 2\frac{1}{dx^2}\left[\epsilon_{m_{i+1,j}} \frac{U_{i+\frac{3}{2},j} - U_{i+\frac{1}{2},j}}{dx}\right.\right.$$

$$\left. - 2\epsilon_{m_{i,j}} \frac{U_{i+\frac{1}{2},j} - U_{i-\frac{1}{2},j}}{dx} + \epsilon_{m_{i-1,j}} \frac{U_{i-\frac{1}{2},j} - U_{i-\frac{3}{2},j}}{dx}\right]$$

$$- \frac{1}{2dxdy}\left[\epsilon_{m_{i+1,j+1}}\left(\frac{U_{i+\frac{1}{2},j+1} - U_{i+\frac{1}{2},j}}{dy}\right.\right.$$

$$\left.\left. + \frac{V_{i+1,j+\frac{1}{2}} - V_{i,j+\frac{1}{2}}}{dx}\right) - \epsilon_{m_{i-1,j+1}}\left(\frac{U_{i-\frac{1}{2},j+1} - U_{i-\frac{1}{2},j}}{dy}\right.\right.$$

continued on the next page.

(149)

Turbulent Kinetic Energy Transport Equation (continued from previous page):

$$+\frac{V_{i,j+\frac{1}{2}} - V_{i-1,j+\frac{1}{2}}}{dx}\Bigg) - \epsilon_{m_{i+1,j-1}}\Bigg(\frac{U_{i+\frac{1}{2},j} - U_{i+\frac{1}{2},j-1}}{dy}$$

$$+\frac{V_{i+1,j-\frac{1}{2}} - V_{i,j-\frac{1}{2}}}{dx}\Bigg) + \epsilon_{m_{i-1,j-1}}\Bigg(\frac{U_{i-\frac{1}{2},j} - U_{i-\frac{1}{2},j-1}}{dy}$$

$$+\frac{V_{i,j-\frac{1}{2}} - V_{i-1,j-\frac{1}{2}}}{dx}\Bigg) - \frac{2}{dy^2}\Bigg[\epsilon_{m_{i,j+1}}\frac{V_{i,j+\frac{3}{2}} - V_{i,j+\frac{1}{2}}}{dy}$$

$$- 2\,\epsilon_{m_{i,j}}\frac{V_{i,j+\frac{1}{2}} - V_{i,j-\frac{1}{2}}}{dy} + \epsilon_{m_{i,j-1}}\frac{V_{i,j-\frac{1}{2}} - V_{i,j-\frac{3}{2}}}{dy}\Bigg]\Bigg\}$$

$$- \frac{\alpha_1}{dx^2}\Big[\epsilon_{m_{i+\frac{1}{2},j}}(q_{i+1,j} - q_{i,j}) - \epsilon_{m_{i-\frac{1}{2},j}}(q_{i,j} - q_{i-1,j})\Big]$$

$$- \frac{\alpha_1}{dy^2}\Big[\epsilon_{m_{i,j+\frac{1}{2}}}(q_{i,j+1} - q_{i,j}) - \epsilon_{m_{i,j-\frac{1}{2}}}(q_{i,j} - q_{i,j-1})\Big]$$

$$- \frac{\alpha_2}{dx^2}\Big[\epsilon_{m_{i+\frac{1}{2},j}}(\varphi_{i+1,j} - \varphi_{i,j}) - \epsilon_{m_{i-\frac{1}{2},j}}(\varphi_{i,j} - \varphi_{i-1,j})\Big]$$

$$- \frac{\alpha_2}{dy^2}\Big[\epsilon_{m_{i,j+\frac{1}{2}}}(\varphi_{i,j+\frac{1}{2}} - \varphi_{i,j}) - \epsilon_{m_{i,j-\frac{1}{2}}}(\varphi_{i,j} - \varphi_{i,j-1})\Big]\Bigg\} \tag{149}$$

Eddy Viscosity:

$$\epsilon_{m_{i,j}} = \zeta_4 \, q_{i,j}^{3/10} \tag{150}$$

Mean Square Turbulent Vorticity:

$$\sqrt{N_{i,j}} = \kappa_3 \, q_{i,j} / \epsilon_{m_{i,j}} \tag{151}$$

The description of the computer program developed to solve the equations (145) through (151) is presented in the next section of this chapter.

Variable Mesh Size

The technique of finite differences can be further refined by application of a variable mesh size for problems where differentiation between the areas of principal interest and secondary interest is of significant importance.

Mesh can be made very fine in the area of large velocity and temperature gradients and increased in size within the region where changes of investigated variables are small with respect to the mesh dimensions. This is illustrated on figure (9) below.

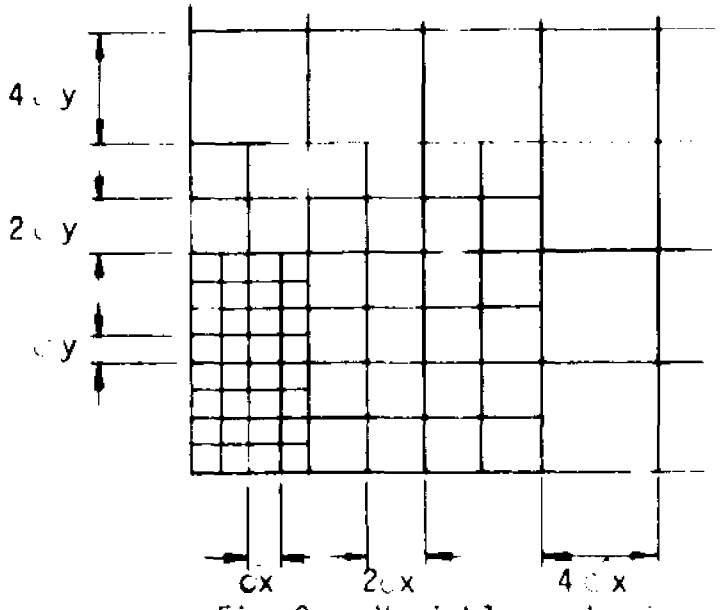

Fig. 9 . Variable mesh size

The advantage of an application of this method is apparent. A very large area of the flow field can be covered with only a small increase in the amount of computations and computer storage. What is also important, is that this can be done without decreasing the accuracy of the results.

A serious difficulty arises, however, when it is necessary to match two regions of different mesh size. An illustration below is self-explanatory and presents the technique that was used to match the variables on the mesh boundaries.

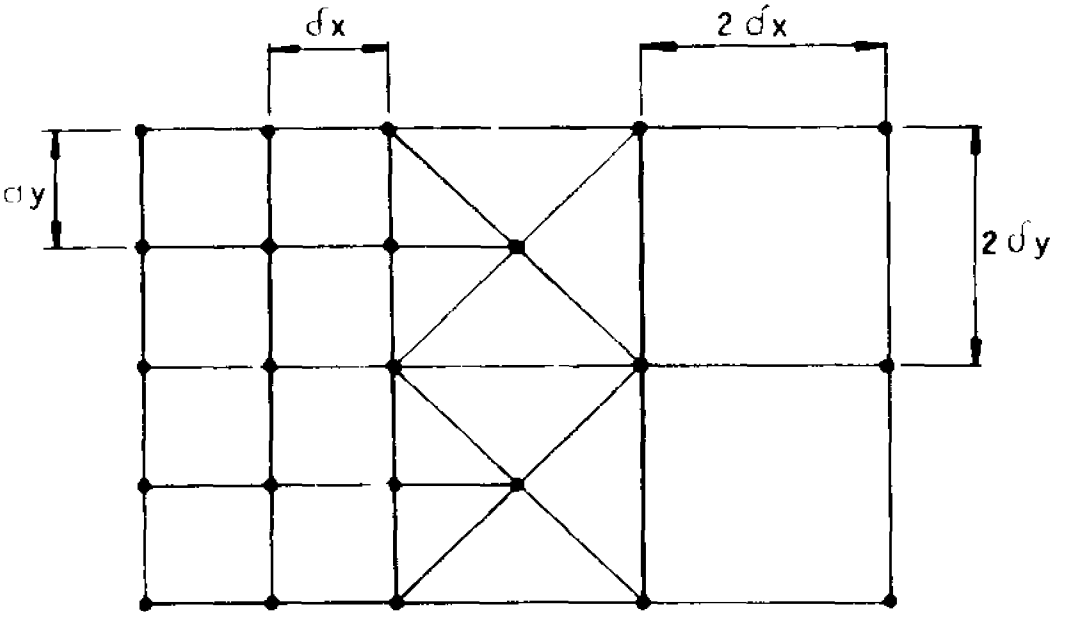

Fig. 10 . Transition between the fine and the coarse net.

Detailed explanation of the technique applied above can be found in reference (17) by Forsythe and Wasow.

Only introductory work was done in the area of variable mesh size because of the problems posed by the solution of Poisson's equation (which is part of the computational cycle). Nevertheless, the results are quite promising and additional effort may be spent in the future in order to finalize this numerical procedure.

The numerical stability analysis for a variable mesh size is no different from the one developed for a constant mesh size, since each of the regions of a variable size net has an individually constant mesh size.

C. COMPUTER PROGRAM

Equations (14^c) through (15^l) have been programmed for solution by a computer. In this section we shall briefly discuss computational procedure, program options and computation time requirements.

Computational Procedure

The computer program is written in FORTRAN IV and consists of a main program and several subroutines.

Solution is time dependent, and an explicit scheme is used to evaluate the variables as functions of time and space coordinates. Although the solution is time dependent, steady state results can also be obtained by performing the computations until an equilibrium is reached, and the dependent variables stop changing, even if we proceed with calculations.

The calculational cycle is separated into two major parts. In summary the procedure of computation is as follows:

1. A temporary field of advanced time velocities is calculated from the Navier-Stokes equations, with a pressure boundary condition at the free surface satisfying the normal stress condition. Correct velocity boundary conditions assure that this temporary velocity field contains the correct vorticity at every interior point in the fluid. The temporary velocity field does not, however, satisfy the continuity equation i.e. $\frac{\partial u_i}{\partial x_i} = 0$.

2. In the second step the temporary velocities are adjusted to their final values so as to preserve the vorticity at every point. A potential function, and a Poisson's equation is employed. The potential is determined by the requirement that the final velocity field satisfies the continuity equation everywhere i.e. $\frac{\partial u_i}{\partial x_i} = 0$. With final velocities

determined, the temperature field and all turbulent variables are calculated and then the program proceeds to the next cycle in time incremented by the appropriate Δt.

Poisson's equation can be solved either by the iteration procedure, or by a direct method. Application of either method depends on the type of problem to be solved. Iteration procedure requires small amount of computer storage space but it can become very costly in computer time. A direct method, in turn, results in great savings of computer time, but then requires a large amount of computer storage.

Program Options

A major option is a choice for a flow to be assumed either laminar or turbulent and then, for either of them there are the following possibilities:

a) Vertical jet in either stationary reservoir, or a cross-stream with no temperature variations.

b) The same as above, with an addition that the jet and ambient temperatures are specified. There is also a choice of a reservoir having uniform temperature throughout, or being temperature (density) stratified.

c) Horizontal jet in either stationary reservoir, or a cross-stream with no temperature variations.

d) The same conditions as in (c), with the addition that jet and ambient temperatures are specified. The reservoir may be of uniform temperature, or temperature (density) stratified.

For any of the options it is possible to investigate effects of buoyancy and stratification, intensity of turbulence in the flow field with turbulent viscosity distribution, in addition to getting velocity, pressure and temperature distributions.

These options were developed for a regular rectangular, or square

computational net. We can apply all the options over the variable mesh size mentioned earlier. The advantage of this net was already described.

Computation Time Requirement

The amount of computer time necessary to reach steady state depends on two factors, namely, character of the flow i.e. laminar or turbulent, and the method that was used to solve Poisson's equation (i.e. iterations, or a direct technique). As mentioned, the direct method should be applied whenever possible (provided that the storage required is not too large) as computation time may be cut down very seriously in comparison with the iteration technique.

When the iteration technique was used, it was found that turbulent flows required less computer time than laminar ones. Although the turbulent flow equations are far more complicated than those for the laminar flow, the number of iterations is cut down, due to a larger dissipation of energy by turbulent motion. The actual amount of time necessary to reach steady state for a particular flow depends on the type of computer used and may vary from a few hours time on IBM 360, to only several minutes on IBM 370.

III. EXPERIMENTAL FACILITY

The experimental system was designed with the objective of modeling the two dimensional flow field of a thermal discharge in the initial stage of its development, as well as, in a steady state process.

The major equipment of the system consisted of:

1. A test tank in which experiments were conducted. Main dimensions: 3.66m. length, 0.20m. width, 0.50m depth. The discharge nozzle centered across the tank was 0.001m. wide.
2. Hot water tank with dimensions: 0.25m.x 0.38m.x 0.50m. It provided a supply of hot water with desired temperature and pressure head.

The measurements of velocity and temperature were taken by the following instruments:

1. Velocity was measured by a temperature compensated probe of a hot film element, gold plated quartz with temperature compensating coil. A constant temperature anemometer (DISA type 55A01) coupled with another anemometer (DISA type 55D05) were used for these measurements. Minimum velocity limit for the probe was 0.01m/sec.
2. Temperature measurements were taken by an array of copper-constantan thermocouples. The magnitude of temperature was read on an electronic thermometer (Comark 1200 series). Estimated accuracy of measurements was 0.05°C.

The jet structure was also recorded photographically. Two different methods of observation were applied:

1. A projector, and a specially designed screen with slides were used to observe the development and intensity of the temperature field as well as the motion of the fluid.
2. Green dye was added to the hot water supply to trace the jet boundaries.

A Graflex camera and black and white film were used to record the trajectories of the jets.

Experimental Cycle: Thermal Discharge to a Still, Infinitely Long Reservoir of Uniform Temperature.

Modeling of the flow in the initial stage of its development poses no serious design problem. To accomplish the task of accumulating data for a steady state process the following operational cycle was devised:

Hot water enters the tank through the discharge nozzle, mixes with the cold water and then, due to momentum and buoyancy forces, reaches the surface and spreads out horizontally.

Eventually the head of the thermal layer reaches the end of the tank and is discharged through a filter which regulates the rate of outflow and keeps system in balance.

Cold water is supplied to the tank through the entire tank floor to assure that its velocity is negligibly small. (Velocity at the floor is of order of 0.001m/sec.) The cold water lost in the mixing process is thus replaced.

This operational cycle can be carried on for a long interval of time.

The serious problem that was encountered while conducting experiments was posed by an enormous quantity of very small air bubbles. Air accumulated on the surface of velocity and temperature probes had a very adverse effect on the accuracy of the readings. The problem was successfully solved by an application of air traps on hot and cold water supply systems.

The experimental system and its components are illustrated on the following pages.

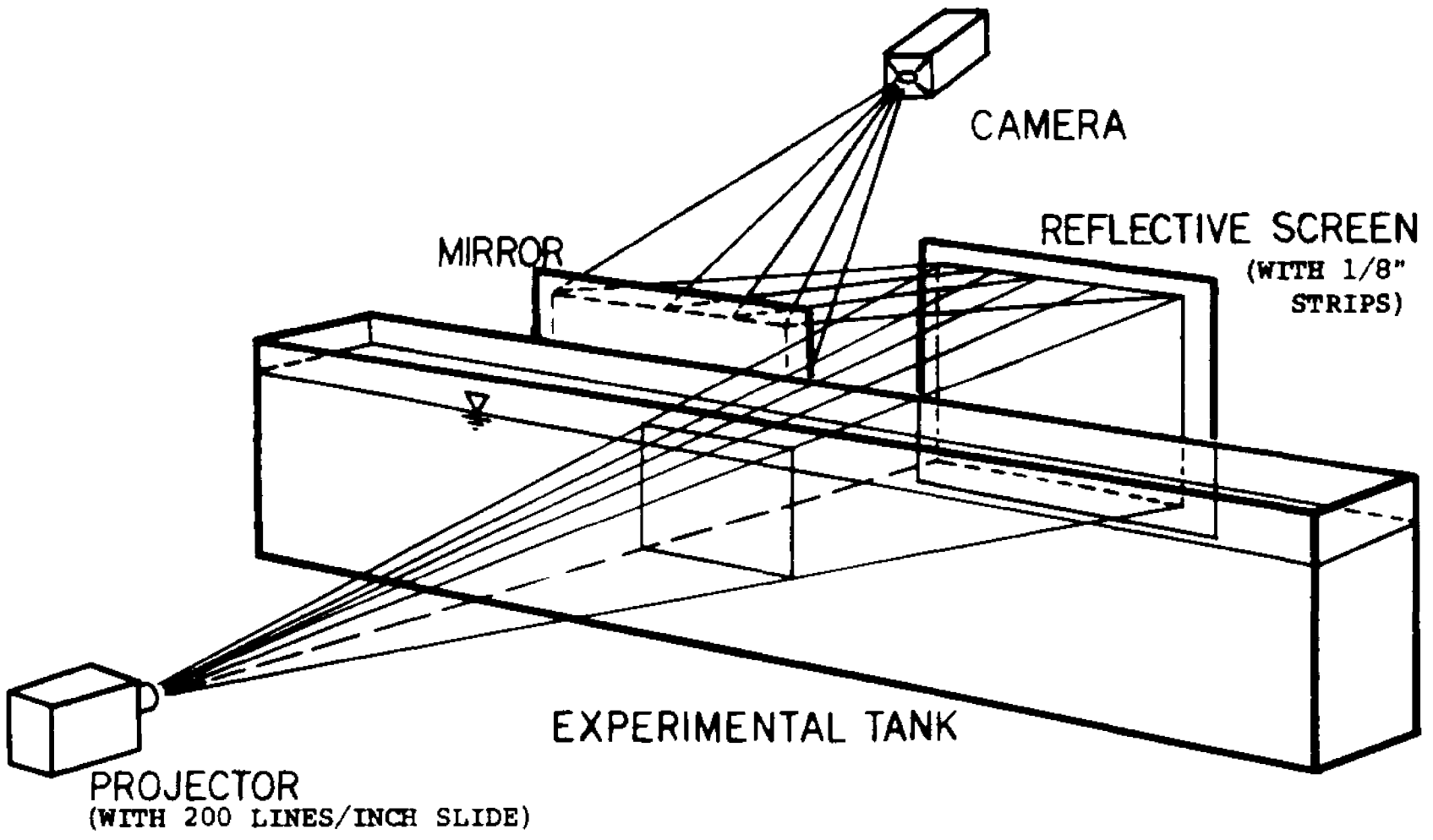

FIG.11 EQUIPMENT PLACEMENT FOR OBSERVATION OF TEMPERATURE DISTRIBUTION

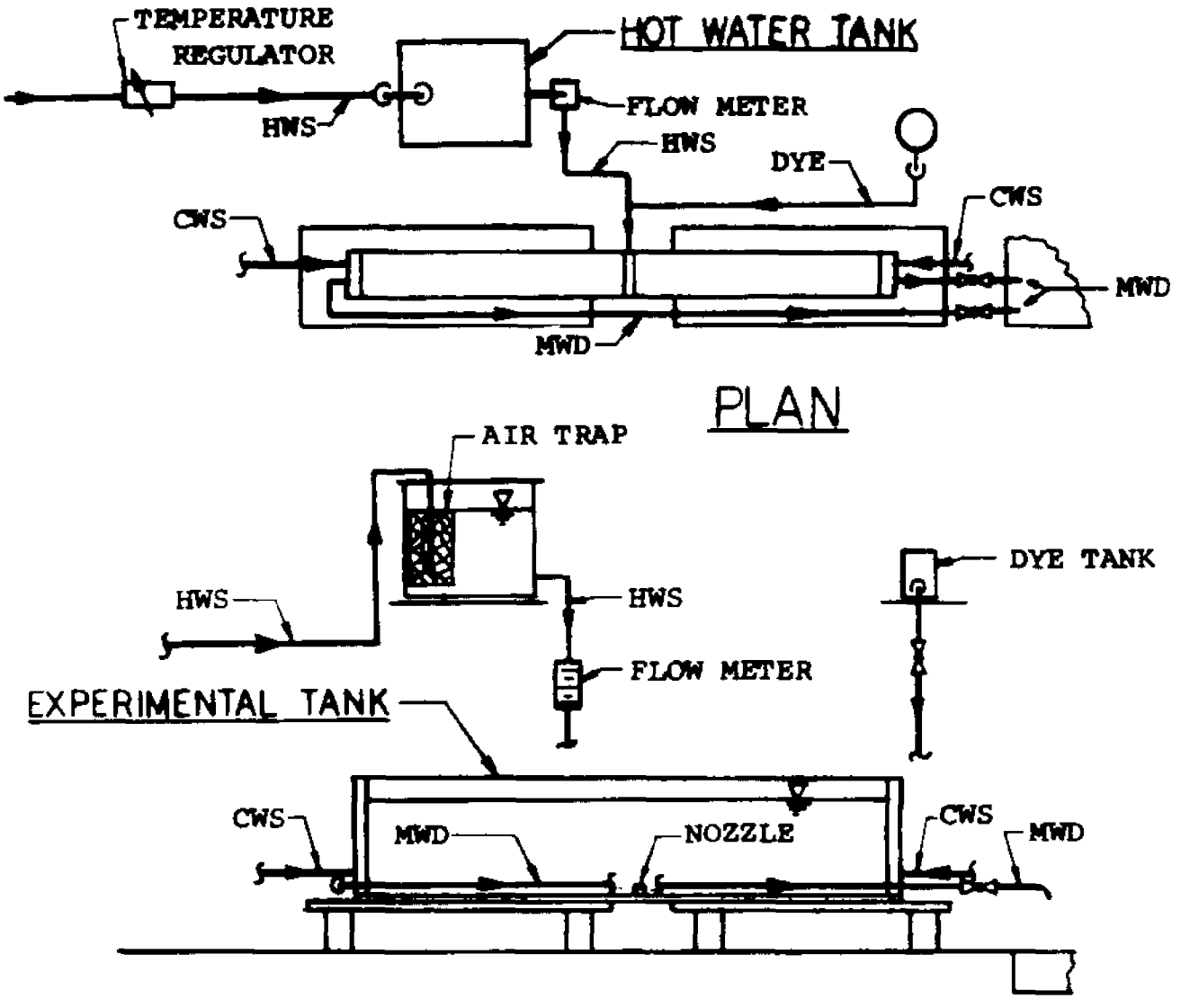

FIG 2. EXPERIMENTAL SYSTEM

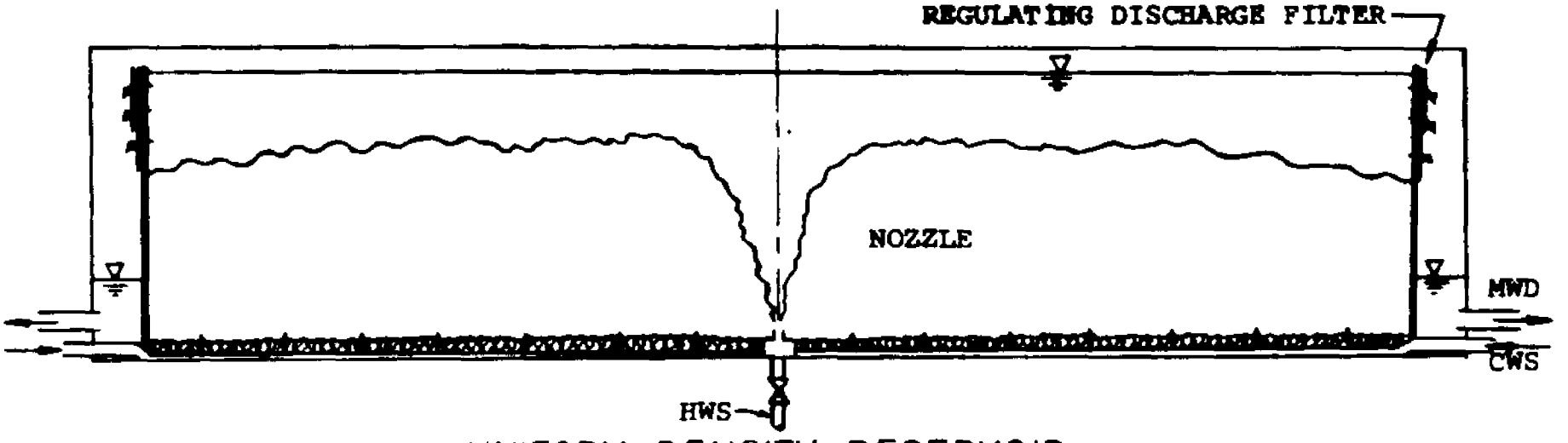

UNIFORM DENSITY RESERVOIR

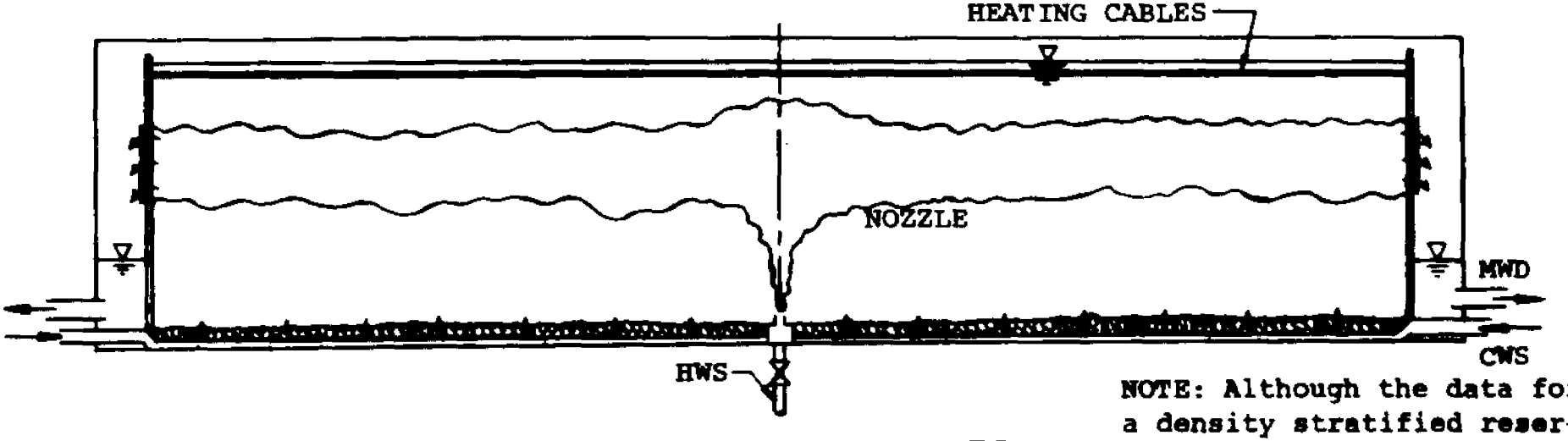

DENSITY STRATIFIED RESERVOIR

FIG13 EXPERIMENTAL TANK SET UP

NOTE: Although the data for a density stratified reservoir were not obtained, it was possible to develop conditions for a discharge to a stratified reservoir and it is shown above.

IV. EXPERIMENTAL RESULTS

In this chapter, the experimental results are presented. The discharges, according to the structure of the flow field will be classified as being deep, or shallow, depending on the flow pattern and size of the thermal layer.

The shallow discharges are defined as such where the entire region (from top to bottom) is affected by turbulent mixing. There is no thermal layer since all the space is filled by the discharge water and the temperature on the vertical cross-section is either uniform, or varies slightly.

The flow pattern of a deep discharge is significantly different. The thermal layer is formed on the water surface (when the equilibrium state is reached) and the lower (cold water) region is not affected by the mixing.

As far as various parameters are concerned, the size of the discharge nozzle and the reservoir depth are most descriptive in characterizing the discharge.

In this investigation, shallow discharges had 1:5 nozzle to depth ratio, a border case, 1:16 ratio and deep discharges, 1:500 ratio. The gradual transition from shallow to deep water discharges illustrated by change of temperature and velocity pattern is shown on Fig.(14) and Fig.(15).

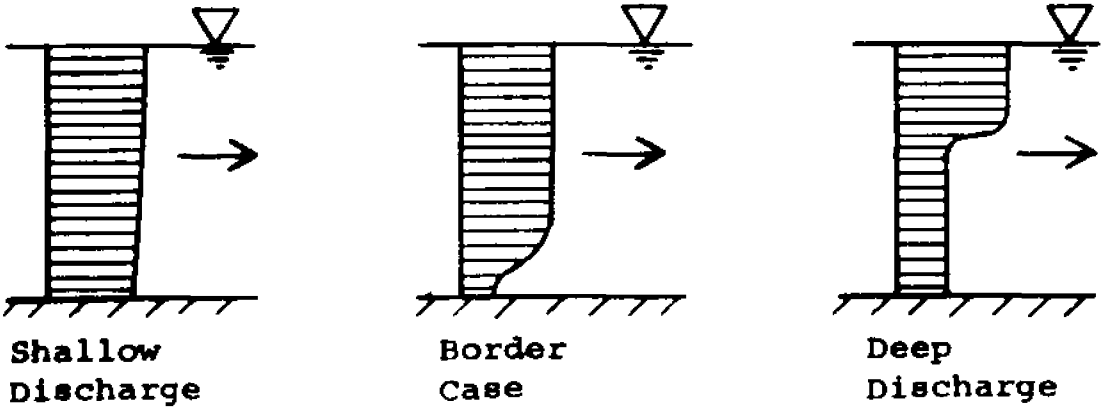

FIG. 14. TEMPERATURE PROFILES

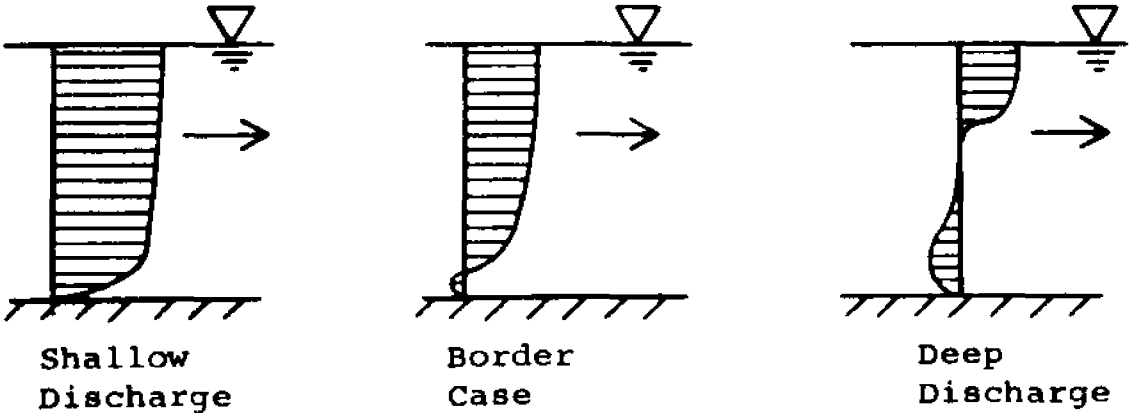

FIG. 15. VELOCITY PROFILES

The arrow points direction of the flow away from the jet center line.

Additional information on the flow pattern of various discharges and other details, is given in this chapter (pp.108,109). The first two sections discuss deep discharges and shallow discharges. In the third section of this chapter, an investigation of the free surface is presented. The shape of the free surface and its dependence on several flow parameters are evaluated experimentally and numerically.

The experimental data were taken, as stated, for the two-dimensional flow. To make sure that the flow is truly two-dimensional and that the impact of the tank walls did not affect the results, the horizontal velocity was measured across the tank from wall to wall at several different cross-sections. The accumulated data are presented on the next page. It may be noticed that the presence of the walls had a negligible impact on the velocity profile.

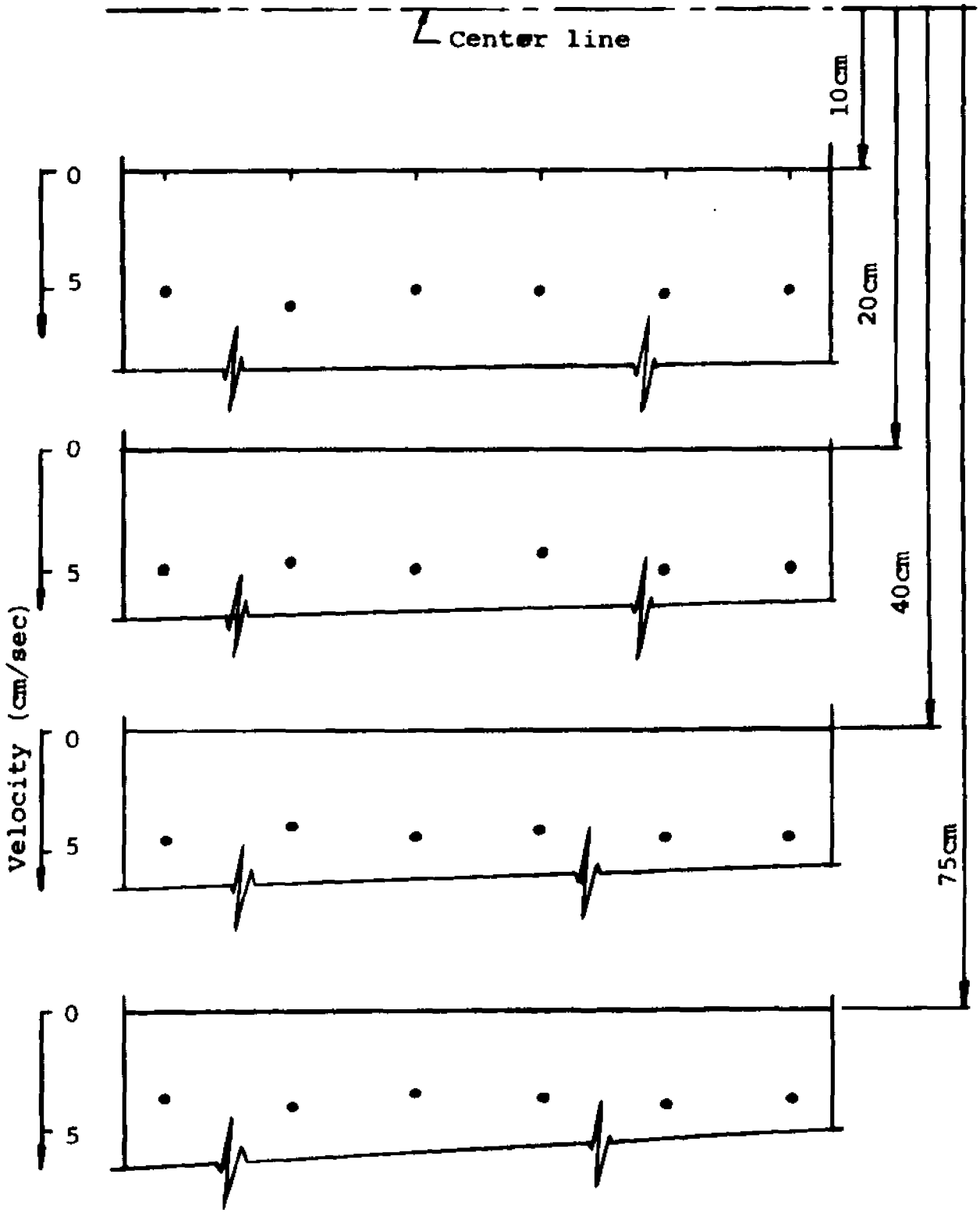

FIG. 16. VELOCITY PROFILES ACROSS THE EXPERIMENTAL TANK TAKEN AT VARIOUS DISTANCES FROM THE TANK AXIS

(Rate of Flow 0.3785 L/M)

1. EXPERIMENTAL RESULTS - DEEP DISCHARGES

The experimental set-up described in the ealier chapter was used to gather the data for a steady, two-dimensional flow. The word "steady" applies to the mean velocity and temperature values, since turbulent fluctuations were present in the large portion of the flow field. Accumulated sets of data covered the temperature and velocity distributions as functions of distance from the jet nozzle, as well as, temperature and velocity distributions as functions of depth and distance from the jet axis in the far field.

The measurements were taken for several different rates of flow, i.e., 0.18925 liters/minute, 0.37850 liters/minute, 0.56775 liters/minute and 0.75700 liters/minute per centimeter of nozzle length.

To develop a relation between the structure of velocity and temperature fields for each discharge rate of hot water, several jets of different hot water temperatures were investigated. Hot water was supplied at $15^{o}C$, $20^{o}C$, $30^{o}C$, $40^{o}C$, $50^{o}C$ and $60^{o}C$. The temperature of the cold water in the reservoir varied between $15^{o}C$ and $16^{o}C$.

The results are presented in graphs on the following pages. These graphs illustrate temperature and velocity distributions over the investigated field. The curves were obtained by applying polynomial regression analysis of the data points for the larger spreads of data, or simply by drawing the line, interpolating between the points, if the spread was negligible. The small deviation of each of the experimental points is due to the fact that an arithmetic average of the experimental values was taken for each point shown on the graph. The measurements were repeated three to six times at each point to obtain, as accurate, as possible results.

Experimental Results - Notes; Fig. E1. through E13.

To prevent the experimental graphs from being overcrowded with notes, which are common to many of them, the pertinent comments are summarized on this page.

The metric system of units is used to present all the experimental data. This conversion resulted in fractions and uneven numbers when some values were changed from British to metric system.

Distance is expressed in centimeters (CM).

Velocity in centimeters per second (CM/SEC).

Temperature in degrees Centigrade (^{o}C).

Rate of flow in liters per minute (L/Min.), taken per centimeter of nozzle length.

Rates of flow of 0.18925 L/Min., 0.37850 L/Min., 0.56775 L/Min. and 0.75700 L/Min. correspond to rates of hot water flow supplied to jet nozzle of 1 GPM, 2 GPM, 3 GPM and 4 GPM respectively.

For the axial distribution of temperature and velocity the number in the upper right hand corner of each box represents the distance of the cross-section, at which the temperature, or velocity were taken, from the jet nozzle (Fig. E1., E2., E5., E6.).

The vertical axis represents velocity, or temperature, while the horizontal one gives the distance from jet axis.

Note: H - the distance from the jet nozzle is defined on Fig.1.
Only one-half of the profile for velocity and temperature is shown.

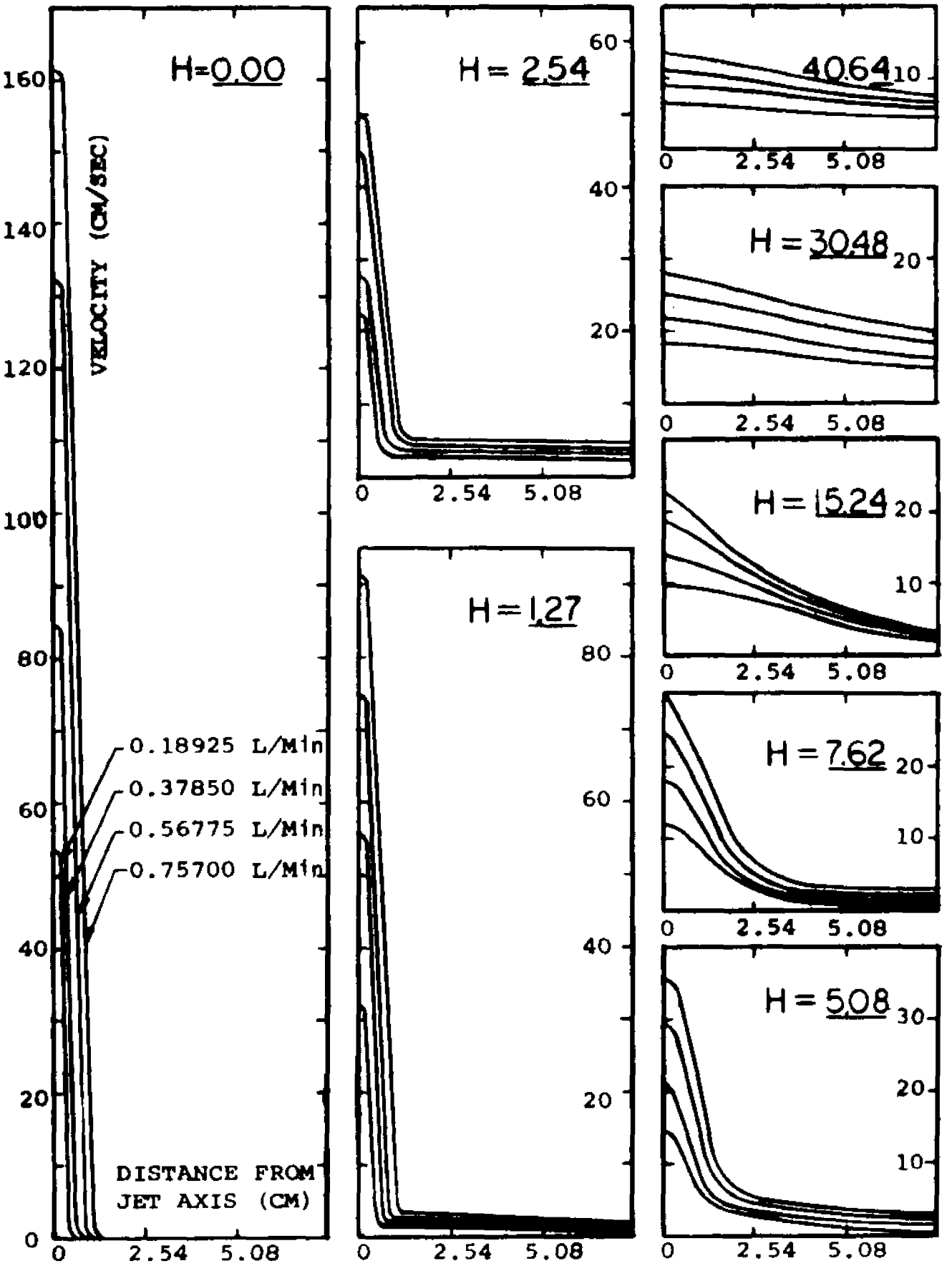

FIG.E1. JET AXIS - VELOCITY DISTRIBUTION PROFILES
Comparison of Velocity Profiles for Various Discharge Rates.
Entering Jet Temperature 30°C.

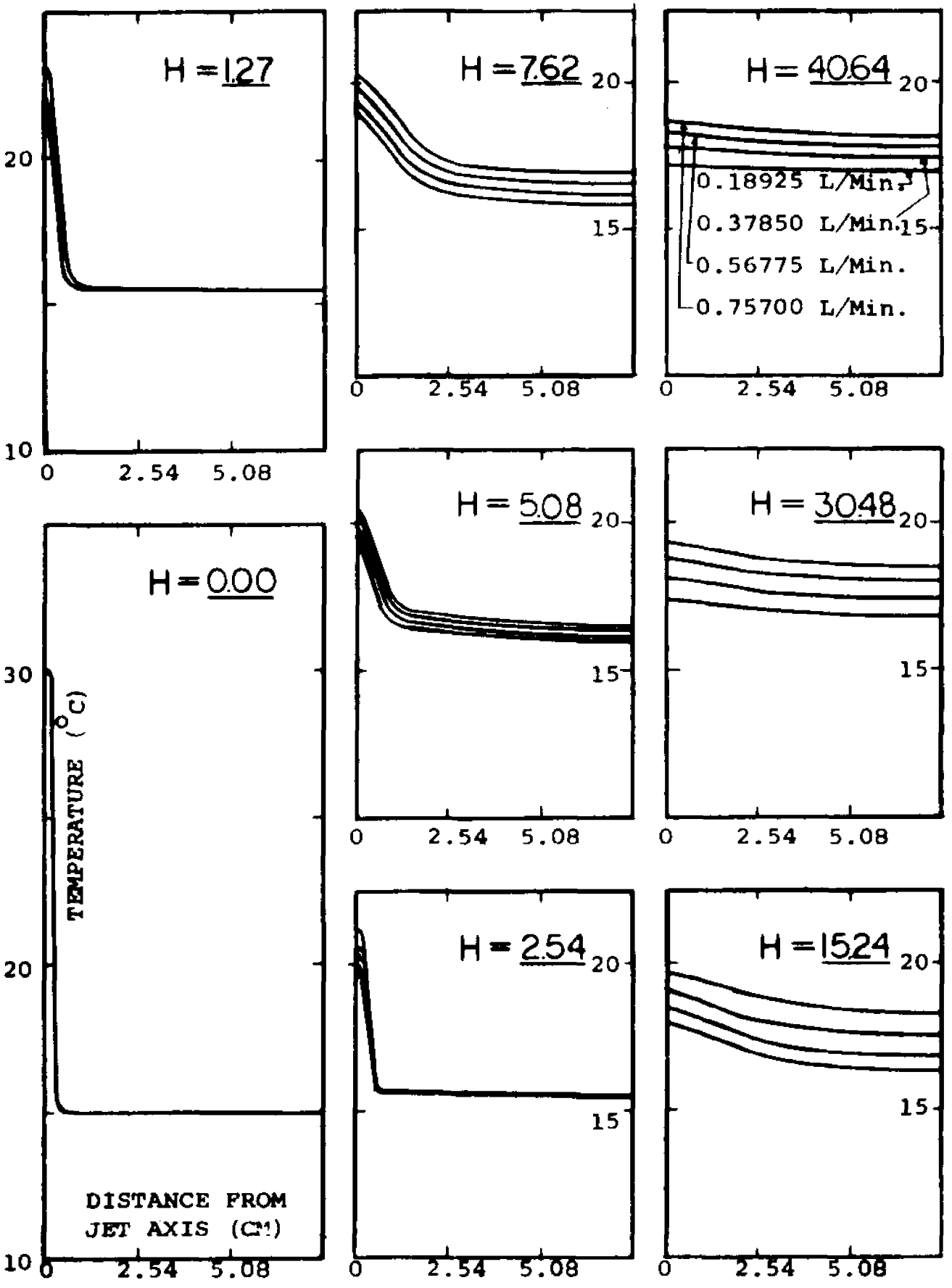

FIG.E2. JET AXIS - TEMPERATURE DISTRIBUTION PROFILES
Comparison of Temperature Profiles for Various Discharge Rates.
Entering Jet Temperature 30°C.

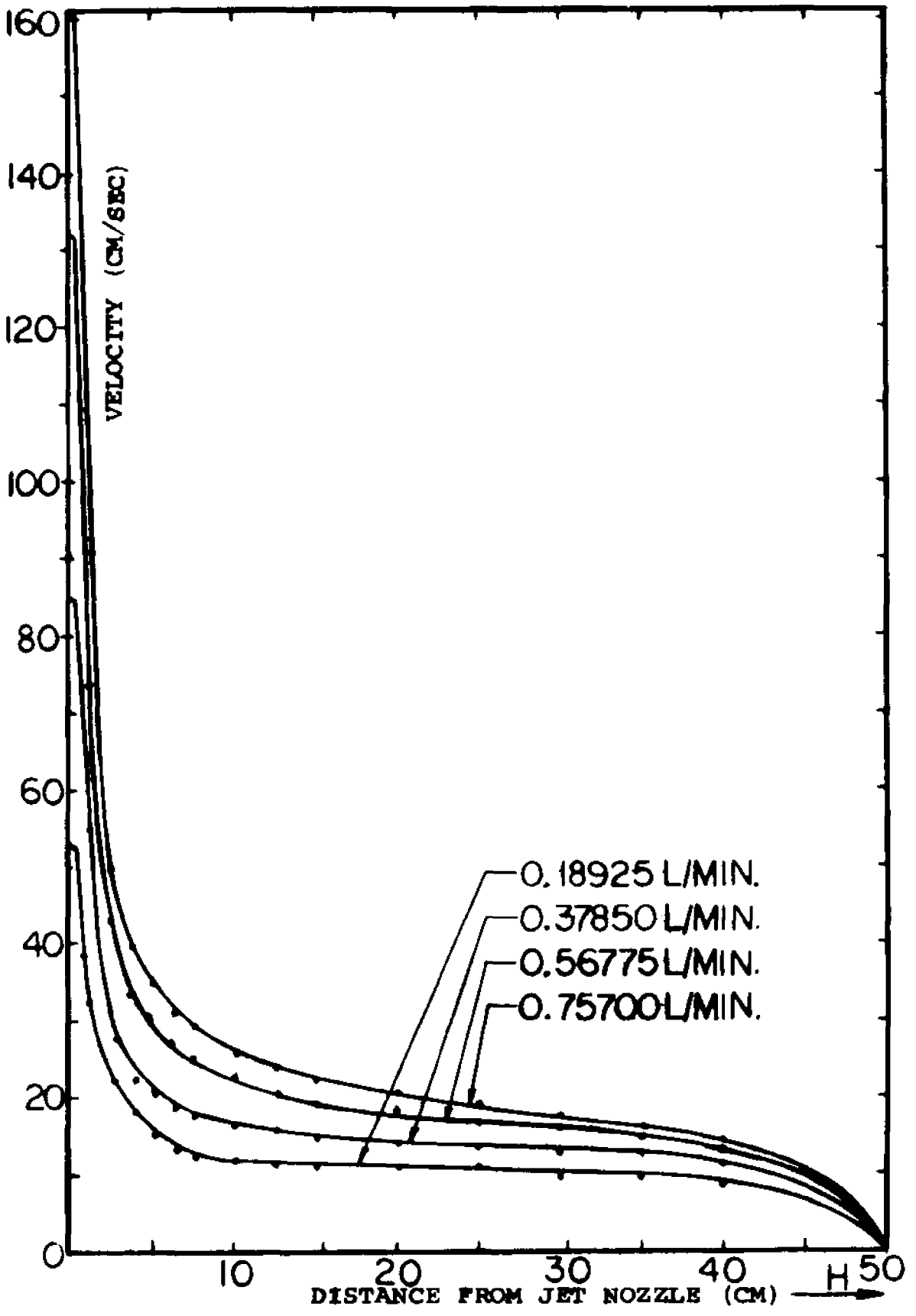

FIG.E3. VELOCITY CHANGE ALONG JET AXIS
Comparison of Velocity Distribution for Various Rates of Flow Entering Jet Temperature 30°C.

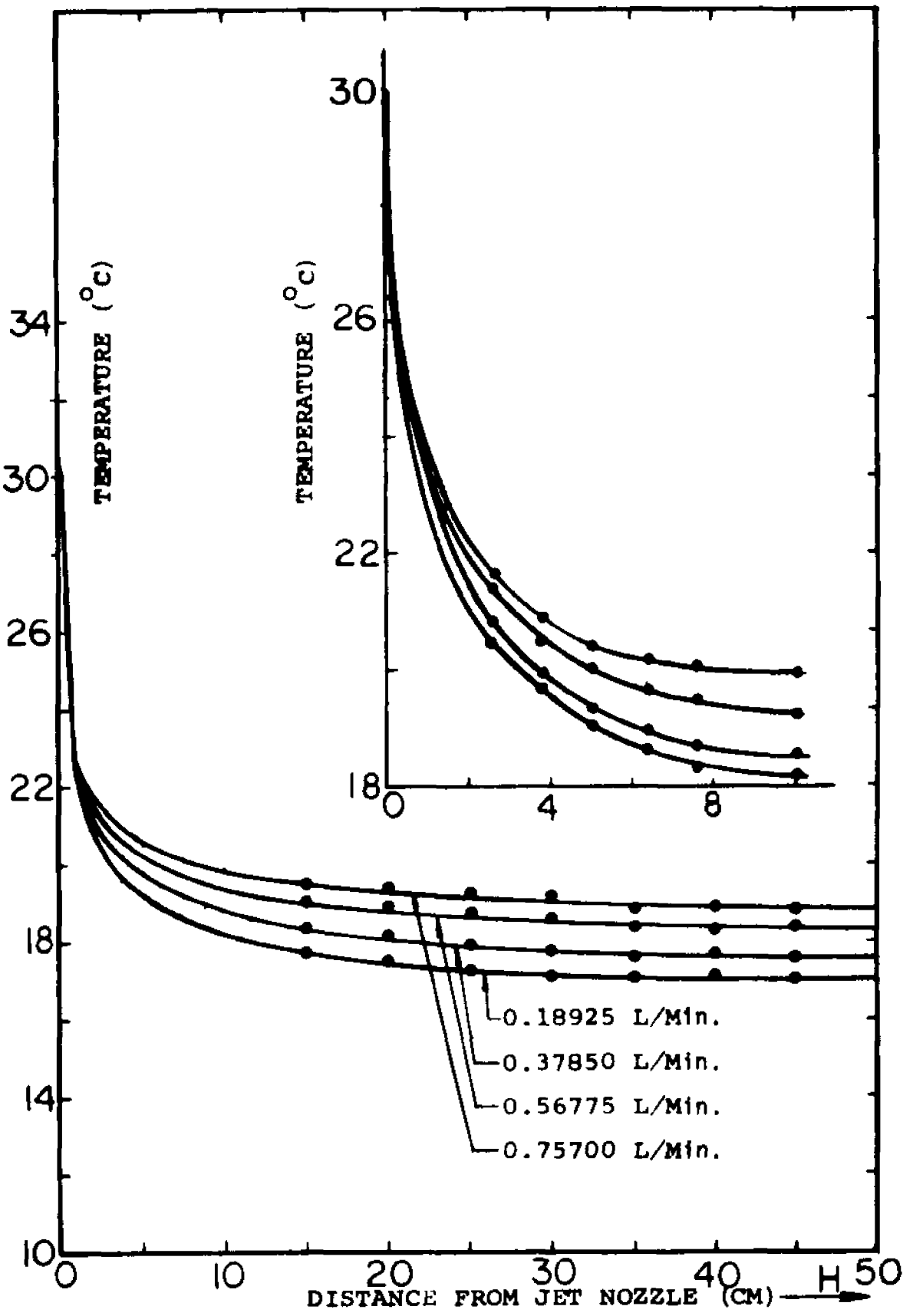

FIG.E4. TEMPERATURE CHANGE ALONG JET AXIS
Comparison of Temperature Distribution for Various Rates of Flow Entering Jet Temperature 30°C.

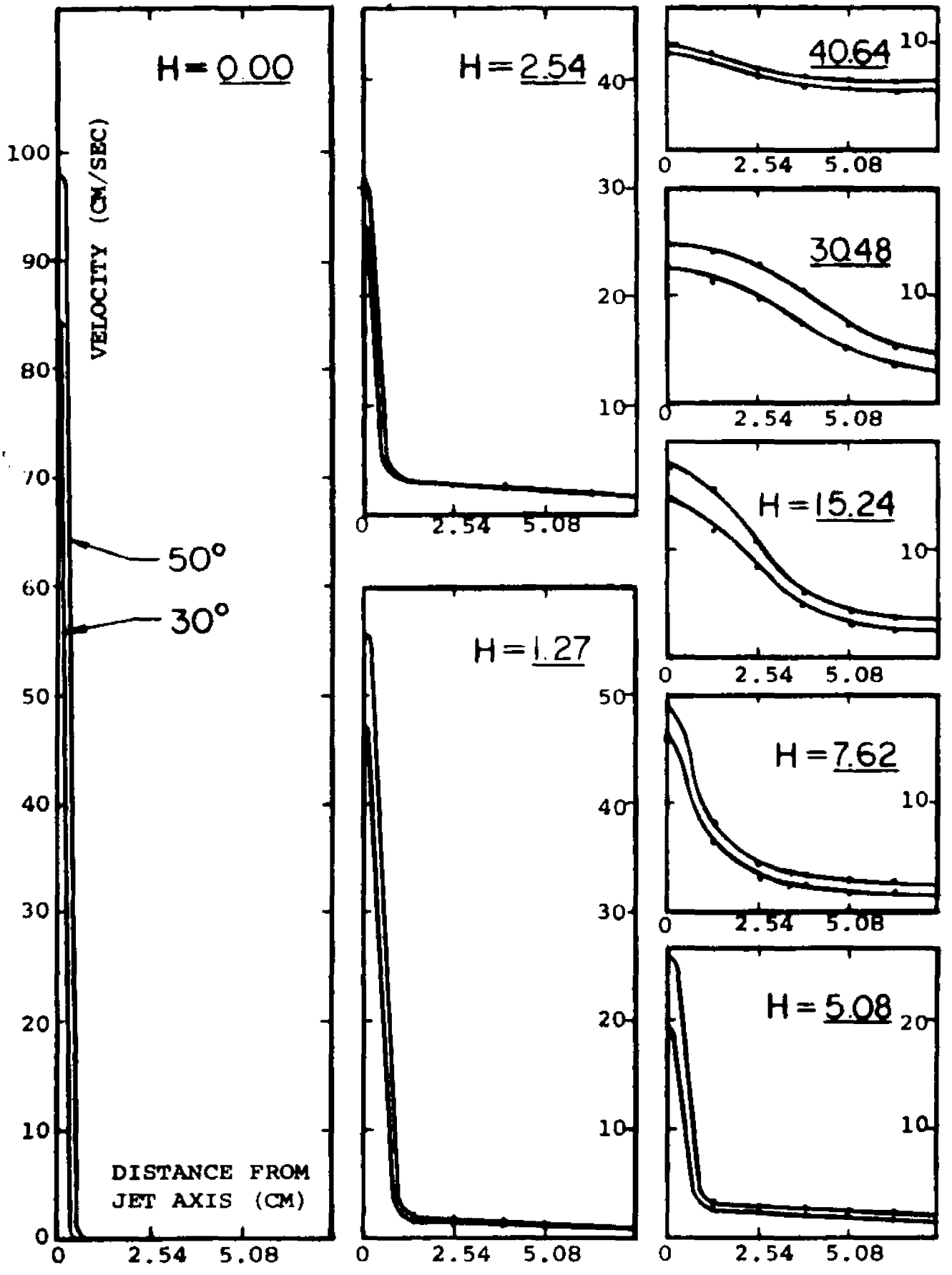

FIG.E5. JET AXIS - VELOCITY DISTRIBUTION PROFILES
Comparison of Velocity Profiles for Various Jet Temperatures
Rate of Flow is 0.37850 L/Min.

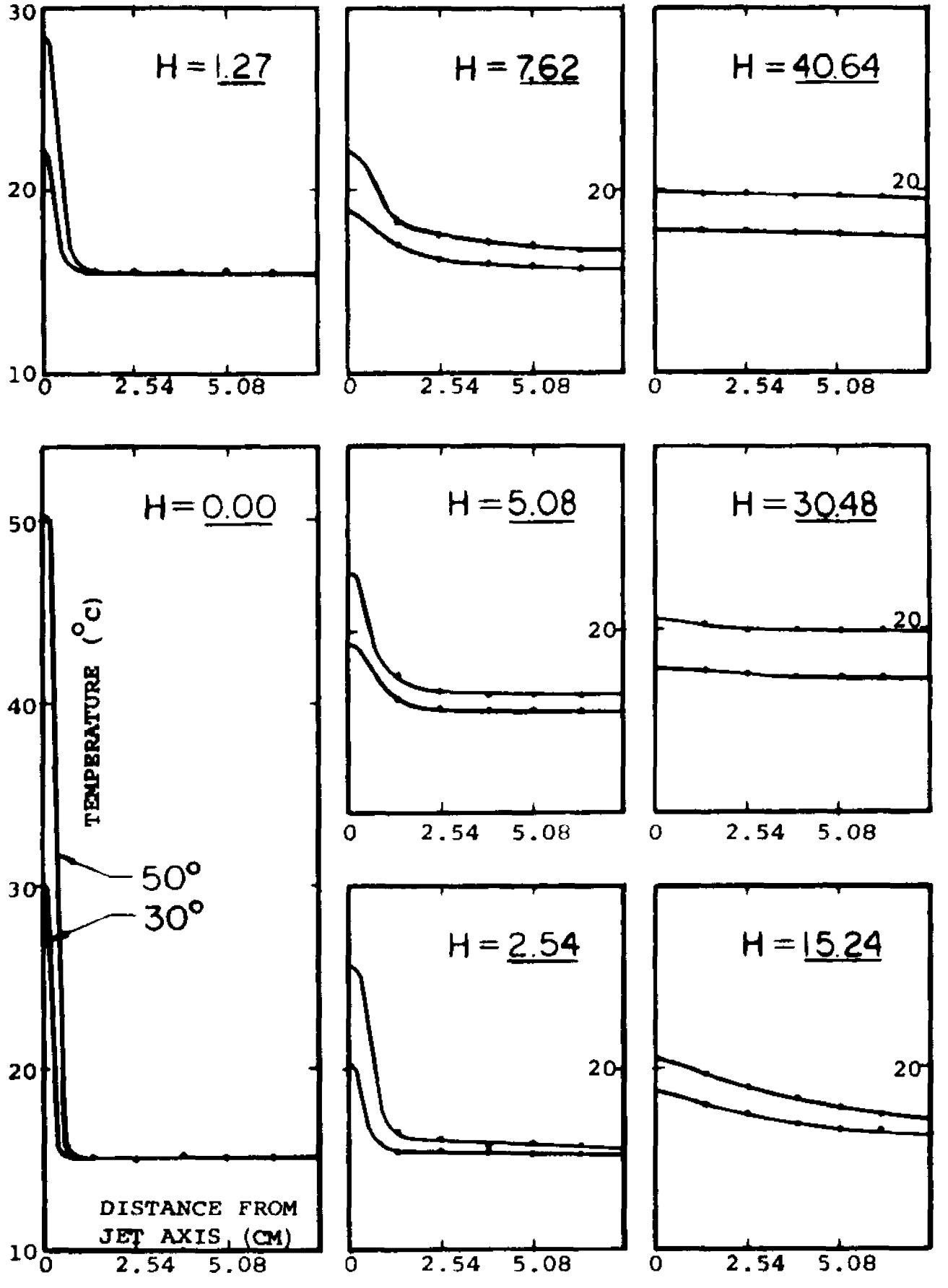

FIG.E6. JET AXIS - TEMPERATURE DISTRIBUTION PROFILES
Comparison of Temperature Profiles for Various Jet Temperatures
Rate of Flow is 0.37850 L/Min.

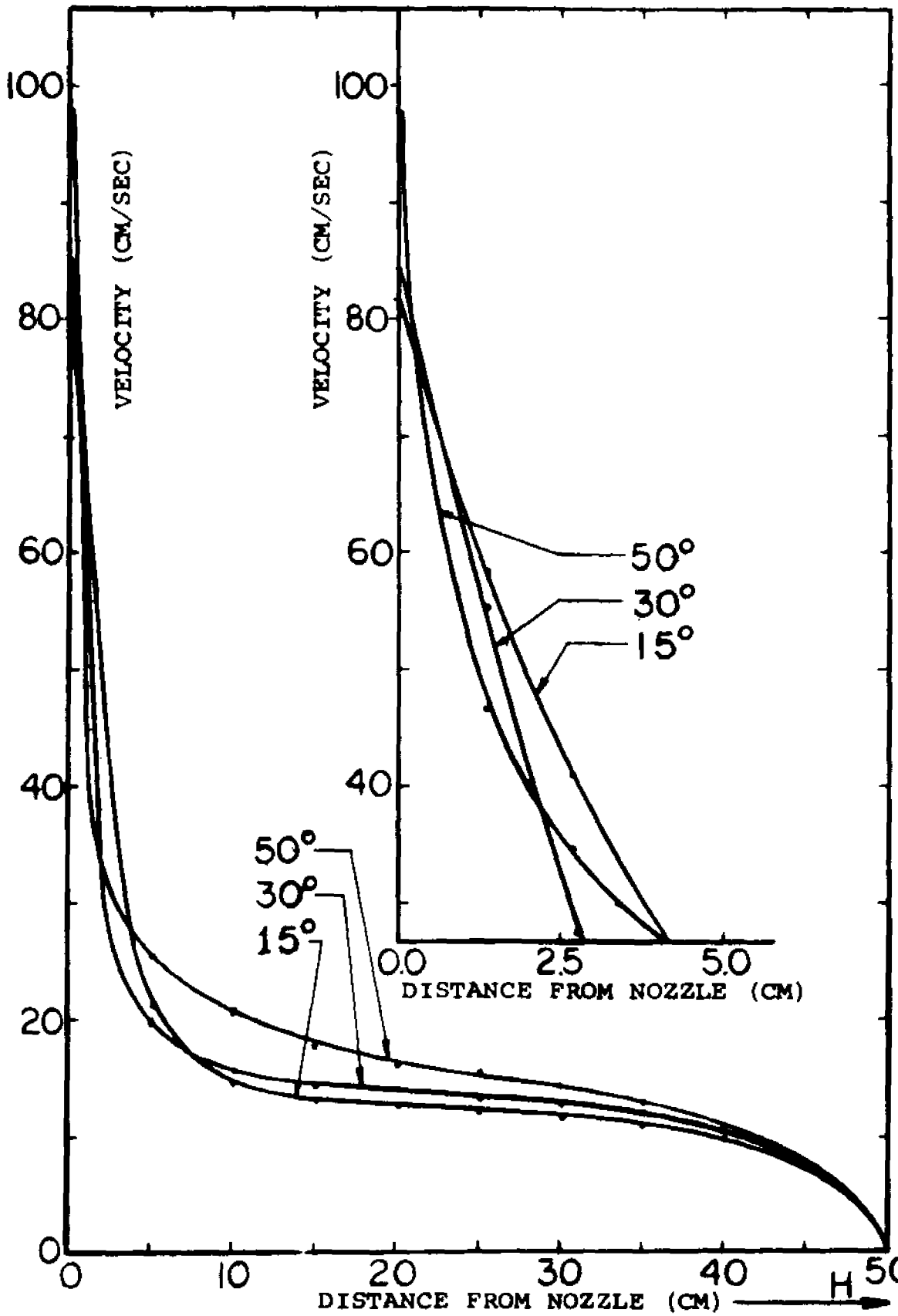

FIG.E7. VELOCITY CHANGE ALONG JET AXIS
Comparison of Velocity Distribution for Various Jet Temperatures
Rate of Flow is 0.37850 L/Min.

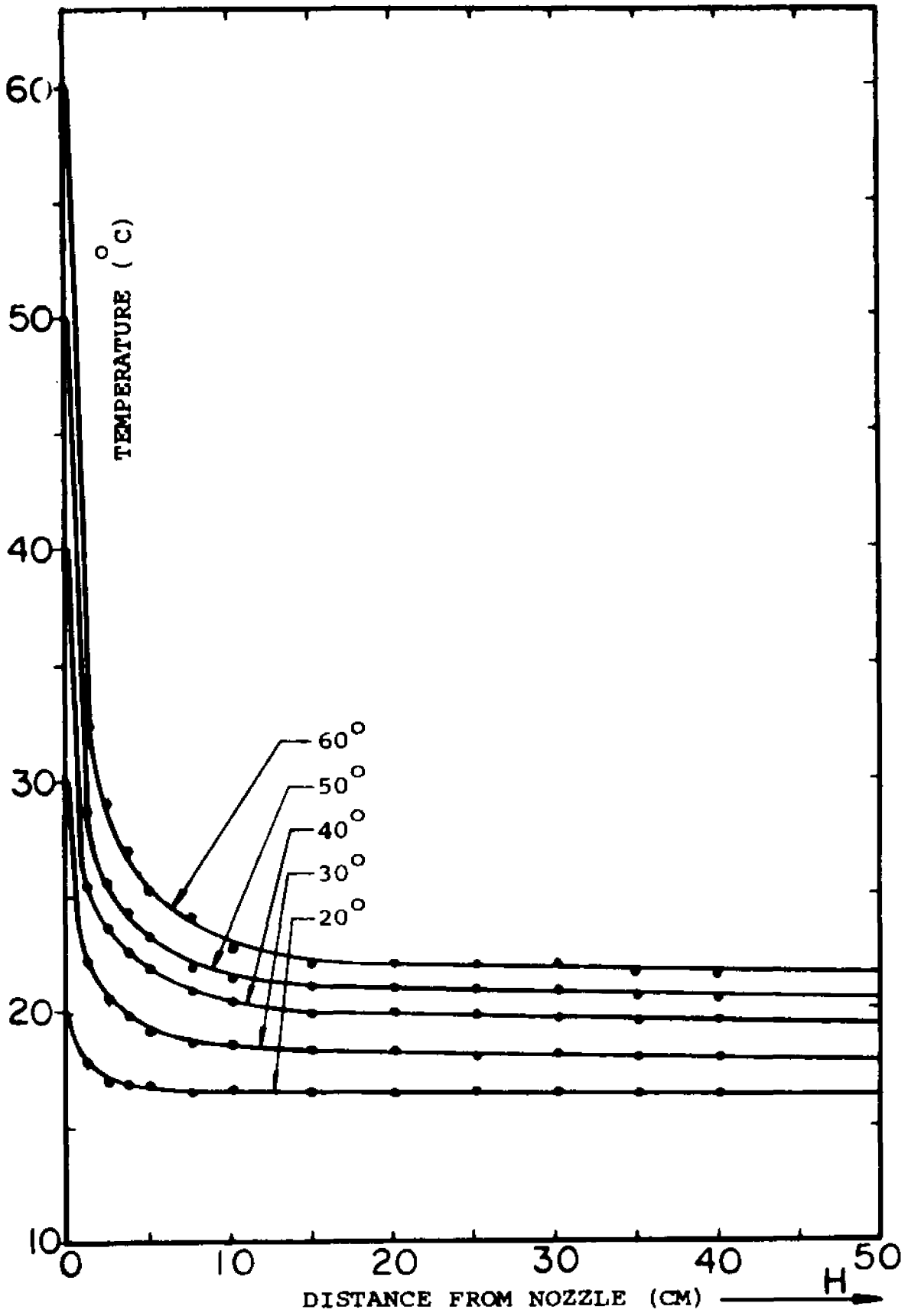

FIG.E8. TEMPERATURE CHANGE ALONG JET AXIS
Comparison of Temperature Distribution for Various Jet Temp's.
Rate of Flow is 0.37850 L/Min.

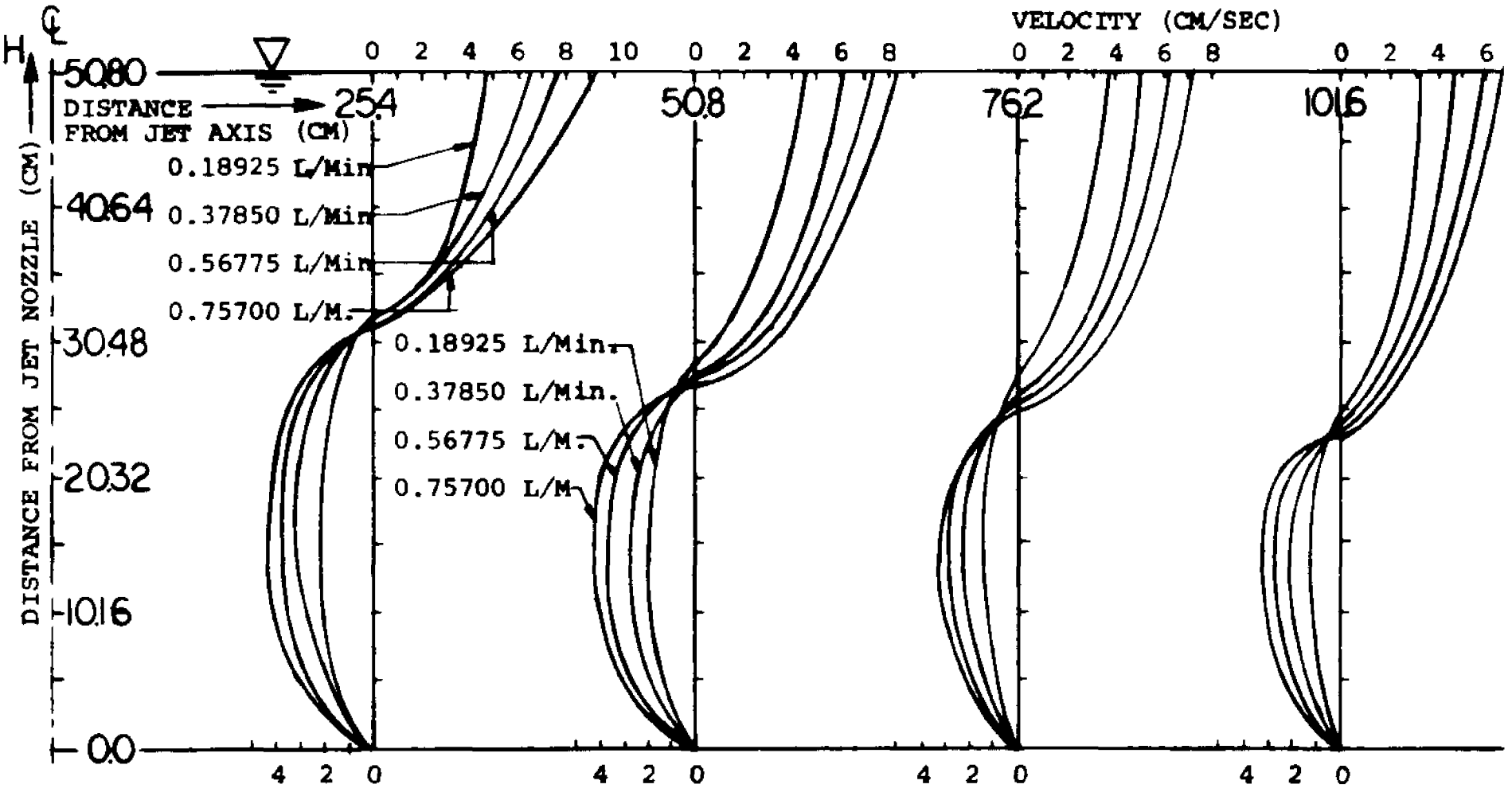

FIG.E9. FAR FIELD - VELOCITY DISTRIBUTION

Comparison of Velocity Distribution Profiles for Various Discharge Rates

Entering Jet Temperature 30°C

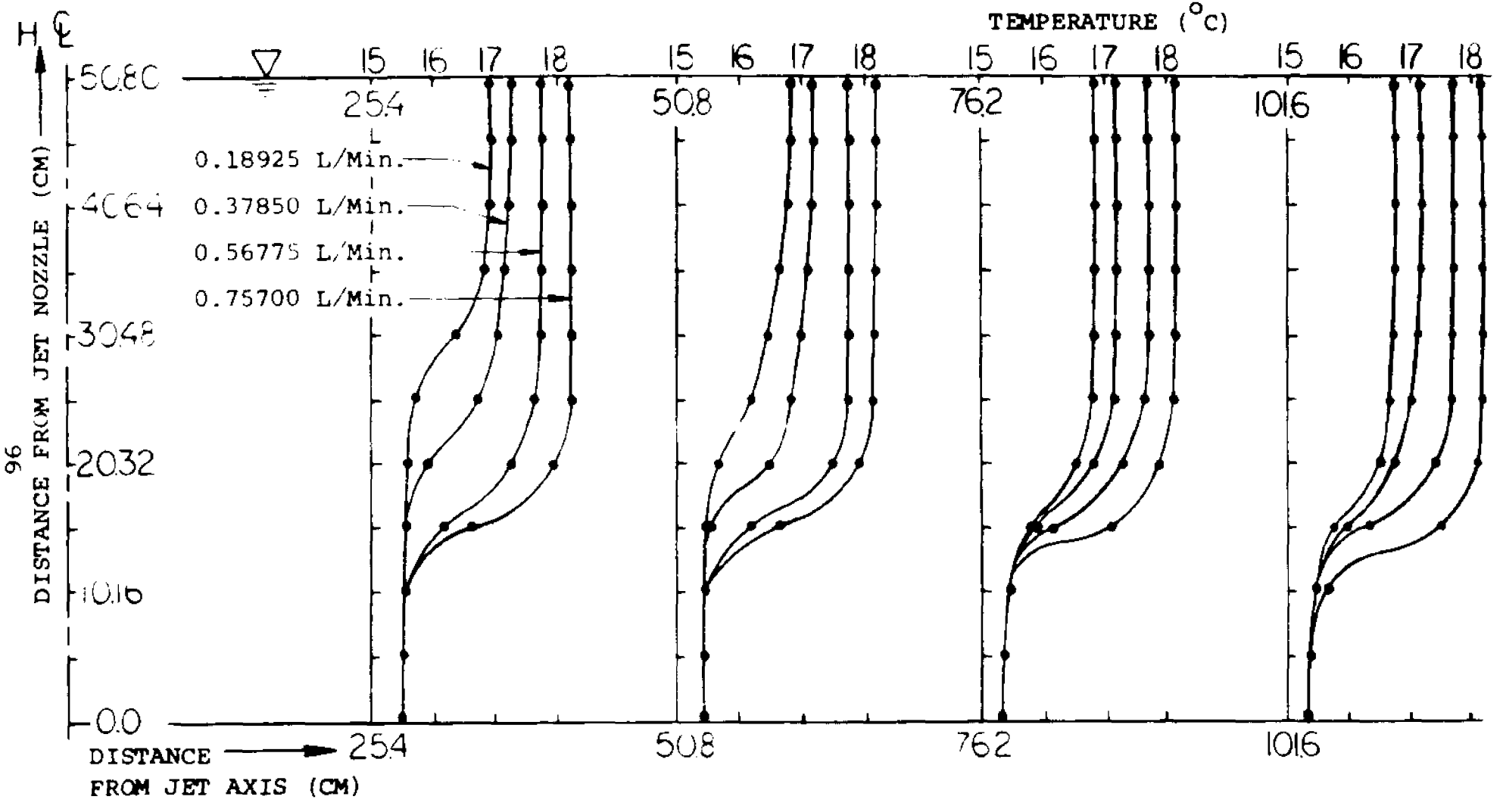

FIG.E10. FAR FIELD - TEMPERATURE DISTRIBUTION

Comparison of Temperature Distribution Profiles for Various Rates of Flow Entering Jet Temperature 30°C.

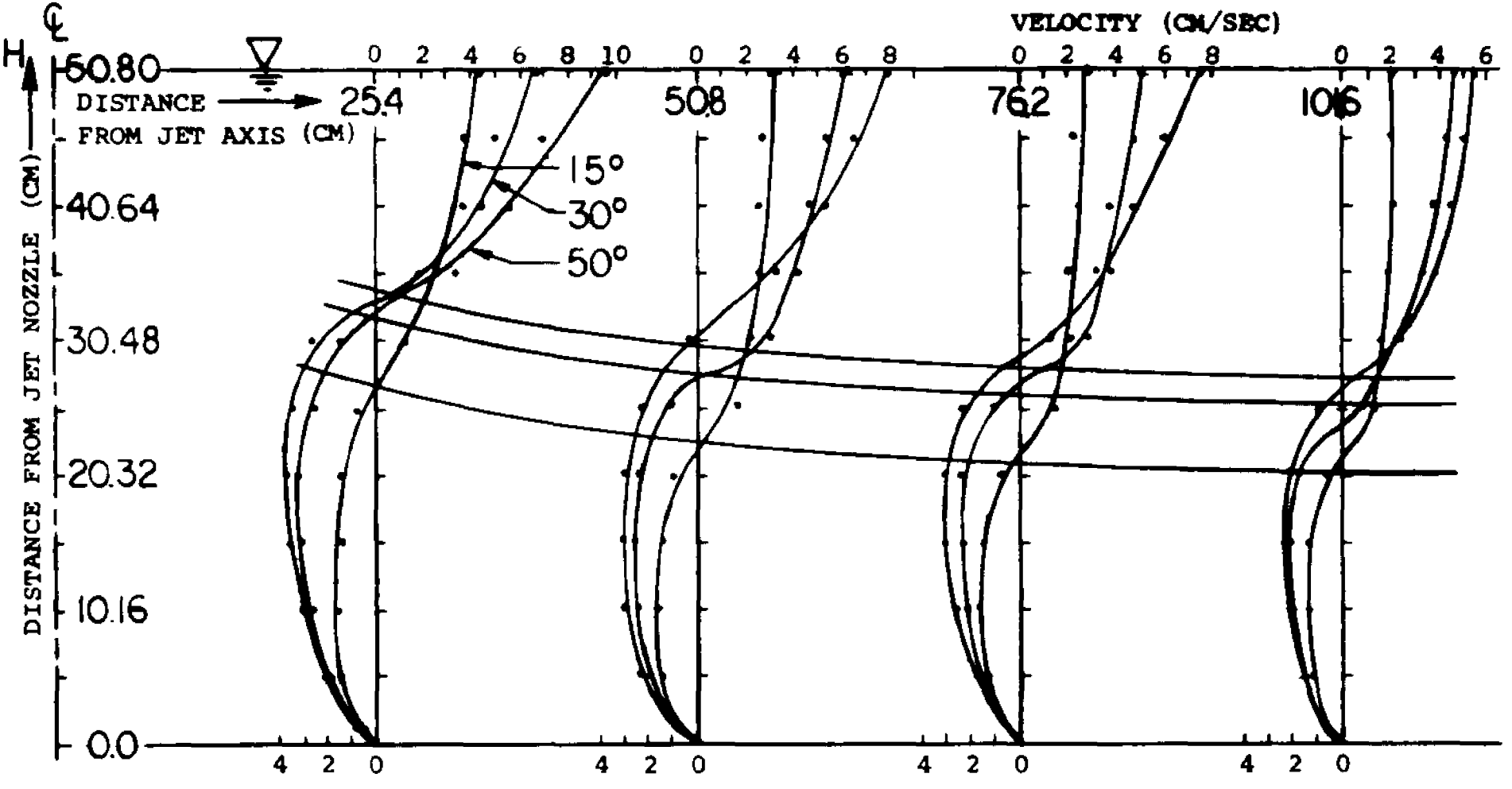

FIG.E11. FAR FIELD - VELOCITY DISTRIBUTION

Comparison of Velocity Distribution Profiles for Various Jet Temperatures

Rate of Flow is 0.37850 L/Min.

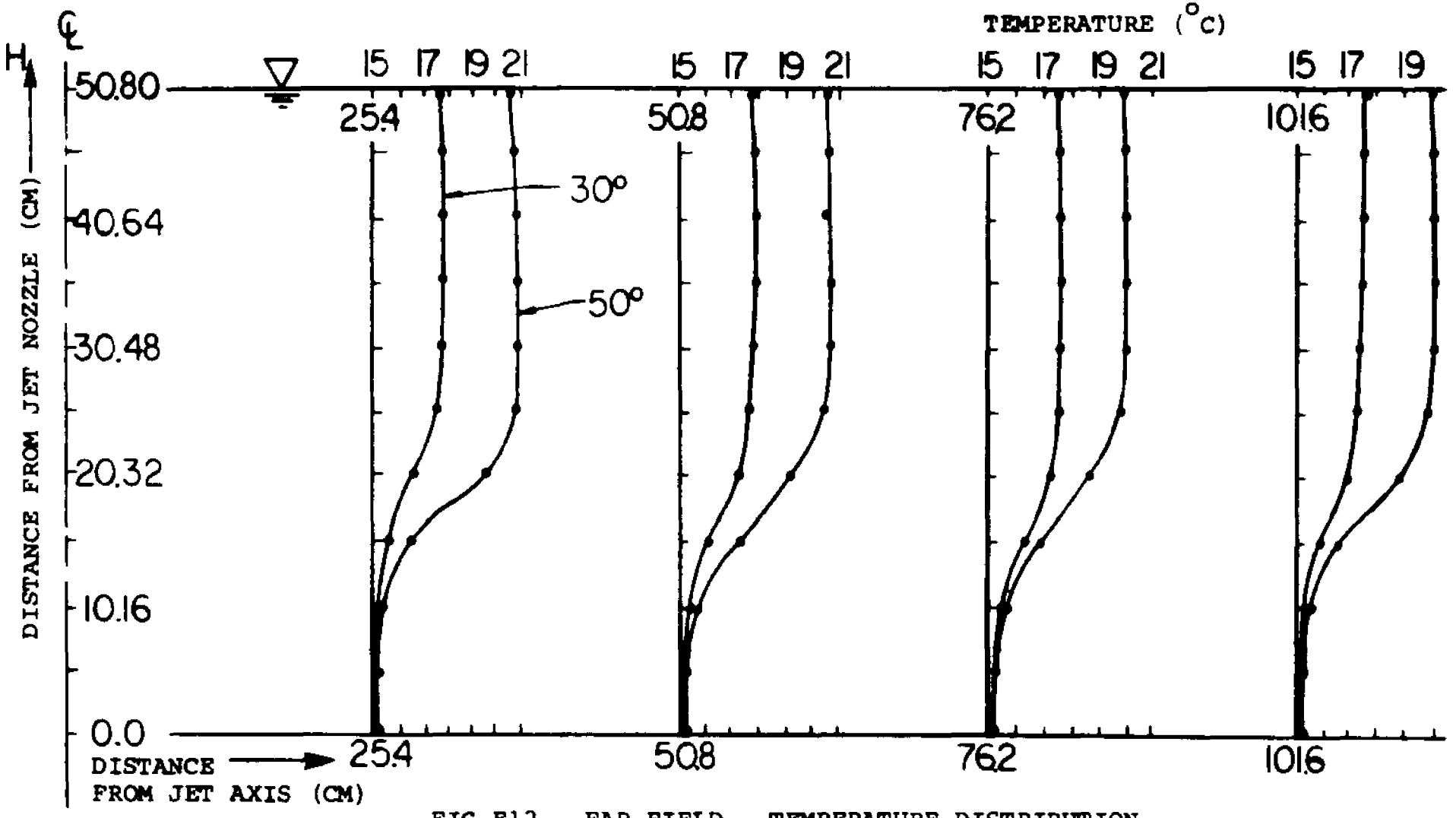

FIG.E12. FAR FIELD - TEMPERATURE DISTRIBUTION

Comparison of Temperature Distribution Profiles for Various Jet Temperatures

Rate of Flow is 0.37850 L/Min.

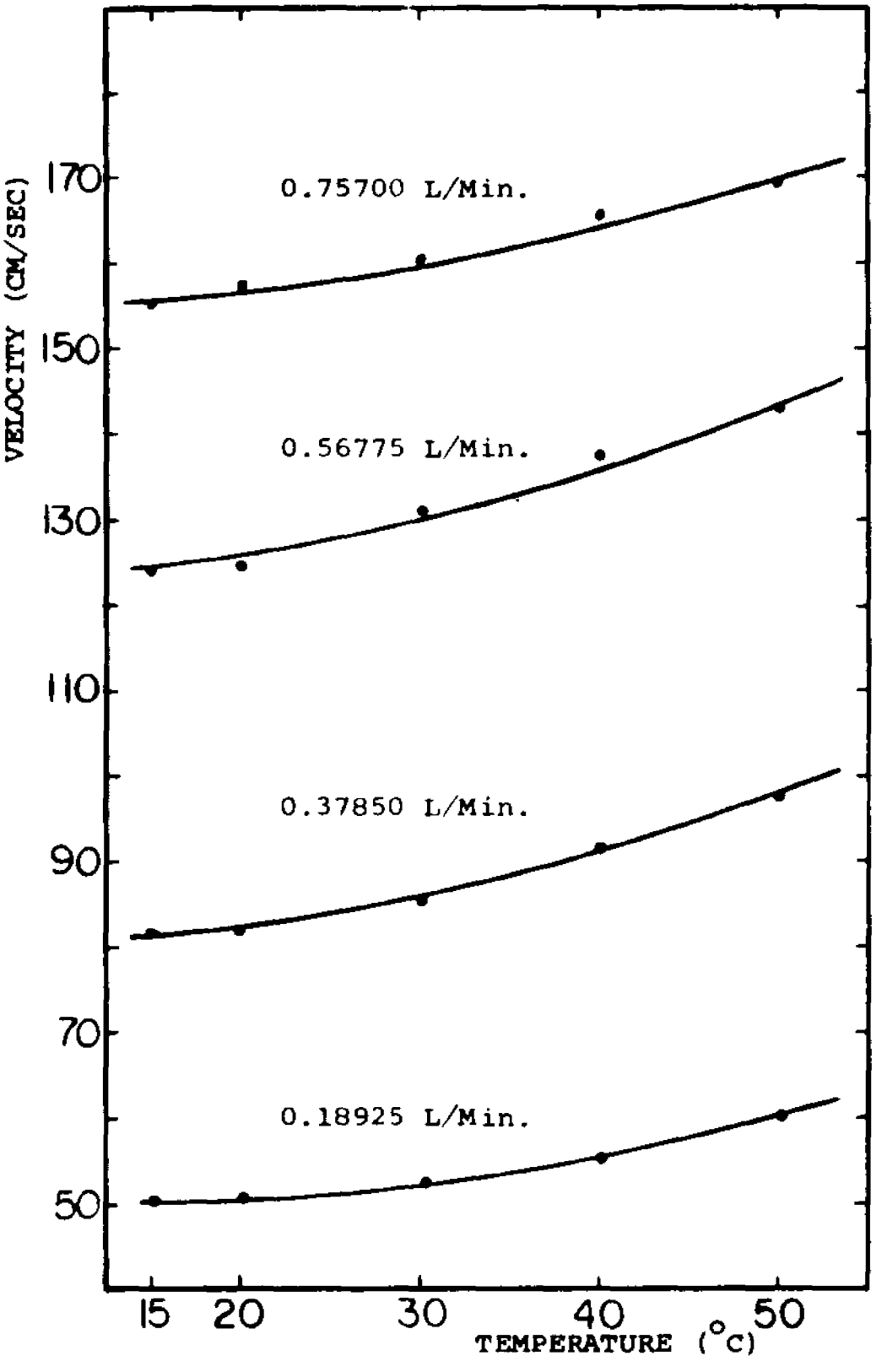

FIG.E13. ENTRANCE VELOCITY AS FUNCTION OF ENTRANCE TEMPERATURE (FOR VARIOUS RATES OF FLOW)

The analysis of the experimental data can be summarized as follows. The entire flow area can be divided into two regions, each with different characteristic features. The vertical flow covers the vicinity of the jet axis and the horizontal flow spreads over the far field.

All investigated jets at any rate of flow and any temperature at the nozzle were strongly turbulent. The turbulent field covered the entire vertical jet region and the initial part of the horizontal spread.

With no large temperature, or velocity gradients to generate turbulence in the horizontal spread, the gradual decay of its intensity was observed. Thus, with an exception of the initial region adjacent to the jet axis, the far field was laminar.

The intensity of turbulence and the size of the turbulent portion were related to the temperature of the discharge and the rate of flow.

Let us proceed with a detailed evaluation of the data in the two regions, starting with the area adjacent to the jet axis.

Near Field - Vertical Jet Region

The jet boundaries determined by the velocity and temperature profiles coincided closely in the initial part of the jet area. This was due to the high velocity of the flow, and negligible conduction in comparison with convection. Farther away, however, from the jet nozzle, the thermal region was significantly greater than the velocity region. This resulted from the fact that conduction and local mixing were of a comparatively large magnitude while the velocity was small.

From the investigation of velocity profiles for various rates of flow it was concluded that the length of the zone of flow establishment was in proportion to the rate of flow.

Analyzing the velocity distribution in the vertical jet (Fig. E1, E3) we can evaluate the impact of the rate of flow on velocity at constant discharge temperature. When the rate of flow is kept constant, jet velocity is a function of temperature difference. It is apparent that the impact of buoyancy force on jet velocity is of the same order of magnitude as inertia force (compare Fig. E1. and E5.).

An interesting phenomenon takes place in the close vicinity of the jet nozzle along the axis when axial velocity drops for various temperatures are compared (Fig. E7). The jets of a higher initial velocity (and entrance temperature) experience a faster velocity drop initially. Later their velocity drop is slower than those of lower initial velocity (and temperature). This results in the double intersection of velocity distribution profiles on the axis in some cases as illustrated on Fig. E7. Apparently this development is due to a very high entrainment of cold water from the ambient.

The high entrainment results from a large velocity gradient. The gradual impact of the buoyancy force slows down the axial velocity drop.

A change of temperature for any entering jet (when rate of flow is kept constant) results in another interesting phenomenon. Jet velocity atthe nozzle increases as the hot water temperature is raised (Fig. E5, E6). Since the amount of hot water supplied to the nozzle does not change, the increase in velocity is possible only by the contraction of the area of the jet flow. This process is illustrated below.

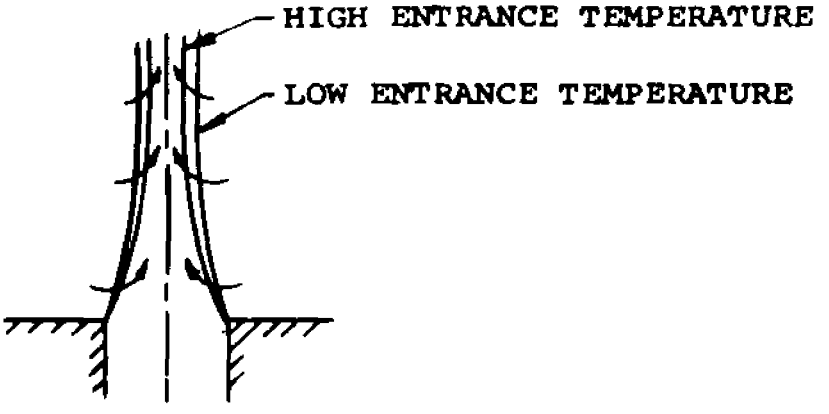

Fig. 17 .Jet Cross-section at the Nozzle vs Temperature Change

The sum of inertia and buoyancy forces will be greater as the temperature is increased (the inertia force is kept constant, since there is constant rate of flow). And so, to accommodate greater velocity and satisfy continuity of the flow there is an apparent narrowing of the jet cross-section.

The temperature profiles are tied with the velocity profiles although not in the way that is assumed by many theoretical investigators. The velocity and temperature profiles are not similar. As it can be seen on Fig. E2 and Fig. E6. the temperature profiles change shapes and get flattened out faster than the velocity profiles.

That is apparently due to thermal conductivity, which increases heat dissipation, and local mixing. Very rapid temperature drop on the axis over a very short distance from the nozzle was observed (Fig. E4 and E8). This is a result of very large entrainment of the cold water from the ambient.

Far Field

The structure of the steady, two-dimensional flow was investigated over the entire cross-section of the tank that is, from the bottom to the water surface.

As mentioned ealier, the horizontal flow field was laminar with some turbulence mostly in the region close to the jet axis. Of particular interest is an interaction between the velocity layer and thermal layer. The velocity layer is also interacting with the flow of ambient water that is entering the jet.

The velocity layer grows in depth as the distance from the jet area increases (Fig. E9 and E11). The growth of layer thickness gradually levels off, as the initial momentum is dissipated and the entrainment of the ambient water into the layer becomes smaller. The thickness of the layer depends on temperature. With the increase of the temperature of the entering jet (at a constant rate of flow) the velocity layer thickness decreases. This fact simultaneously results in in the increase of the magnitude of velocity in the layer since the discharge rate does not change.

The large entrainment of ambient water into the jet results in a development of a negative velocity field in tne lower region of the flow. Again, the higher jet temperature (at the same rate of flow) results in a higher entrainment rate and subsequently in a larger magnitude of velocity in the lower (negative) velocity region. Although it is not obvious from the graphs of the velocity profiles, the region separating the positive velocity field from the negative velocity field is very unstable with large fluctuations of velocity magnitude and direction.

Following the shapes of the velocity profiles it is possible to determine the approximate boundaries of the velocity layer for various temperatures of an entering jet, or for various rates of flow, as it is shown on Fig. E9. and Fig. E11.

It is not possible to make a direct comparison of the effect of the rate of flow, versus that of the temperature of the entering jet, on the velocity layer thickness. But it can be observed quantitatively that increasing the temperature of the entering jet by e.g. $10^{o}C$ has a similar impact on the change in the velocity layer thickness as does doubling the rate of flow (Fig. E11. and E12.). The fact that the temperature changes make such a strong effect on the formation of a velocity layer shows the importance of the buoyancy force on the structure of a thermal layer.

Temperature profiles in the far field (Fig. E10. and E12.) are very different from the velocity profiles (Fig. E9. and E11.).

As mentioned earlier the thermal layer is far greater in depth than the corresponding velocity layer. Its thickness is directly proportional to the rate of flow, although this relationship is not linear.

The fact that the thermal layer is greater in depth than the velocity layer (compare Fig. E10 and E12, with E9 and E11) is of significant importance because the thermal layer overlaps the lower (negative) velocity region. This means, subsequently, that the entraining fluid will not entirely be a cold ambient water, but will be a mixed water of higher temperature (than the ambient) particularly in the upper portion of the jet. This results in an additional increase of temperature in the thermal layer until an equilibrium is reached.

The thermal layer is stable at a sufficiently far distance from the jet area. There is, however, an apparent instability in the area that is close to the jet axis. Investigating the temperature profile at the cross-section which is closest to the jet axis we can see (Fig. E10 and E12) that the temperature at the surface is actually lower than the temperature below, which seems to contradict the influence of the buoyancy force and introduces instability to the flow. This phenomenon can be explained by a visual observation of the jet and is illustrated below.

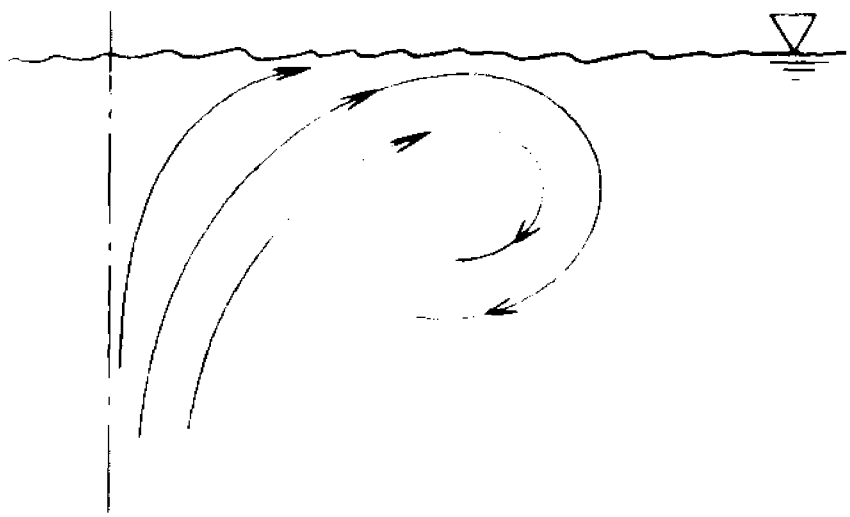

Fig. 18. FLUID MOTION IN THE INITIAL REGION OF HORIZONTAL SPREAD

The excess of velocity on the jet axis at the surface results in a vortex motion and because of that the fluid with highest temperature (and velocity) is turned downward. As we move away from the jet axis, stability is reached by a combination of mixing and buoyancy force.

The temperature drop along the water surface measured from the jet axis was rather small. The largest portion of the drop takes place over the initial section of the thermal layer.

Changes farther away from jet area were very insignificant. This can be explained by the fact that the initial drop is most likely a result of high mixing and convection in that region. In the distant area of the flow temperature decreases only through conduction and radiation. The changes amounted to a few tenths of a degree Centigrade at the most. The distance was too short, and the temperature variation too small, to obtain a meaningful evaluation of the recorded data.

For deep discharges the process of flow development is rather simple. Hot water leaves the nozzle, then mixes with the cold ambient and reaches the surface (due to the combination of inertia and buoyancy force). Then, it spreads in the lateral direction. The vertical velocity component at the surface is usually small due to viscous and turbulent dissipation over a long distance. The excess vertical velocity at the surface produces a rather insignificant downward motion. There is a limited vortex motion as well as limited mixing process. The thermal layer is formed on the reservoir surface and its thickness depends on the earlier mentioned flow parameters.

The case of shallow discharges introduces more possibilities. In one instance, with rather small discharge velocities, the process is similar to the deep discharge case. If, however, the initial velocity of the jet is of a large magnitude, the flow field may be quite different. A free surface region may be analyzed from a conservation of energy point of view. The excess vertical velocity at the surface gets converted into potential energy of elevation which creates a "hump" above the water surface. Then, in turn, due to the gravity force, the mass of flow is directed downward and sideways, creating a very large vortex motion. The higher the "hump", the stronger the vortex. In some instances of a large enough entrance velocity, (and small depth of reservoir) the vortex motion is able to reach the bottom.

The diagrams picturing the velocity fields are presented together, for comparison of the extreme cases, on the next page.

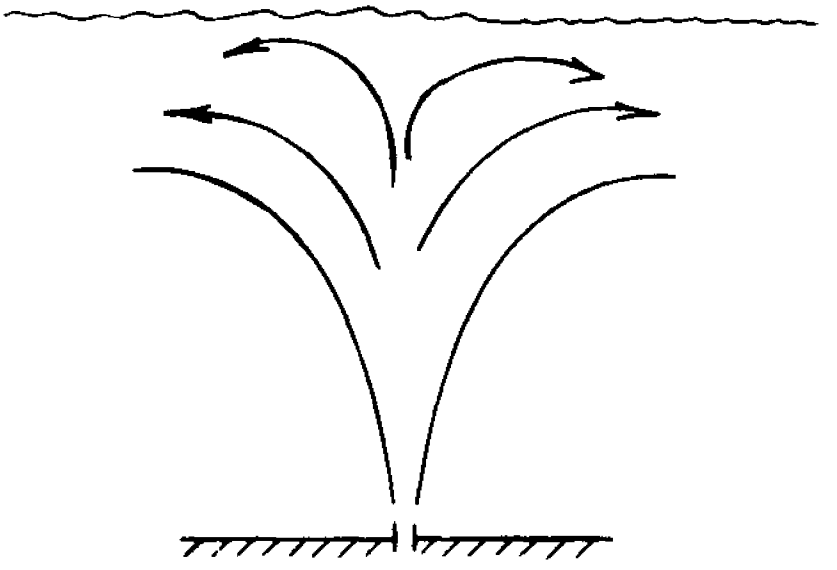

Fig. 19. FLOW PATTERN - DEEP DISCHARGE

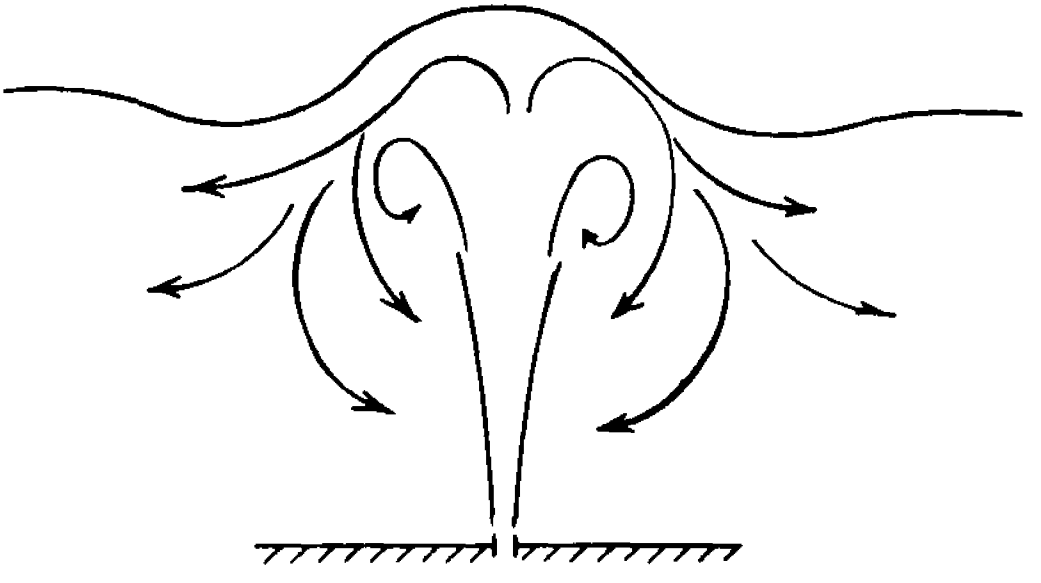

Fig. 20. FLOW PATTERN - SHALLOW DISCHARGE

The more detailed analysis of the free surface structure will be discussed in the next section of this chapter.

2. SHALLOW AND BORDER CASE DISCHARGES

Shallow discharges are investigated in this section. Experimental data accumulated for various flow conditions and numerical solutions are presented. The light technique described earlier was applied and the photographs provided information on the jet boundaries, as well as, the shape and size of the thermal layer.

As it was pointed out already, the flow pattern and the temperature distribution for the thermal jets (in a stationary, not stratified environment) depends on three parameters, namely, the velocity of the discharge, the depth of the reservoir and the size of the discharge nozzle. Depending on the temperature difference between the jet and the environment, the buoyancy force may also be of certain importance.

The detailed analysis of the jet flow and formation of the thermal layer was thoroughly discussed in the section on deep discharges. On the following pages, the differences in the flow structure and additional characteristics of the thermal discharges will be pointed out. There is no point in repeating the material which pertains equally to all kinds of jets.

At first, a thermal discharge with the ratio of depth to nozzle size, 5:1 was considered. Discharges with two different velocities were investigated and the photographs of various stages of flow development presented. In both cases it could be observed that the thermal layer increases in its thickness so far that after a certain interval of time, it will spread from top to bottom. With the passage of time, the temperature becomes uniform (equal to the discharge temperature) since all the cold water gets gradually replaced by hot. Then, since there is no temperature change in the entire field, the velocity distribution is the same as that of a simple jet (there is no buoyancy force) for a steady flow case.

Therefore, only the data on the velocity distribution were accumulated. The numerical solution likewise provides a velocity distribution for a steady case since temperature becomes uniform throughout. The photographs on the next few pages show the development of thermal region and the graphs provide velocity profiles for the same flow conditions.

After 30 sec.

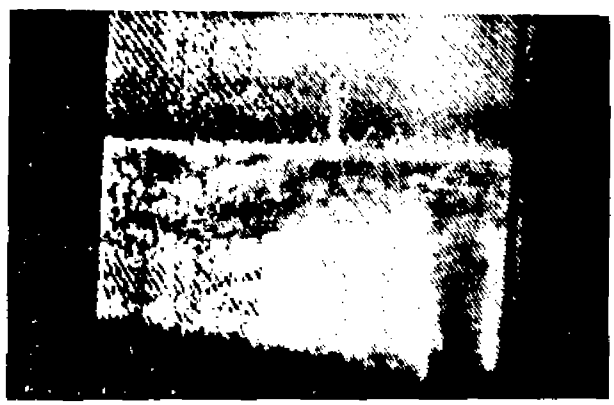

After 1 min.

After 3 min.

Fig. P1. JET AND THERMAL LAYER FORMATION - AS A FUNCTION OF TIME

Rate of Flow	0.56775 L/Min.	Ambient Temperature	$15^{o}C$
Depth of Reservoir	10 cm.	Entering Jet Temperature	$30^{o}C$
Nozzle Size	1.9 cm.		

Time measurement is from the moment the discharge nozzle was open.

After 30 sec.

After 1 min.

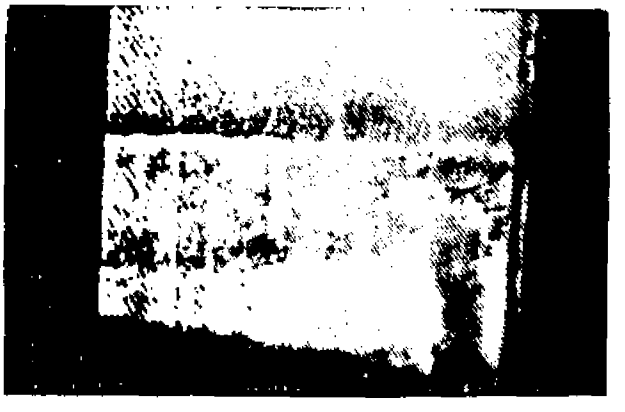

After 3 min.

Fig. P2. JET AND THERMAL LAYER FORMATION - AS A FUNCTION OF TIME

Rate of Flow	0.75700 L/Min.	Ambient Temperature	$15^{o}C$
Depth of Reservoir	10 cm.	Entering Jet Temperature	$30^{o}C$
Nozzle Size	1.9 cm.		

Time measurement is from the moment the discharge nozzle was open.

In the next case, the nozzle size was reduced by half to 0.31cm. where the rate of flow and the depth were kept the same. This resulted in the entrance velocity being two times higher than previously. The flow pattern changed considerably as can be noticed on the photographs on the next page. Visual observation of the flow structure proved to be difficult in this case but the computer investigation provided additional details about the temperature and the flow development. The excess vertical velocity at the surface was turned downward (some of it sideways) which brought hot water from the surface to the bottom. Complete mixing resulted and then this warm water started to spread in the lateral direction. The photographs presented on the next page show the temperature field development at a few time intervals. For the reason mentioned above there are no visible boundaries between the hot and cold regions. There is also no visible difference with the passage of time due to a very thorough mixing which results in a very gradual temperature change.

There is no point in presenting either the experimental data on velocity and temperature distributions or a numerical solution for a steady case. The temperature is uniform since all the cold water gets gradually replaced by hot water. Then, since there is no temperature change in the entire field, the velocity distribution is the same as that of a cold jet in a cold environment (for a steady case).

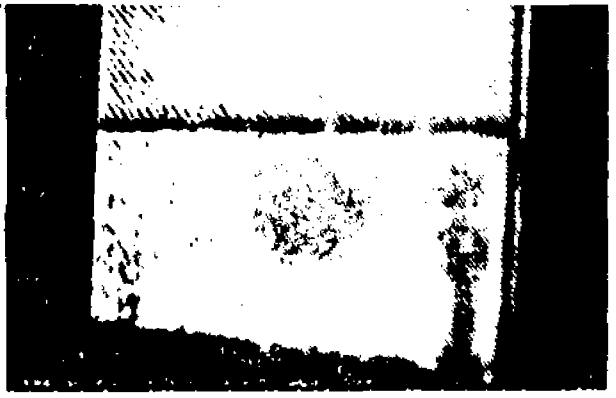

After 30 sec.

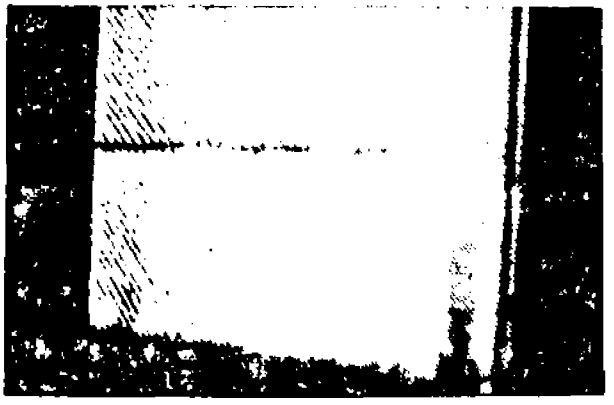

After 1 min.

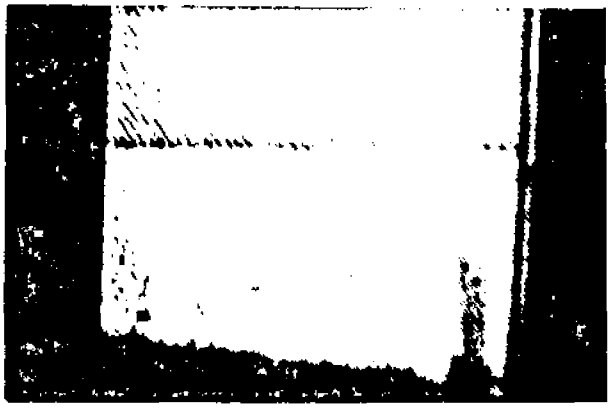

After 3 min.

Fig. P3. JET AND THERMAL LAYER FORMATION - AS A FUNCTION OF TIME

Rate of Flow	0.75700 L/Min.	Ambient Temperature	$15^{0}C$
Depth of Reservoir	10 cm.	Entering Jet Temperature	$30^{0}C$
Nozzle Size	0.31 cm.		

Time measurement is from the moment the discharge nozzle was open.

Proceeding to another range of discharges, the ratio of depth to nozzle size is 16:1. The rate of flow is kept the same as in the previous instances for shallow discharges. The flow structure here is now more similar to the deep discharges. The thermal layer is formed near the water surface The cold region below the thermal layer is the source of entrainment of ambient water to the jet and therefore it has a direction toward the jet axis.

The photographs of the thermal field presented here are of the same discharge rate but of different depth of reservoir and they are shown on Fig.(E15) through (E22).

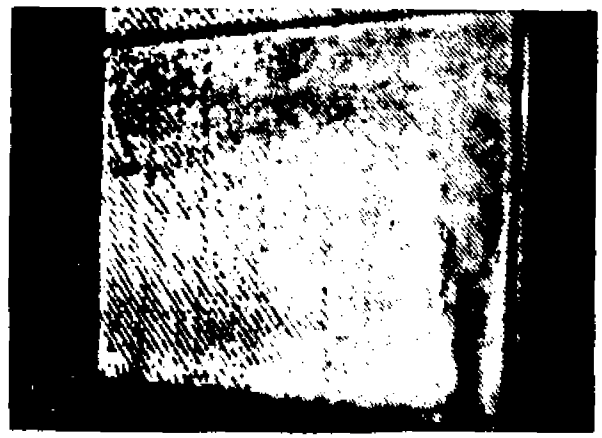

Depth of Reservoir 20 cm.

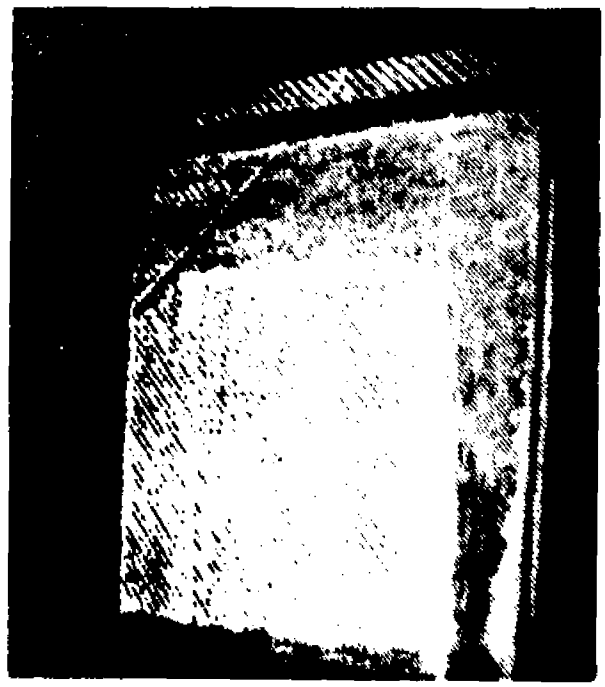

Depth of Reservoir 30 cm.

Fig. P4. JET AND THERMAL LAYER FORMATION - STEADY FLOW PATTERN

Rate of Flow	0.75700 L/Min.	Ambient Temperature	$15^{o}C$
Nozzle Size	1.25 cm.	Entering Jet Temperature	$30^{o}C$

Let us start with an analysis of the velocity and temperature at the jet axis. Both experimentally and numerically, it can be observed that velocity of the thermal jet is due apparently to the impact of the buoyancy force. The velocity and temperature decrease is much smaller here than in the deep discharge case. The fact that the turbulence is of much lower magnitude results in smaller mixing and diffusion and consequently in slower dissipation of energy and thermal energy.

When the velocity is investigated along the jet axis for shallow discharges we can notice that there is a very slow velocity decrease in the area close to the jet nozzle and then a much faster velocity drop farther away from the nozzle. For comparison, in case of a deep jet a rapid velocity drop is immediate. This phenomenon is explained by the existance of a potential core (corresponding to the earlier described region of flow development). The potential core is quite significant in the case of shallow discharges and preserves the entrance velocity from the impact of mixing and entrainment fluid. Since the nozzle for deep discharges was 1mm. in size and the flow was very turbulent it was difficult to observe the presence of the potential core and its impact on the flow characteristics.

3. FREE SURFACE FORMATION

In addition to the experimental data about the velocity and temperature fields, the formation of the shape of water surface directly above the discharge nozzle was investigated.

Depending on the relation between the three parameters, that is, velocity of the discharge, size of the discharge nozzle and the depth of reservoir, the free surface may form a "hump" in the place of discharge. This "hump" is of no concern for deep water discharges. The turbulent and viscous dissipation is sufficient to reduce the vertical velocity component to a negligible value. For shallow discharges, however, the "hump" formed on the water surface may be of considerable height.

The elevation of the surface was measured for various ratios of nozzle size to depth. As was mentioned earlier, the presence of the "hump" has a very serious impact on the flow pattern. In the following pages experimental and numerical results are presented. The rate of discharge (or entrance velocity) was kept constant to define the dependence of elevation of water surface on discharge velocity and depth. The shape of the free surface, as it was evaluated on the computer, is superimposed on the photographs of the free surface.

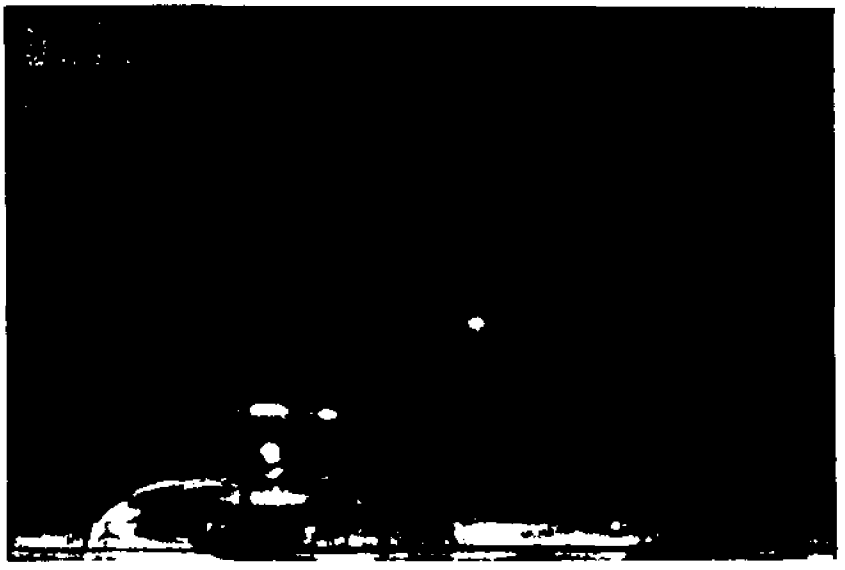

Fig. P5. FREE JET

Rate of Flow 0.75700 L/Min.
Nozzle Size 1.25 cm.
Grid Size 5cm. x 5cm.

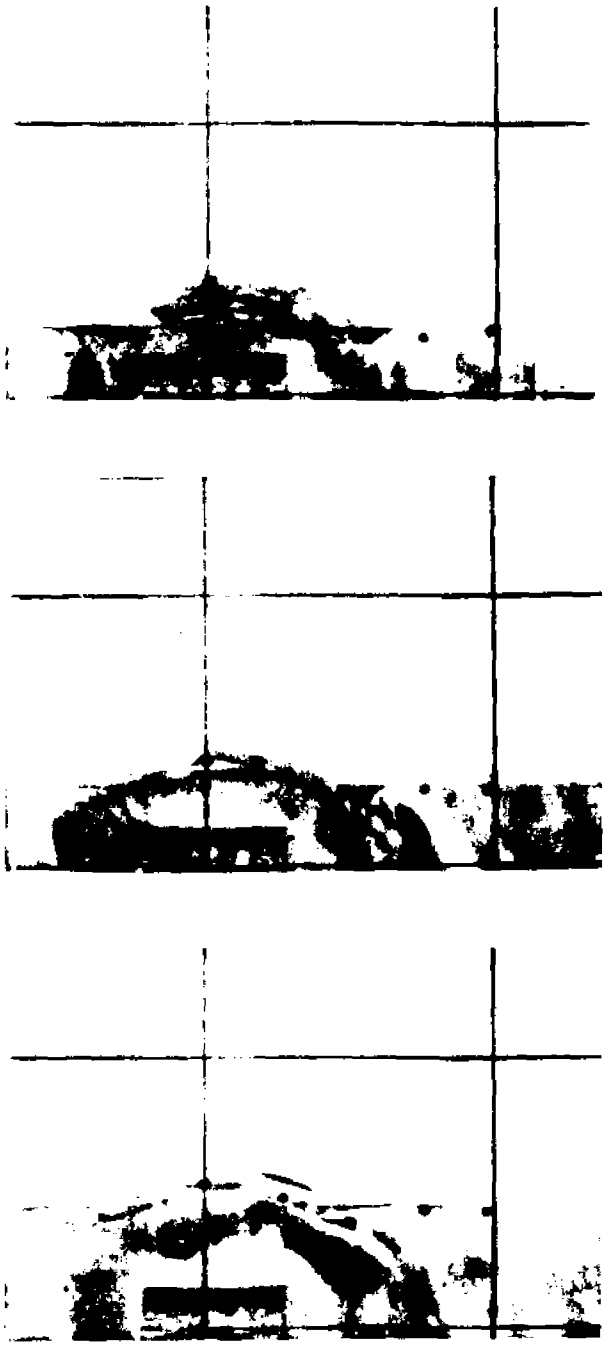

Fig. P6A. FREE SURFACE FORMATION - AS A FUNCTION OF DEPTH

Rate of Flow 0.66250 L/Min.
Nozzle Size 1.25 cm.
Grid Size 5cm. x 5cm.

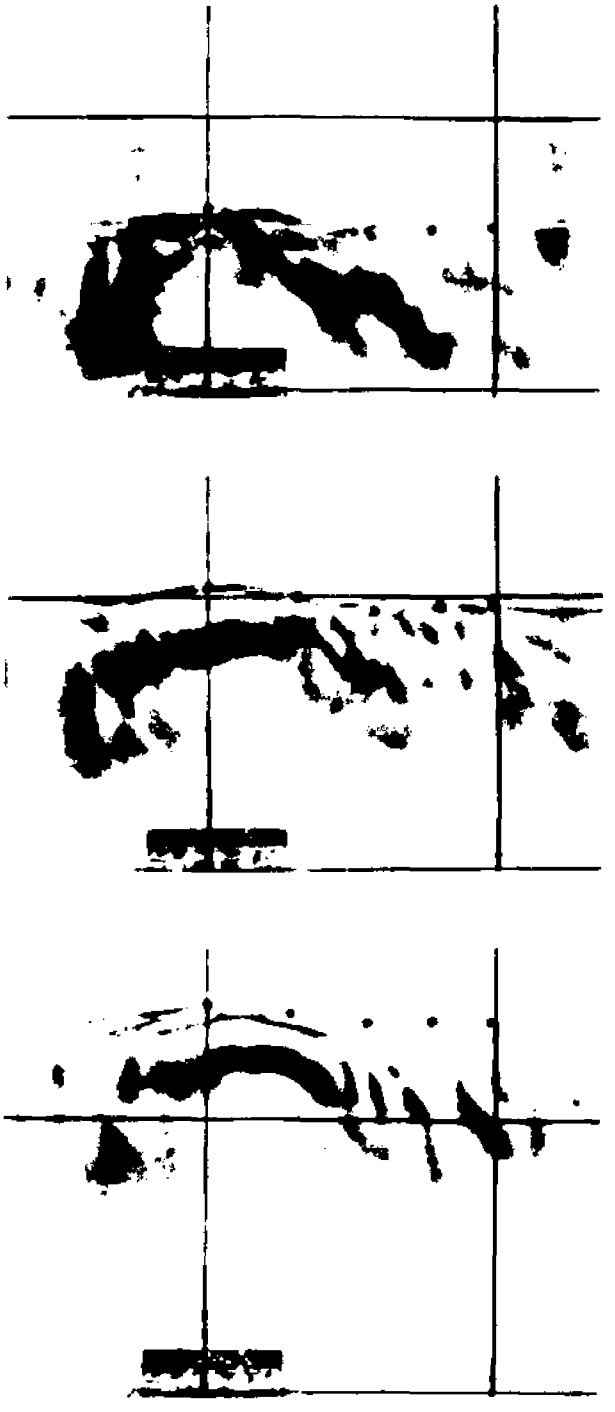

Fig. P6B. FREE SURFACE FORMATION - AS A FUNCTION OF DEPTH

(Continuation of P6A.)

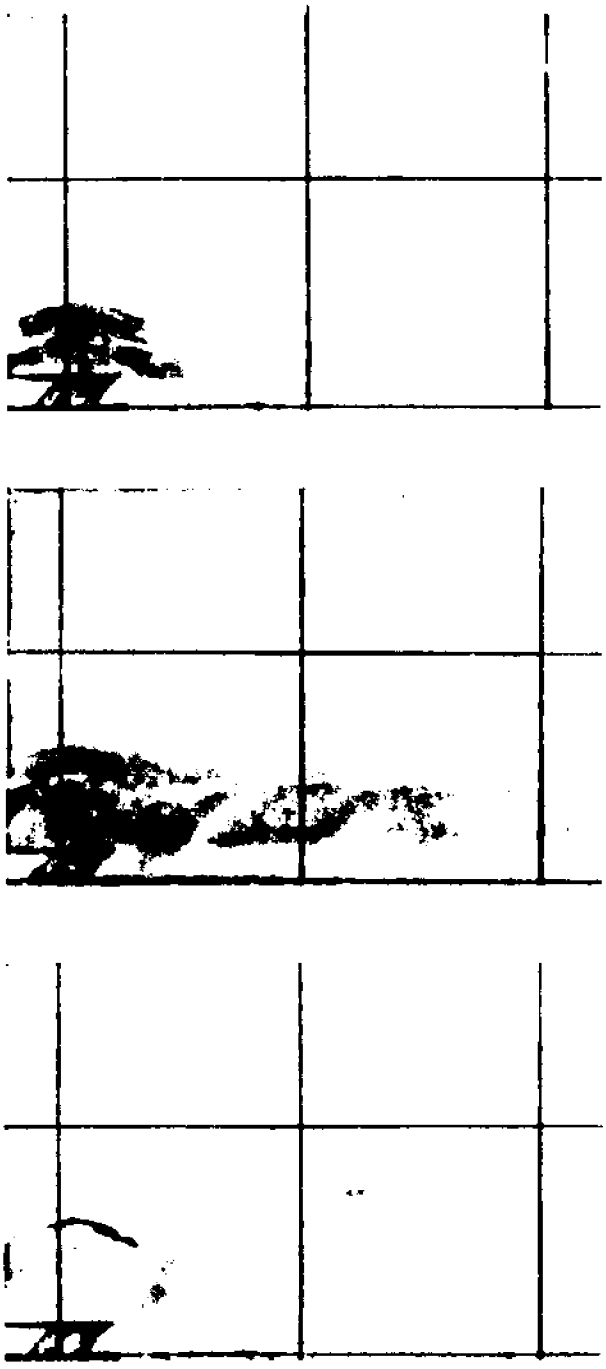

Fig . P7A. FREE SURFACE FORMATION - AS A FUNCTION OF DEPTH

Rate of Flow 0.75700 L/Min.
Nozzle Size 1.25 cm.
Grid Size 5cm. x 5cm.

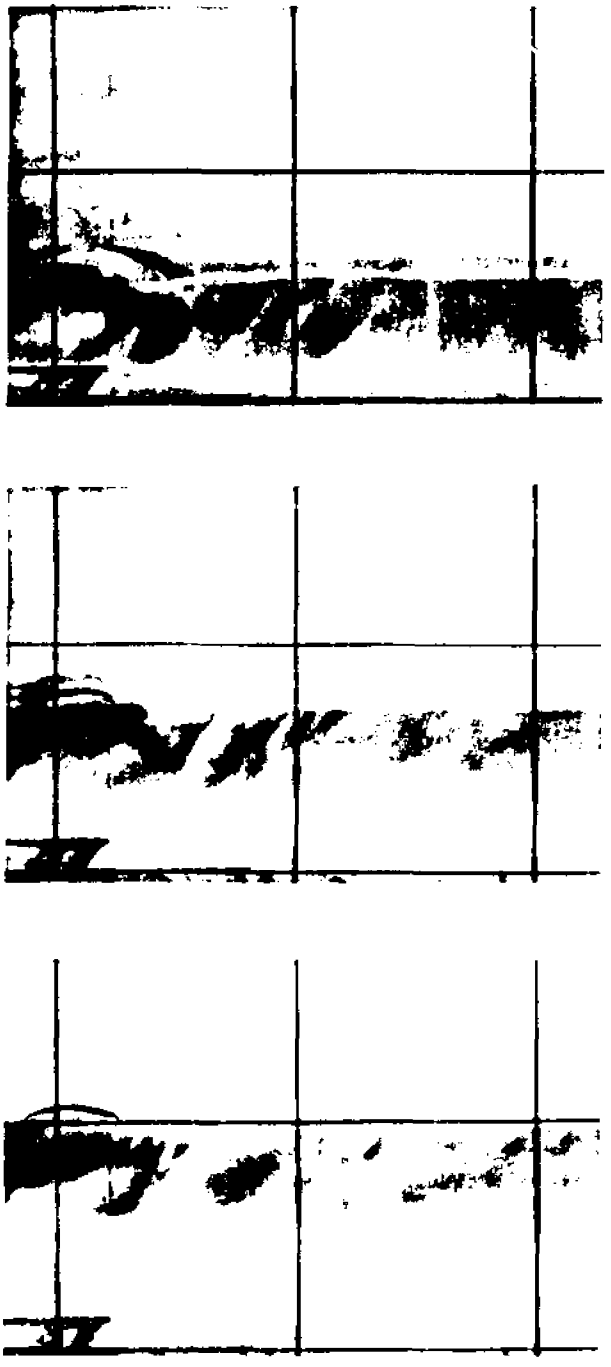

Fig. P7B. FREE SURFACE FORMATION - AS A FUNCTION OF DEPTH

(Continuation of P7A.)

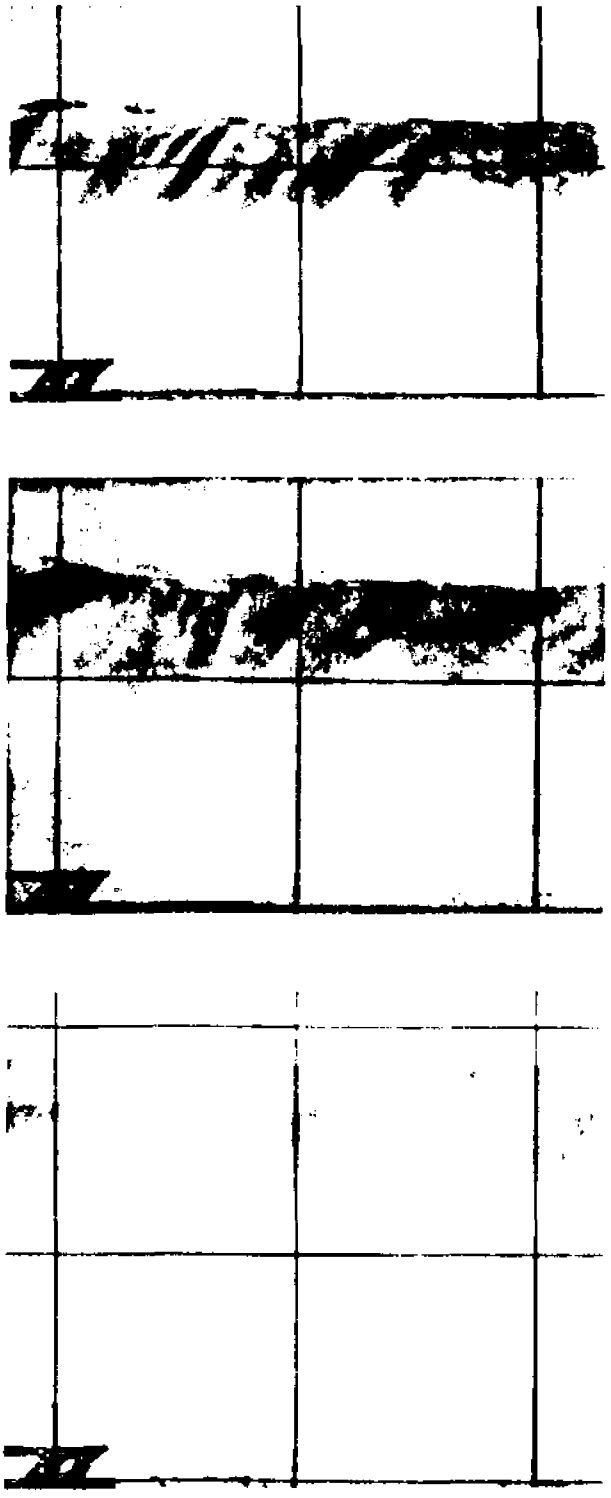

Fig. P7C. FREE SURFACE FORMATION - AS A FUNCTION OF DEPTH

(Continuation of P7B.)

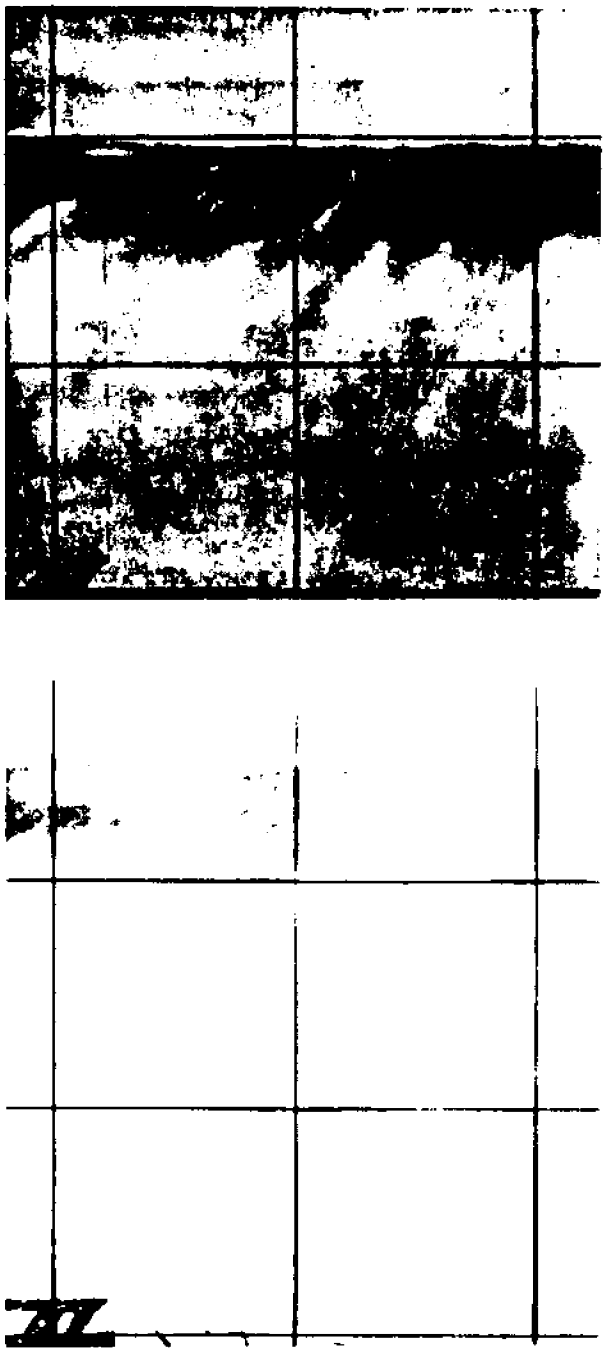

Fig. P7D. FREE SURFACE FORMATION - AS A FUNCTION OF DEPTH

(Continuation of P7C.)

As expected, the elevation of free surface is in inverse proportion to the tank depth, although, it should be pointed out that this relation is not linear.

There is a gradual decrease of the elevation of the free surface and when the ratio of the jet nozzle to the tank depth is 1:10 or less, the water surface becomes almost flat.

Summary

There is a very rapid drop of temperature and velocity along the jet axis in the area immediate to the jet nozzle. This is the result of a high turbulence level and a large entrainment of the ambient fluid. With the increase of the entrance velocity or temperature, there is an increase of velocity and temperature gradients along the jet axis.

The investigation of the relationship between the jet temperature and initial momentum shows that buoyancy force is a significant factor in the magnitude of velocity value. Its impact is stronger for the flows with low entrance velocities (rate of flow 0.18925 L/Min.) where an increase of temperature by $35^{o}C$ yielded up to a 20% rise in velocity. The same temperature difference for a higher rate of flow (0.75700 L/Min.) increased velocity by about 8%.

The observation of the far field shows that the thickness of the thermal layer depends on the temperature of the discharge (higher temperature results in a thinner thermal layer). The temperature of the thermal layer is related to the discharge velocity (mixing) where an increase of velocity results in the lowering of the temperature of the thermal layer.

In contrast, the buoyancy force is far less significant for shallow discharges where the impact of momentum prevails. Mixing, vortex motion and also the thermal layer take much larger portion of the field. In extreme cases it may result in the elimination of entrainment of any ambient fluid into the jet. In certain conditions, temperature may become uniform from top to bottom without any appreciable gradient. The drop in velocity, or temperature, on the jet axis is much smaller than for the deep discharges. This apparently resulted because of the size of the potential core which is proportionally much larger in the shallow discharges.

The elevation of the free surface depends on the jet entrance velocity and also the depth of reservoir and the size of the discharge nozzle. This elevation may be of considerable magnitude if the discharge is very shallow and then it will have a strong impact on the structure of the flow (vortex motion). With an increase in depth, relative elevation of the free surface gradually becomes negligible.

V. NUMERICAL RESULTS AND THEIR COMPARISON WITH EXPERIMENTS

In this chapter numerical results are discussed. The earlier developed finite difference equations with appropriate initial and boundary conditions were solved on the computer for a variety of flows.

In the first part, the numerical results are compared with the experiments. The graphs representing numerical solutions are shown on the background of experimental data to check their validity and accuracy. The comparison was made for the vertical, hot and cold water discharges where the ratios of nozzle to reservoir depth were taken as 1:5 and 1:16. It is necessary to point out that a vast majority of industrial applications lie in this similar range.

The shallow and medium range discharges were applicable to testing of the numerical results. The computational grid necessary to cover the field to yield an accurate enough solution does not in these cases, require excessive computer storage. Whereas, the computations of the deep discharges require a much larger amount of computer storage and computer time. Later in this chapter some additional numerical results will be presented.

The numerical solutions are plotted as curves on Fig.(E14) through (E22) while the dots represent the experimental data. First the axial flow will be considered. The velocity profiles Fig.(E15) and (E16) at the jet axis closely resemble experimental results near the axis, but they are off some distance away. The discrepancy between numerical and experimental results can be explained by the fact that apparently the hot film probe responded to a cross flow in the area of the vicinity to jet borders. That resulted in excessive readings in that region. Numerical evaluation of velocity along the axis Fig (E17) and (E18) coincides very closely with experimental results. The same comment may be made about temperature distributions where numerical solutions are very close to the experimental data Fig. (E19), (E20) and (E21).

For very shallow discharges, the gathering of the experimental data encounters serious difficulties. As illustrated on Fig. (20) there is high mixing and turbulence and so it is hard to determine the magnitude and particularly the direction of the velocity in this region with a strong vortex motion. Unless the velocity magnitude is large enough that one can observe visually the direction of the flow, it is difficult and sometimes impossible to find the direction of the flow. Anemeter readings of the hot film probe become meaningless when the direction of the flow is not known. For this reason, the numerical solution is of very significant importance. The computer solution lends itself also to a graphic presentation (that is a streamline pattern and a vectorially pictured velocity field), provided a plotter with a microfilm printer is available.

In the far field, (Fig. (E 21) and (E 22)) numerical results are in agreement with the experimental data with respect to velocity as well as to the temperature profiles.

Again, the computer results provide clearer information for certain regions of the flow field than could be obtained experimentally. This particularly applies to the lower part of the thermal layer where unstable conditions develop. This process was described earlier; it is also apparent from an analysis of the velocity profiles in the far field. In the surface layer the warm water spreads horizontally and the velocity vector is directed away from the jet centerline. In the lower region, the cold water moves toward the jet, being used as as entraining fluid. In the region of contact between the two layers (the surface layer and the lower layer), there is considerable shear and vortex motion with fluctuations of velocity. It becomes very difficult to measure either the magnitude or the direction of the velocity and, thus, to establish the border of the surface layer. From the numerical solution, the velocity profile is obtained and the thickness of the surface layer may be accurately determined.

The shape of the free surface was evaluated numerically through the application of the principle of the conservation of energy. The energy of vertical velocity at the free surface was converted into the energy of elevation. At the free surface, the dissipation of energy may be considered negligible. The relative height of the free surface can be calculated from the $H = V^2/2g$ relation using free surface at infinity as the base. The results were plotted against the background of the photograph showing the cross-section of the free surface.

The numerical solution may also be used to evaluate the entrainment. Experimentally, the entrainment is usually estimated indirectly by measuring the jet cross-section and relating the coefficient of entrainment to the velocity gradient. The computer program permits a direct computation of the amount of ambient water entering the jet.

The interaction of the jet with a current is demonstrated on the next page. The trajectories of the two jets are shown: one, where the jet velocity to the current velocity ratio is 1:2, and the second where the ratio is 1:4. Both, the jet and the ambient were of the same temperature.

Summary

The numerical solutions presented here covered the area of the shallow discharges for the near and far field velocity and temperature distributions. The problem of a discharge with a cross-flow and the formation of a free surface were also investigated.

All the flows investigated experimentally were turbulent and therefore for comparison between the experimental data and the numerical results it was necessary to apply the turbulent version of the computer program.

In the far field, as well as, in the far field, there is good agreement between the experimental data and the numerical results. The numerical solution offers large flexibility in application and allows the accurate evaluation of the regions that are difficult for experimental investigations.

VI. GRAPHS - EXPERIMENTAL AND NUMERICAL RESULTS

The numerical and experimental results are presented in the following pages. The numerical solutions are presented as curves on the background of dots representing the experimental data.

For greater flexibility the results were shown in the dimensionless form. Vertical distance is a percentage of the total length between the discharge nozzle ard the free surface. The horizontal distance is a ratio of length to the size of the discharge nozzle. The dimensionless velocity is a ratio of the local velocity to the velocity of the entrance. Dimensionless temperature is a ratio of the difference between the local and ambient temperatures to the difference of the entrance and ambient temperatures.

For the axial distribution of temperature and velocity the number in the upper right hand corner of each box represents the distance of the cross-section,at which the temperature, or velocity were taken, from the jet nozzle

It is important to mention that since the discharges were symmetrical, only one-half of the profile for the velocity or temperature is shown.

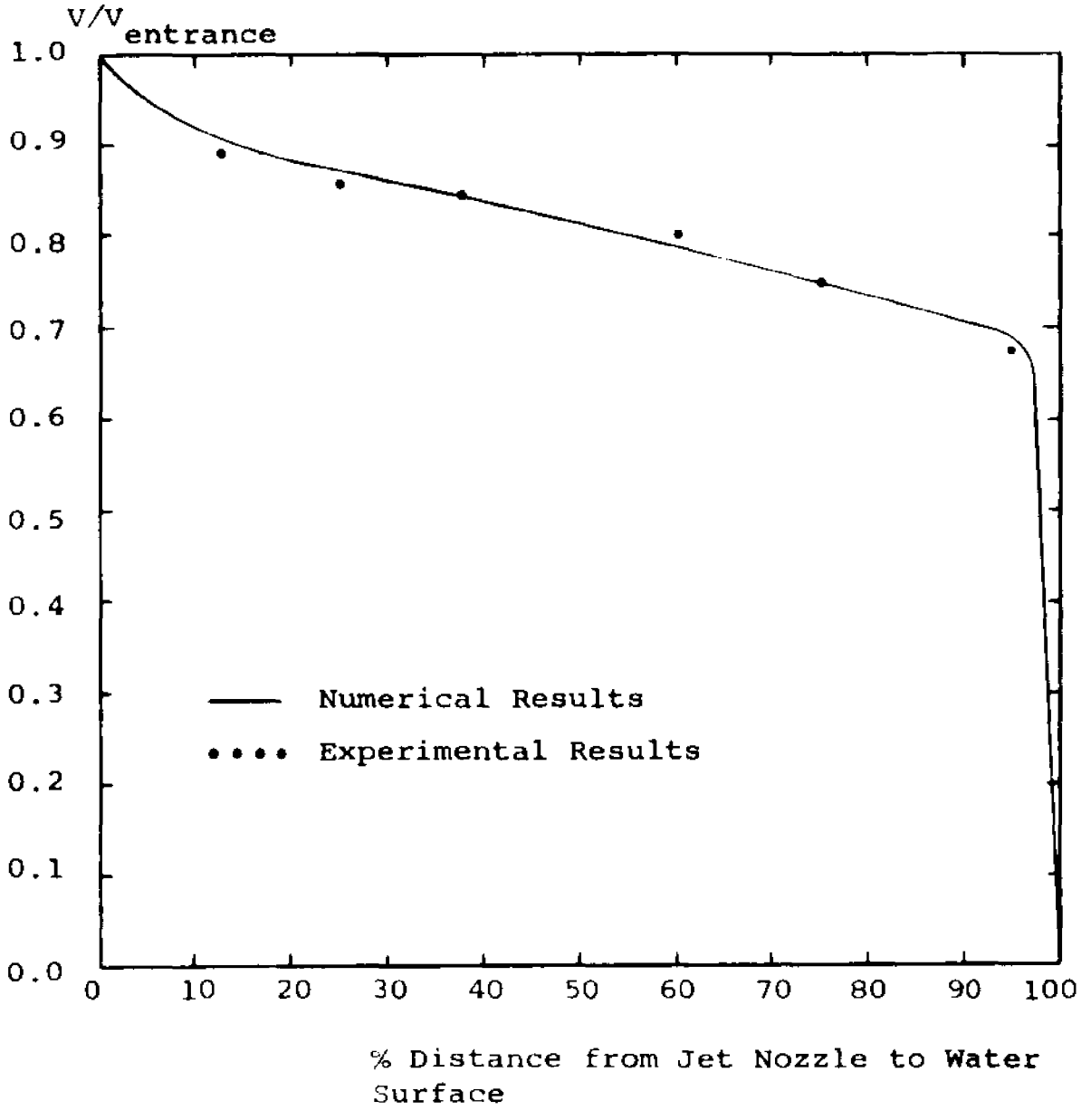

FIG. E14. NONDIMENSIONALIZED VELOCITY DISTRIBUTION ALONG JET AXIS - SIMPLE JET

Rate of Flow 0.56775 L/Min.
Depth of Reservoir 10cm.
Nozzle Size 1.9cm.

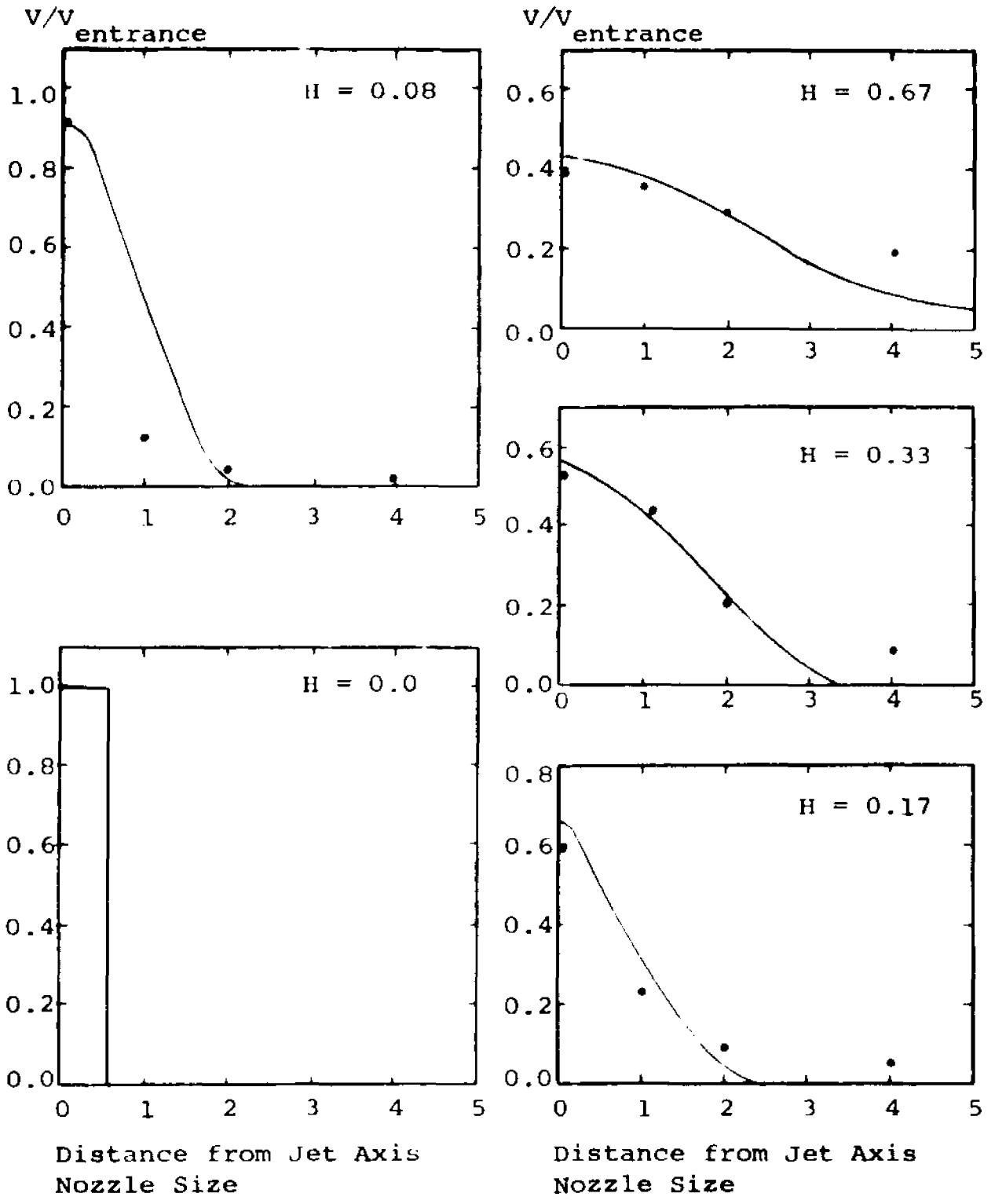

FIG. E.15. NONDIMENSIONALIZED VELOCITY AT JET AXIS

THERMAL JET

H - Distance from Jet Nozzle/Depth of Reservoir
Rate of Flow 0.56775 L/Min. Ambient Temperature 15°C
Depth of Reservoir 30cm. Entering Jet Temperature 30°C
Nozzle Size 1.9 cm.

Measurements were taken at 5 vertical locations

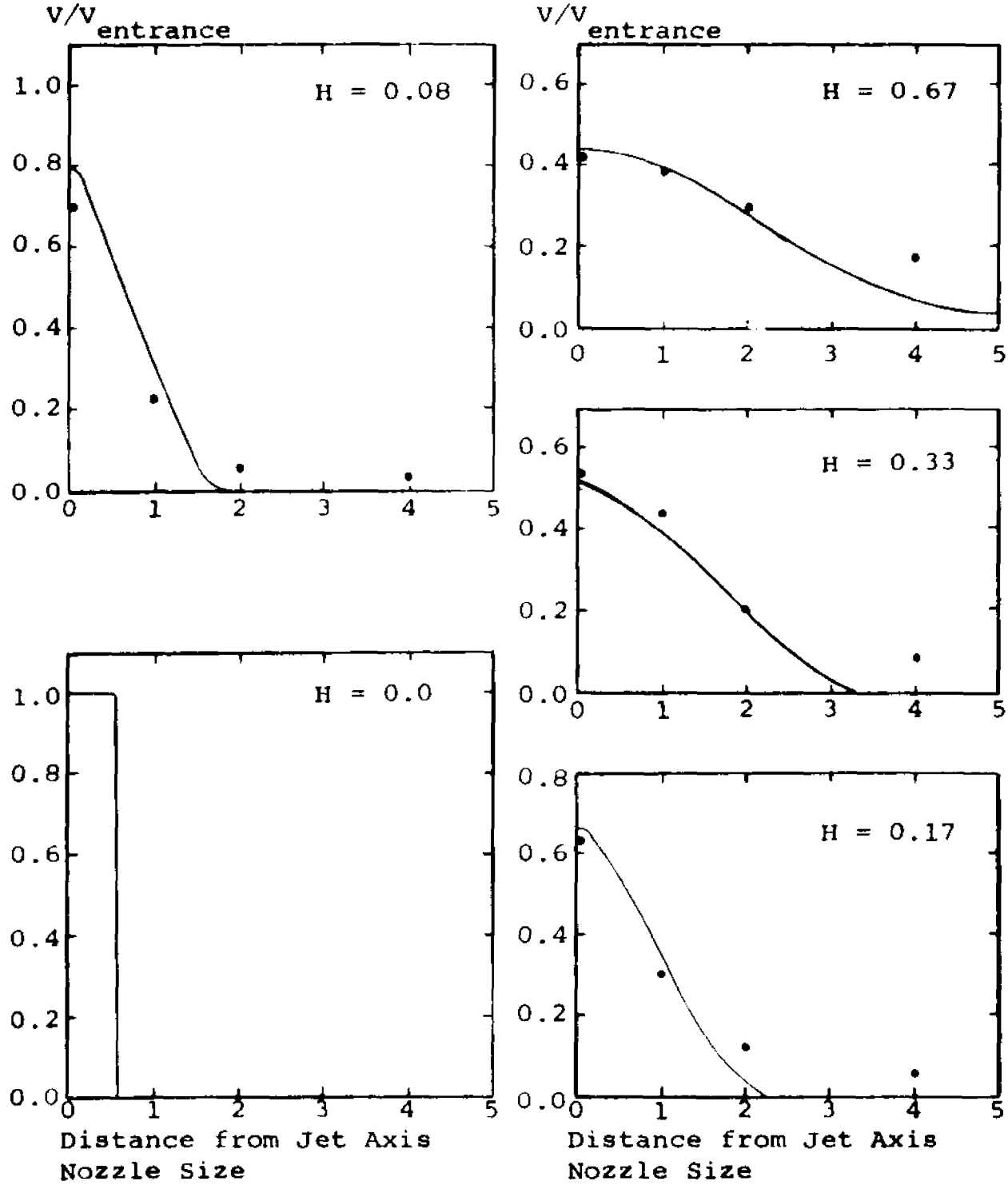

FIG. E.16. NONDIMENSIONALIZED VELOCITY AT JET AXIS

SIMPLE JET

H - Distance from Jet Nozzle/Depth of Reservoir
Rate of Flow 0.56775 L/Min. Nozzle Size 1.9 cm.
Depth of Reservoir 30 cm.

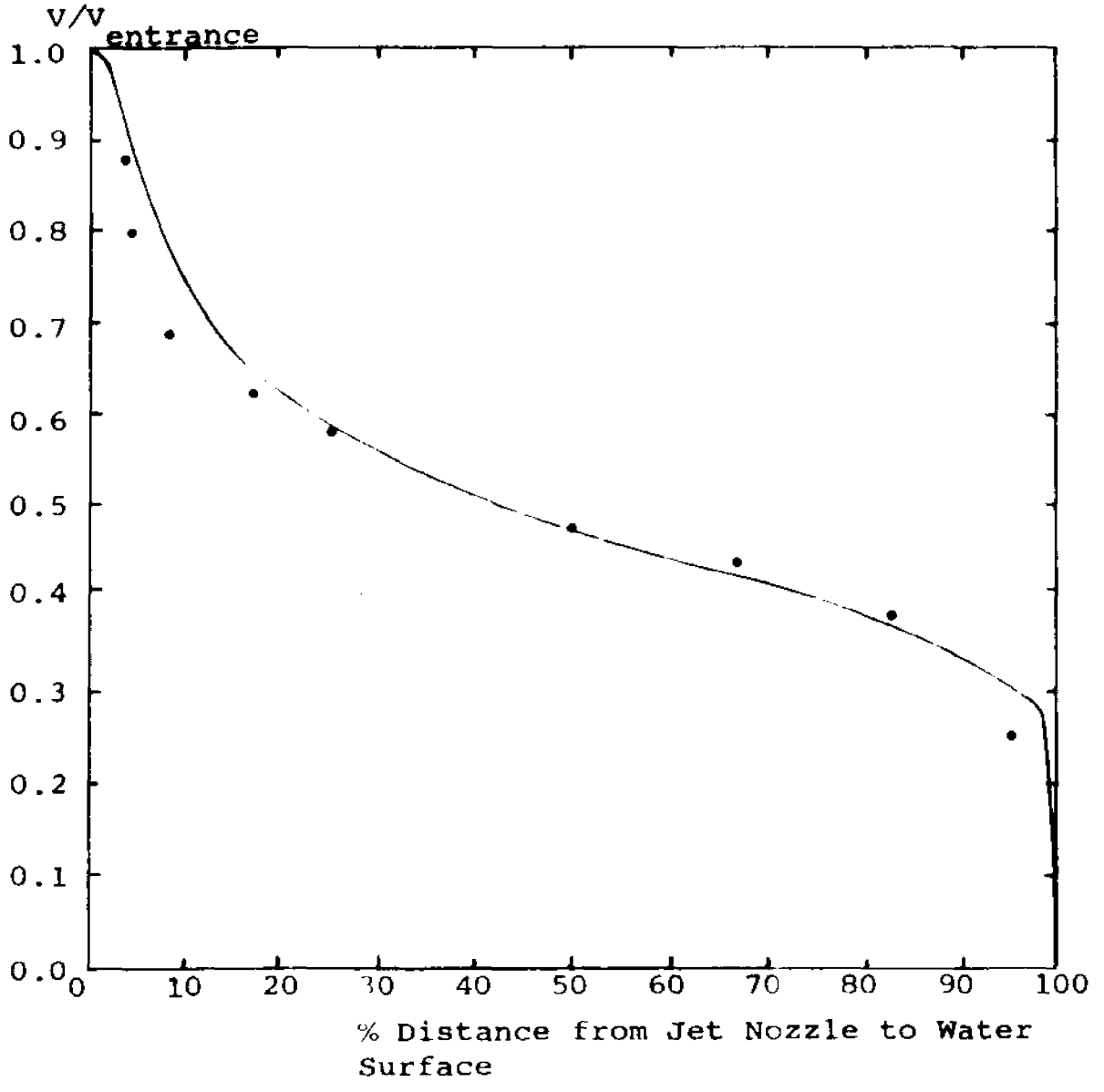

FIG. E17. NONDIMENSIONALIZED VELOCITY DISTRIBUTION ALONG JET AXIS - SIMPLE JET

Rate of Flow 0.56775 L/Min.
Depth of Reservoir 30 cm.
Nozzle Size 1.9 cm.

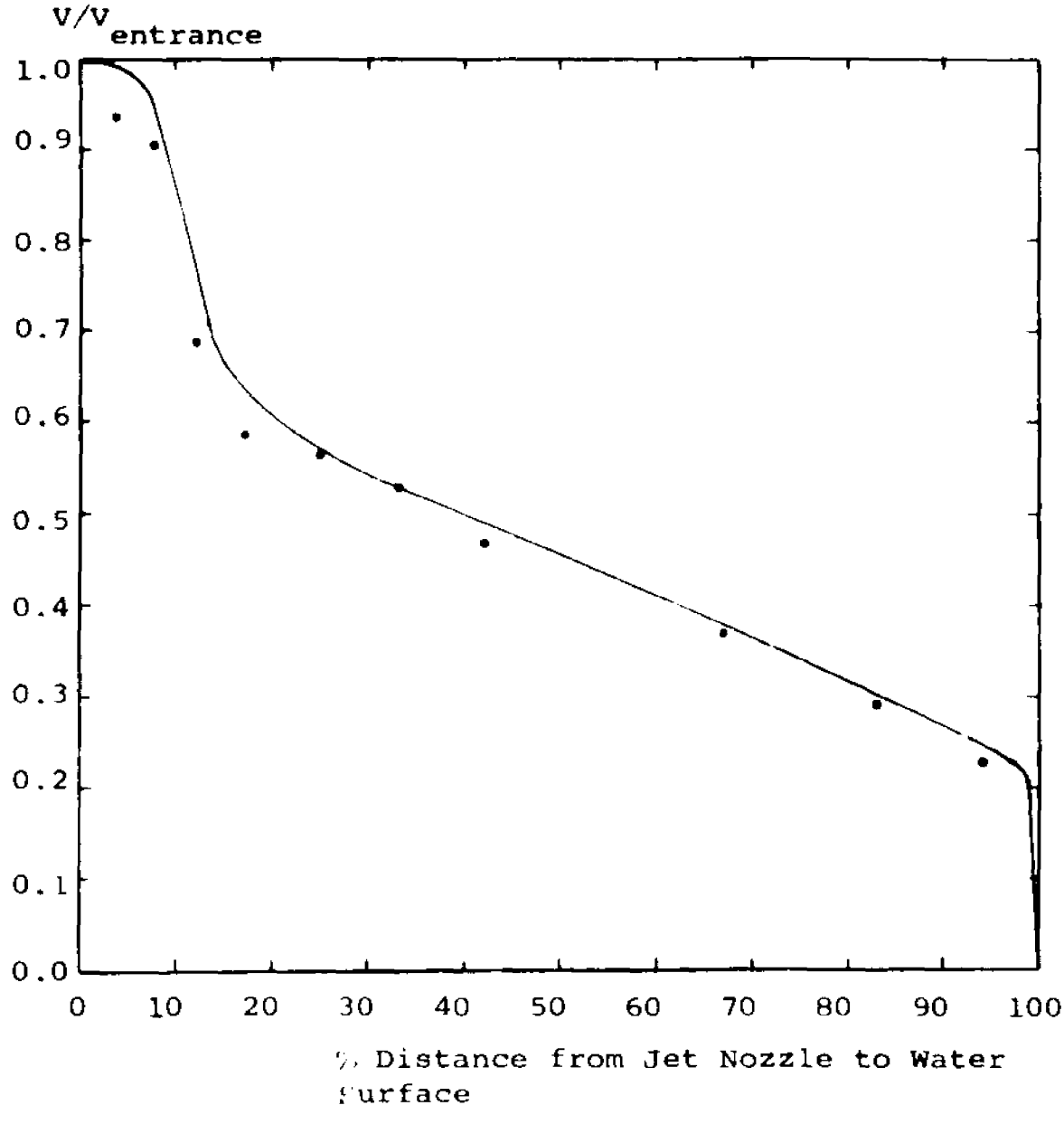

FIG. E18. NONDIMENSIONALIZED VELOCITY DISTRIBUTION ALONG JET AXIS - THERMAL JET

Rate of Flow 0.56775 L/Min.
Depth of Reservoir 30cm.
Nozzle Size 1.9cm.
Ambient Temperature 15°C
Entering Jet Temperature 30°C

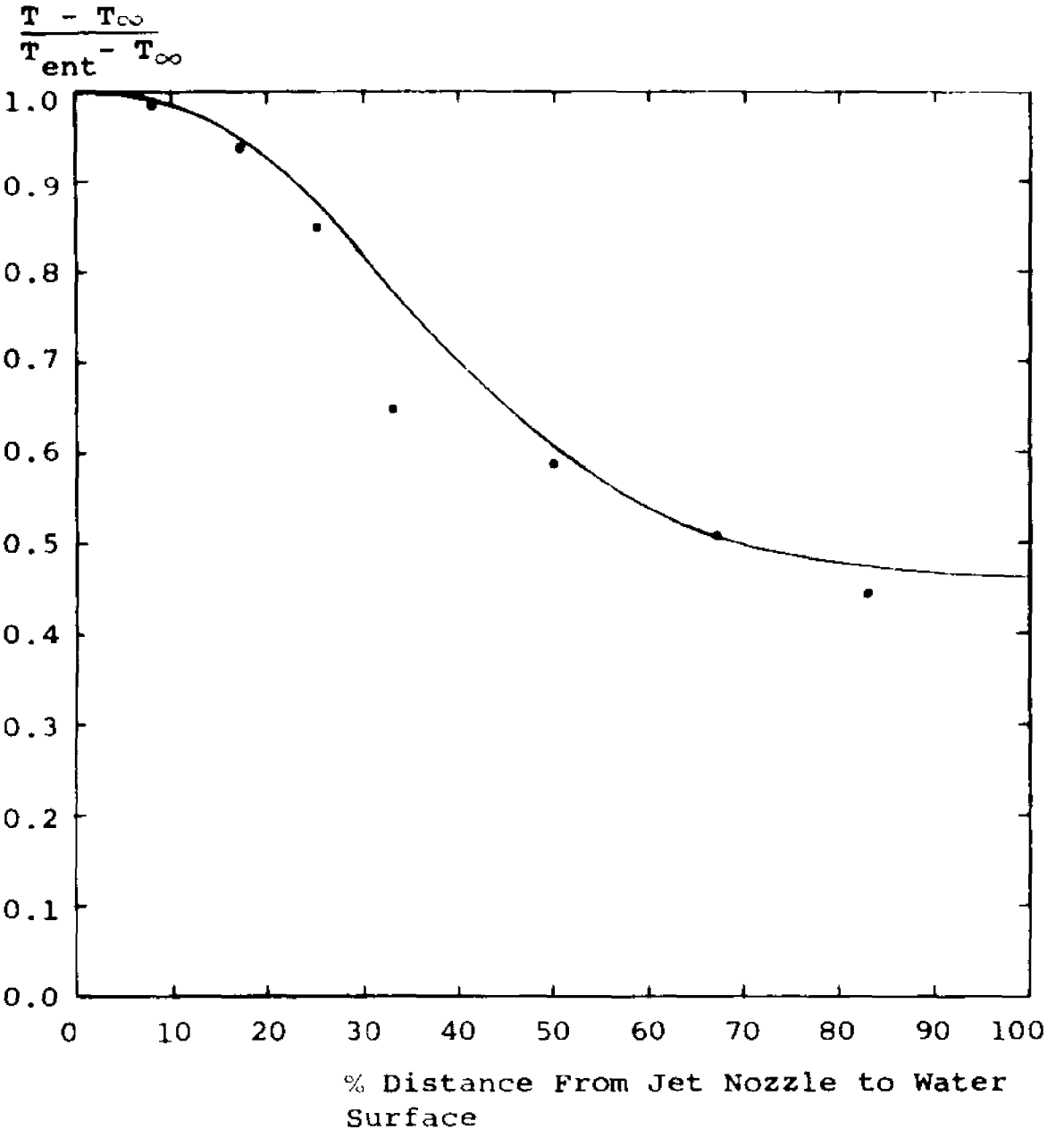

FIG. E19. NONDIMENSIONALIZED TEMPERATURE DISTRIBUTION ALONG JET AXIS - THERMAL JET

Rate of Flow 0.56775 L/Min.
Depth of Reservoir 30cm.
Nozzle Size 1.9cm.
Ambient Temperature 15°C
Entering Jet Temperature 30°C

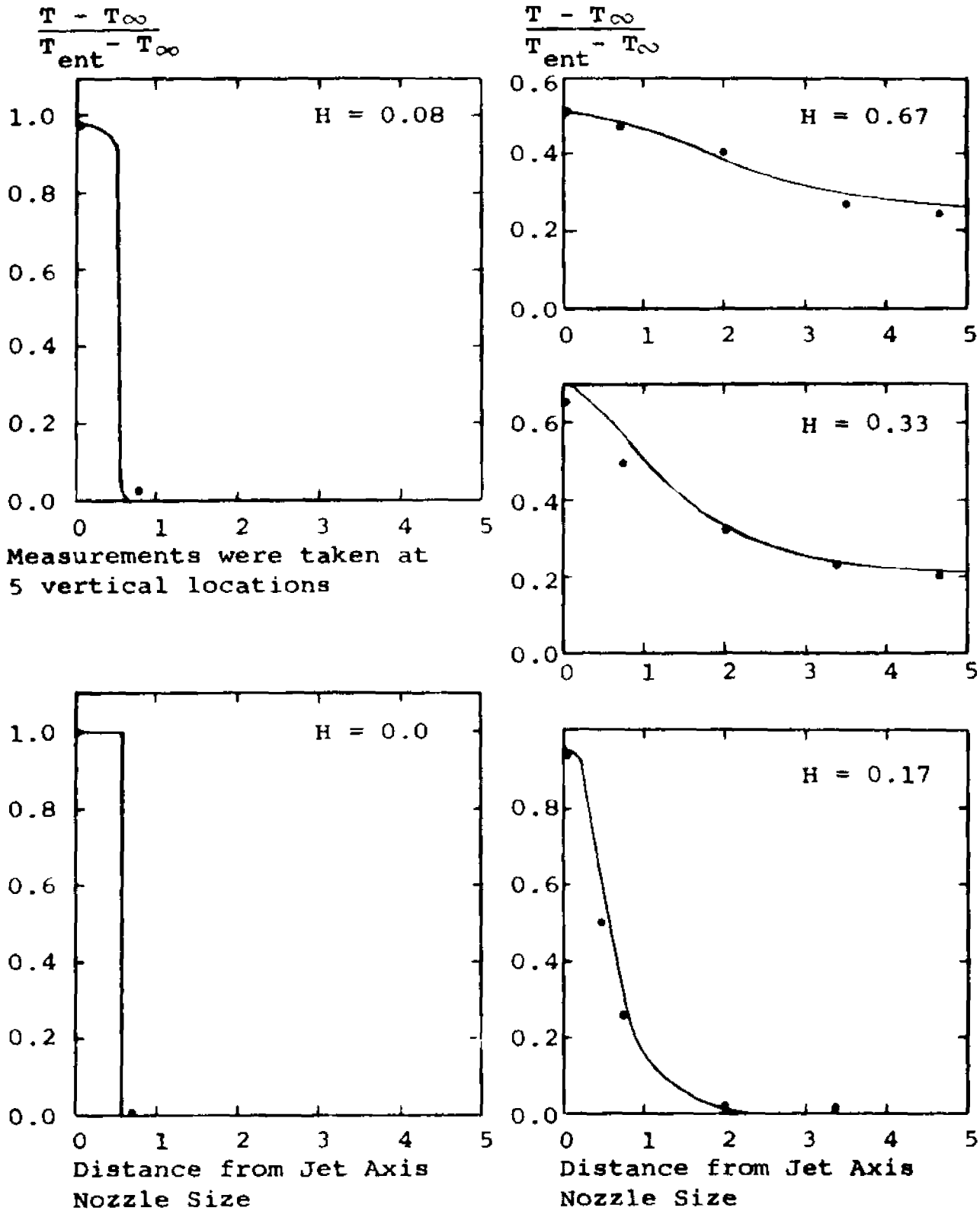

FIG. E.20. NONDIMENSIONALIZED TEMPERATURE AT JET AXIS

H - Distance from Jet Nozzle/Depth of Reservoir
Rate of Flow 0.56775 L/Min. Ambient Temperature $15^{o}_{o}C$
Depth of Reservoir 30 cm. Entering Jet Temperature $30^{o}C$
Nozzle Size 1.9 cm.

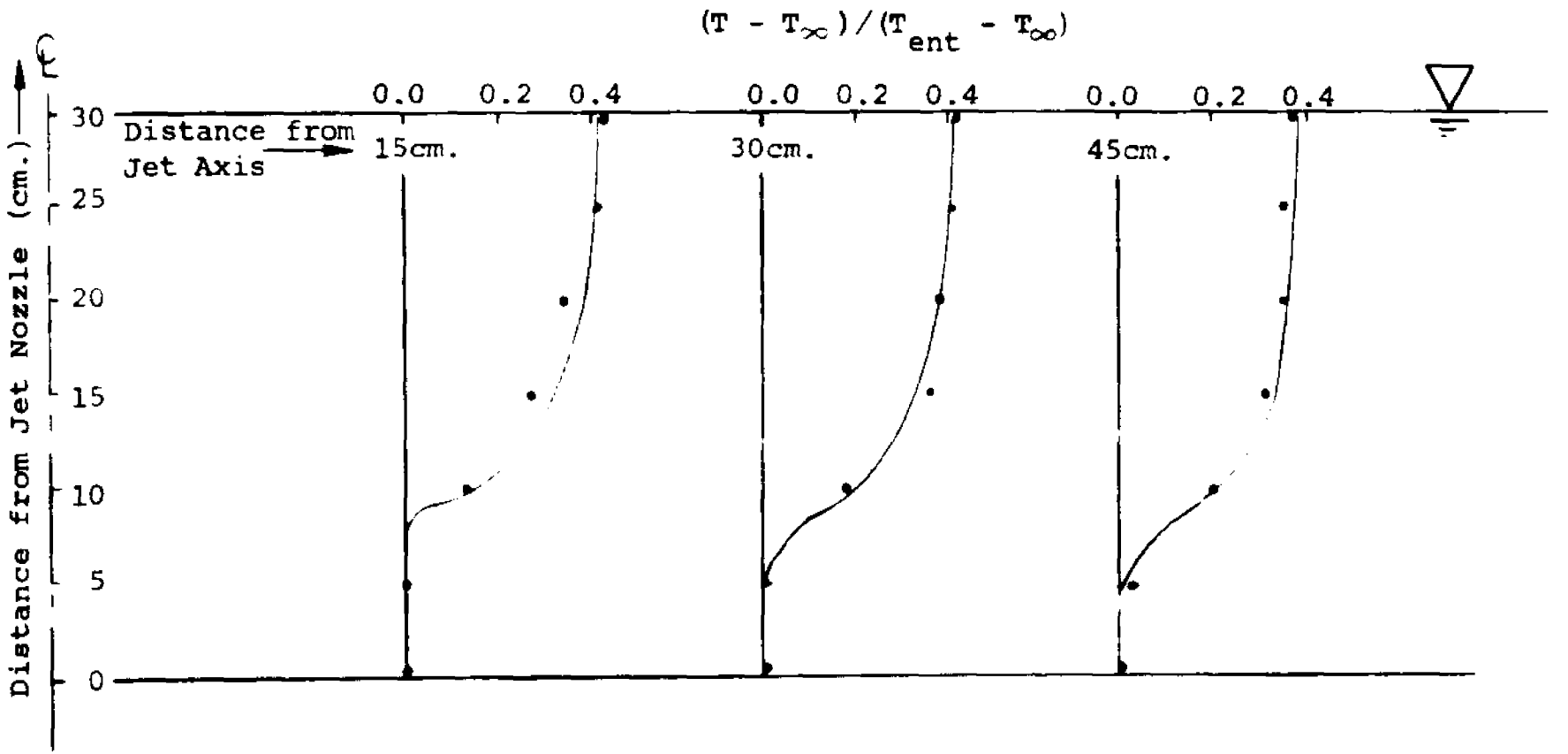

FIG. E21. NONDIMENSIONALIZED TEMPERATURE PROFILES IN THE FAR FIELD

Rate of Flow	0.56775 L/Min.	Ambient Temperature	15°C
Depth of Reservoir	30 cm.	Entering Jet Temperature	30°C
Nozzle Size	1.9 cm.		

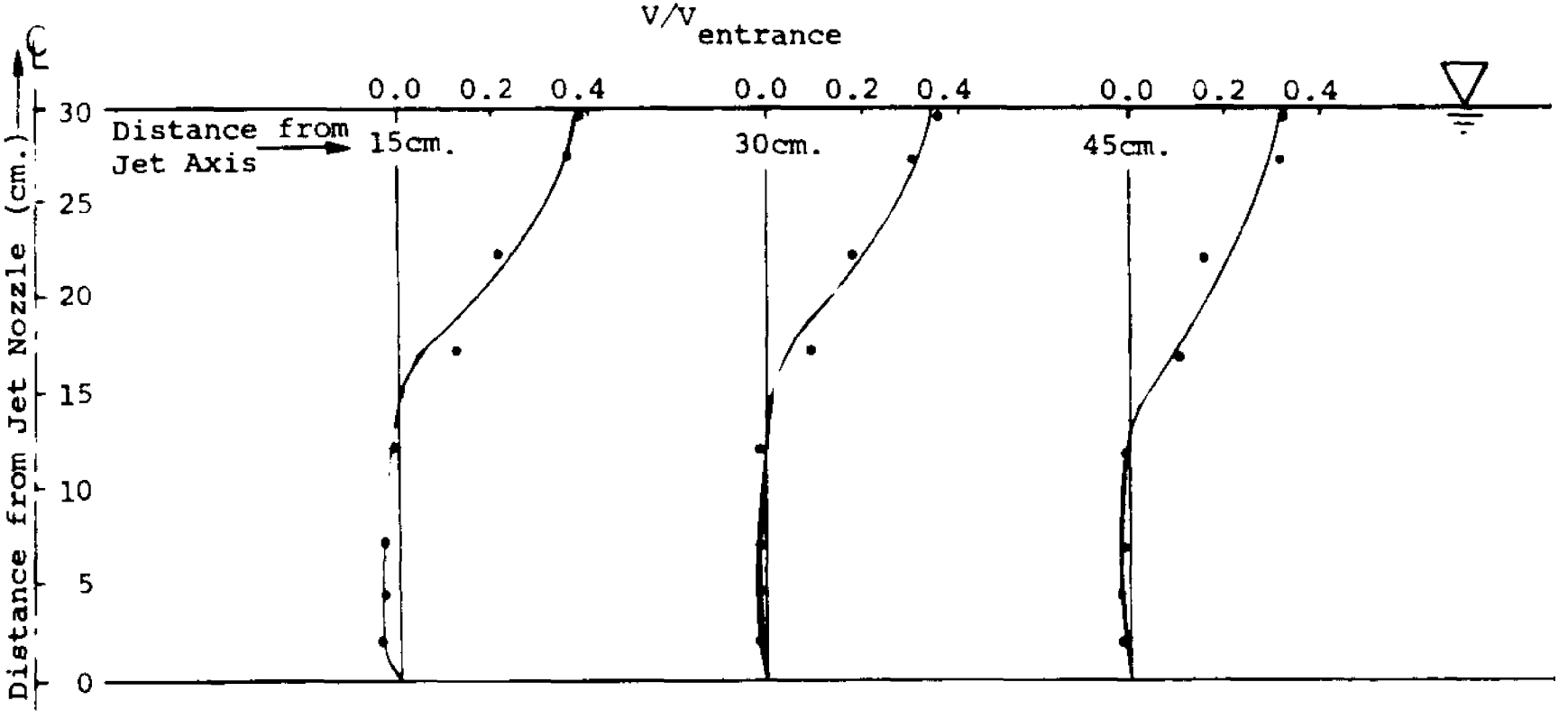

FIG. E22. NONDIMENSIONALIZED VELOCITY PROFILES IN THE FAR FIELD - THERMAL JET

Rate of Flow	0.56775 L/Min.	Ambient Temperature	15°C
Depth of Reservoir	30 cm.	Entering Jet Temperature	30°C
Nozzle Size	1.9 cm.		

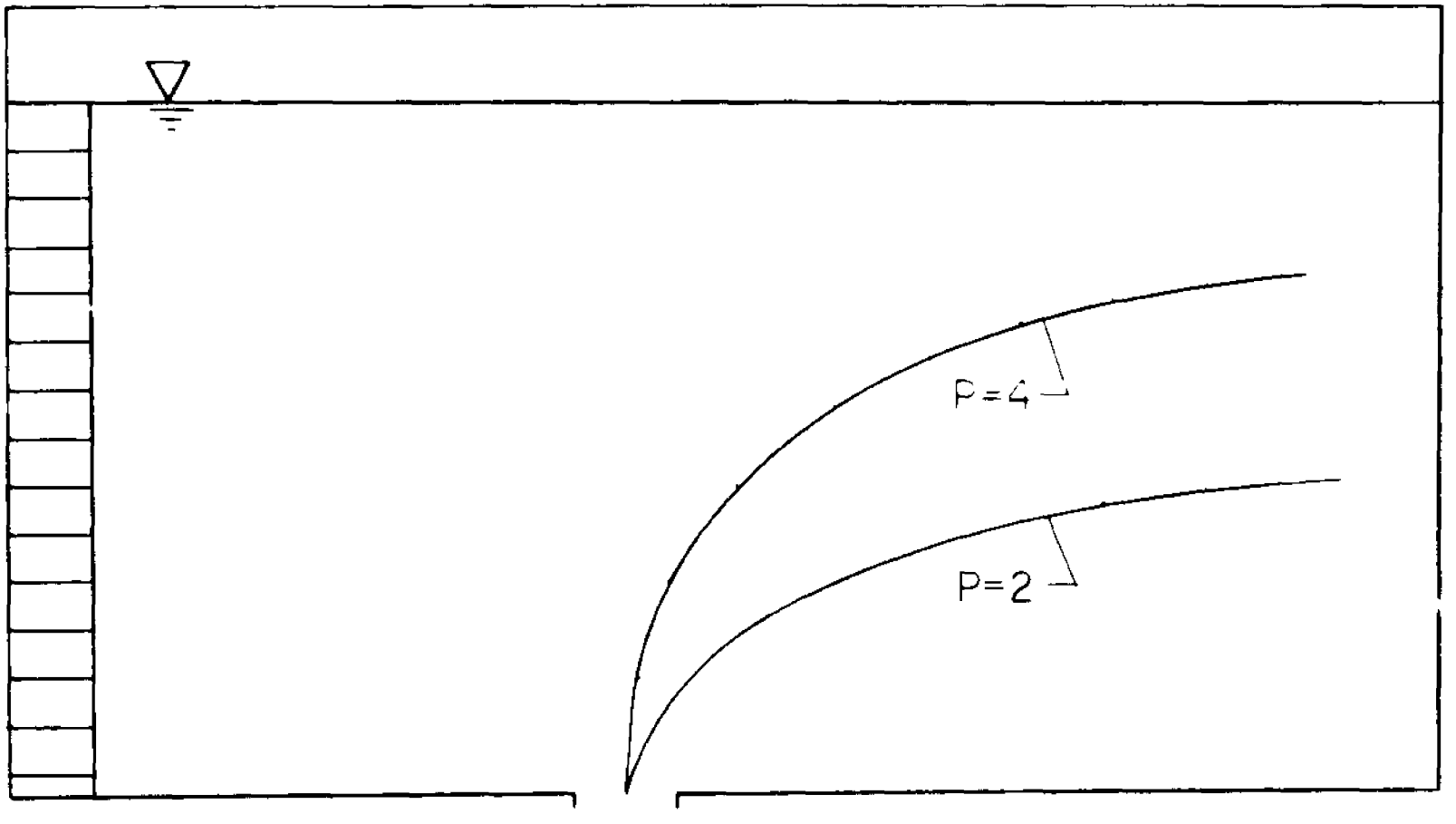

FIG. E23. TRAJECTORIES OF JET IN A CROSS - FLOW

$$P = \frac{\text{Jet Velocity}}{\text{Current Velocity}}$$

VII. DISCUSSIONS AND CONCLUSION

In this chapter, a brief summary of this research will be given. The discussion on numerical and experimental results, applicability of used methods and assumptions, limitations and other comments will be presented.

The primary result of this dissertation was the development of theoretical background and numerical solution of a thermal jet problem. The computer program is general enough to include major types of two-dimensional, time dependent flows. The turbulent energy spectrum in the wave number k space was analyzed on the way to an evaluation of the physical phenomena and certain expressions in turbulence. This provided a closure for a system of turbulent flow equations.

Not only can the velocity, temperature and pressure distribution in the flow field be obtained but also the turbulence intensity, eddy viscosity and mean square vorticity as well. The types of flow that may be investigated include horizontal and vertical discharges with stationary, or flowing ambient, where the reservoir may be stratified or of a uniform temperature distribution. Depending on the number of flow parameters and external conditions, discharges may be of laminar or turbulent character. To accommodate this fact, there are two versions of the solution developed i.e., the laminar and the turbulent one. The applicability of either one is discussed later in this chapter.

The physical modeling of the flow was also a part of this dissertation. The vertical jets of various discharge rates and temperatures were investigated. The depth of the reservoir and the discharge nozzle size were varied also.

Thus, flow patterns in both deep and shallow discharges were examined. Experimental data on velocity and temperature distributions were gathered and a comparison of numerical and experimental results was made.

The numerical evaluation of turbulent flows is of very significant importance. There are very few limiting cases where some analysis is applicable to a problem. Otherwise, numerical methods are necessary to obtain solutions. The equations of transport are strongly coupled, nonlinear partial differential equations. Even with the assumption of the isotropic turbulence, the equations for turbulent flow are extremely complicated and, therefore, the application of finite difference methods to them is not trivial. It is not possible, at present, to perform numerical calculations of turbulent flows unless the turbulence is presented by some appropriate model. The turbulent flow expressions developed here permit, in a relatively simple way, an evaluation of the impact of turbulence on the flow.

Many numerical solutions of turbulent flow problems include a large number of universal constants which were introduced during the evaluation of correlations of various turbulent quantities. Although it is not obvious from the immediate inspection, in most cases only a very restricted range of a numerical value of a certain constant will lead to satisfactory results. Although it was not possible to eliminate them (universal constants), there are very few of these constants present in this solution. Their magnitude is based on experiments, or was evaluated and tested by previous investigators and in the present work. It is necessary to mention that the values of 1.6 and 1.8 for σ were also applied in the program. It was found that the numerical solution was not sensitive to the changes of σ in this range due apparently to the very large magnitude of other terms.

Applicability of Laminar and Turbulent Solutions

The laminar approximation of the flow has a computational advantage over a turbulent one because it is a lot simpler. Thus, it would be reasonable to use the laminar flow assumption wherever possible. The applicability of either assumption will now be discussed.

For the flows with a very low velocity, laminar approximation is sufficient, since the viscous dissipation is of primary importance and turbulence is nonexistant, or of a very small intensity. The inertia forces in the flow field are balanced by the viscous forces and the laminar solution is in good agreement with reality.

For higher magnitudes of velocity, however, the laminar solution does not work. The inertia forces, which now have a considerable magnitude cannot be satisfactorily balanced by the viscous forces alone and tne numerical solution blows up. This is very well justified by the physical process. In the case of a turbulent flow assumption, large velocities and velocity gradients generate turbulence of a high intensity and subsequently, the turbulent dissipating mechanism. To an increase of velocity corresponds an increase of turbulence intensity. Then, turbulent viscosity increases as well as the turbulent dissipation and, thus, the system balances itself.

It should be added here that similar situations develop if instead of a large velocity, there is a large temperature gradient. An unstable situation may develop if the buoyancy force is not balanced. The reason is the same as the one described above.

The restrictions discussed earlier apply to the jet problems where there is a continuous supply of momentum. If the momentum is not supplied to the flow continuously, but once or, sporadically, at some time intervals, the earlier restriction about the laminar flow mau be seriously relaxed. The danger of the solution blowing up is much smaller because viscous forces will eventually dissipate supplied energy. Holding the solution stable may require very small time step dt in some cases. Its magnitude (dt) being in some inverse proportion to the momentum that is supplied. This has to be investigated very carefully.

Limitations of the Numerical Solution

The main problem is the size of the computer storage. The mesh size, at least in the region immediate to the jet nozzle, must be no larger than the nozzle itself. That presents no problem for the shallow or medium discharges but when the ratio of the depth to the nozzle size becomes 50:1, 100:1 or even larger, the demand of computer storage becomes too high. Variable mesh size offers some flexibility which permits an extension of the range of solutions. That is also restricted, however, because the ratio of dx to dy in any particular region should be within certain limits, otherwise, distorted results are obtained, or instability develops.

The table presented here gives an estimate about storage requirements for various sizes of computational grids for laminar and turbulent flows:

Size	Variables laminar	Variables turbulent	Total lam.	Total turb.	Storage laminar	Storage turb.
10 x 20	10	14	2000	2800	8000	11200
20 x 20	10	14	4000	5600	16000	22400
40 x 40	10	14	16000	22400	64000	89600

Together with the increase of the grid size the amount of computer time necessary to reach steady state also increases.

In addition to a large number of variables, the turbulent flow calculations are much more complicated because of the complex character of turbulent flows. It is, however, not the complexity of expressions that is a major factor in the required computer time, but it is the evaluation of the potential function (that is, solution of the Poisson's equation) by iterations, on each time step that is so time consuming. Size of the time step dt which is dependent on the magnitude of entrance velocityand temperature difference is also very important. The larger the velocity (or temperature difference), the smaller the time step, and subsequently a longer time for computations is necessary to reach a steady state.

The range of magnitude of entrance velocity is large and is quite sufficient to cover cases of industrial applications for thermal discharges. The absolute limit is not specified, since it would depend on a number of flow parameters particular to a given situation. Temperature may be defined more closely. It must be higher than freezing and may extend to the region below the boiling point. Near the boiling point the Boussinesq assumption on incompressibility would not hold up. Temperature range is also quite sufficient for industrial applications.

Accuracy of Experimental Measurements

The measurement of velocity becomes a complex problem when there is a temperature change in the flow field. Hot film probe readings are in some proportion to the heat transfer from the probe by convection. There is no difficulty in velocity measurement in the fluids of uniform temperature, but if the temperature is not constant it is necessary to compensate for its changes. For that reason, the temperature compensated probe was used. The reaction of the anemometer scale to the velocity changes is almost instantaneous. The reaction for the temperature compensation is somewhat slower (of the order of a few seconds), so there is a possibility of some error being introduced into the readings. Since, however, the data were gathered for a steady flow, the error would be averaged out and the obtained readings were accurate enough.

Another difficulty that may distort the data in certain circrumstances is because of the fact that the anemometer readings may be affected by a cross-flow. In other words, the probe would respond not only to the velocity component parallel to its axis, but also to some extent to the velocity in the other directions. In the regions of the flow where the direction of the velocity is rather well defined, the readings would be accurate enough. In the area of high mixing and vortex motion, however, the results may become seriously distorted. To obtain most accurate data, hot film results were verified by the Pitot tube readings whenever possible.

The measurement of temperature posed no difficulties for the accumulation of steady flow data.

VIII. BIBLIOGRAPHY

1. Abraham, G., "Horizontal Jets in Stagnant Fluid of Other Density," Proc. ASCE, J. Hyd. Div., HY1 (Jan. 1967), pp. 63-68.
2. Abramovich, G. N., "The Theory of Turbulent Jets," English edition translated by Scripta Technica, MIT Press, Cambridge, Mass. (1963).
3. Albertson, M. L., Dai, Y. B., Jensen, R. A. and Rouse, H., "Diffusion of Submerged Jets," Trans. ASCE, 115 (1950) pp. 639-97.
4. Anwar, H. O., "Behavior of Buoyant Jet in Calm Fluid," Proc. ASCE, J. Hyd. Div. 95 HY4 (July 1969) pp. 1289-1303.
5. Bampfield, J. F., "A Moire Pattern Technique for the Detection of Shockways," NOL Report No. NOLTR 67-57, (Jan. 1968)
6. Brock, R. R., "Power Law Solutions for Vertical Plumes," Proc. ASCE J. Hyd. Div. 96 HY9 (Sept. 1970) pp. 1803-17.
7. Brooks, N. H., "Diffusion of Sewage Effluent in an Ocean Current," Cal. Inst. of Technology, Civil Eng. Dept.
8. Chorin, A. J., "Numerical Solution of the Navier-Stokes Equations," Math. Comp. 22 745 (1968).
9. Chorin, A. J., "A Numerical Method for Solving Incompressible Viscous Flow Problems," J. of Comput. Phys. 2 (1967) pp. 12-26.
10. Daly, B. J., Harlow, F.H., "Transport Equations in Turbulence," Phys. of Fluids vol. 13 No. 11 (Nov. 1970) pp. 2634-49.
11. Donaldson, du P. C., Rosenbaum, H. and Sullivan, R., "Theoretical Study of the Generation of Atmospheric Clear Air Turbulence," AIAA Paper No. 70-55 (1970).

12. Fage, A., Falkner, V. M., "The Transport of Vorticity and Heat through Fluids in Turbulent Motion," Proc. Roy. Soc. (London) A, vol. 135.

13. Fan, L. N. and Brooks, N. H., Discussion of Ref. 1, Proc. ASCE, J. of Hyd. Div., HY 2 (March 1966), pp. 423-29.

14. Fan, L. N., and Brooks, N. H., "Numerical Solutions of Turbulent Buoyant Jet Problems," W.M. Keck Lab. of Hydraulics and Water Resources, Report No. KH-R-18, Cal. Institute of Technology.

15. Fan, L. N., "Turbulent Buoyant Jets into Stratified or Flowing Ambient Fluids," W.M. Keck Lab. of Hydraulics and Water Resources, Report No. KH-R-15, Cal. Institute of Technology (Jan. 1969).

16. Förste Von J., "Die ebene laminare Stromung in einem Halbraum bei kleiner Reynolds-Zahl," Zamm 43 (1963) Hoft 7/8, pp. 353-59.

17. Forsythe, G. E., and Wasow, W. R., "Finite Difference Methods for Partial Differential Equations," John Wiley & Sons Inc. (1960).

18. Fromm, J. E., "Numerical Solutions of the Nonlinear Equations for a Heated Fluid Layer," Phys. of Fluids vol. 8 No. 10 (Oct. 1965).

19. Grigg, H. R., and Stewart, R. W., "Turbulent Diffusion in a Stratified Fluid," J. of Fluid Mech., 15 (1963), pp. 174-86.

20. Harlow, F. H., and Nakayama, P. I., "Turbulence Transport Equations," Phys. of Fluids vol. 10 No. 11 (Nov. 1967).

21. Hinze, J. O., "Turbulence," McGraw Hill Book Company (1969).

22. Hirst, E. A., "Analysis of Round, Turbulent, Buoyant Jets Discharged to Flowing Stratified Ambients," Oak Ridge National Laboratory, (June 1971).

23. Hirst, E. A., "Analysis of Buoyant Jets Within the Zone of Flow Establishment," Oak Ridge National Laboratory, (Aug. 1971).

24. Hirt, C. W., "Computer Studies of Time-Dependent Turbulent Flows," Phys. of Fluids, Suppl. II (1969), pp. 219-27.

25. Keffer, J. F., and Baines, W. D., "The Round Turbulent Jet in a Cross-Wind," J. of Fluid Mech., 15 (1963) pp. 481-96.

26. Kovasznay, L. S. G., and Nee, V. W., "Simple Phenomenological Theory of Turbulent Shear Flows," Phys. of Fluids vol. 12 No. 3 (1969), pp.473-84.

27. Lawler, G. P., "Mathematics of Estuarine Pollution," Engineering Aspets of Marine Waste Disposal, (June 1965) by Quirk, Lawler and Matusky Engrs.

28. Lawler, J. P. and Leporati, J. L., "Receiving Water Temperature Distributions from Power Plant Thermal Discharges an Estuarine Model," (Feb. 1969), by Quirk, Lawler and Matusky Engrs.

29. Lawler, Leporati, Lawler, "Receiving Water Temperature Distribution from Power Plant Thermal Discharges - Lake Model," Engineering Aspects of Marine Waste Disposal, (May 1968), by Quirk, Lawler and Matusky Engrs.

30. Mahajan, B. M., and John, J. E. A., "Mixing of a Shallow Submerged Heated Water Jet with an Ambient Reservoir," AIAA Journal, vol.9 No. 11, (Nov.1971), pp. 2135-40.

31. Lykov, A. V., and Mikhaylov, Y. A., "Tieoria Tieplo i Masso Pierienosa," Moskva, 1963 Gosudarstviennoye Energietichеskoye Izdatielstvo.

32. Morton, B. R., "On a Momentum - Mass Flux Diagram for Turbulent Jets, Plumes and Wakes," J. of Fluid Mech., 10 (1961) pp.101-12.

33. Morton, B. R., "Forced Plumes," J.of Fluid Mech., 5 (1959) pp. 151-63.

34. Morton, B. R., "Entrainment Models for Laminar Jets, Plumes and Wakes," Phys. of Fluids vol. 10 No. 10 (Oct. 1967).

35. Morton, B. R., Taylor, G. I., and Turner, J. S., "Turbulent Gravitational Convection from Maintained and Instantaneous Sources," Proc. Roy. Soc. London, A234 (1956), pp. 1-23.

36. Pai, S., "Fluid Dynamics of Jets," D. Van Nostrand Co. Inc., 1954.

37. Ricou, F. P., and Spalding, D. B., "Measurements of Entrainment by Axisymmetrical Turbulent Jets," J. of Fluid Mech., 11 (1961), pp. 21-32.

38. Saffman, P. G., "A Model for Inhomogeneous Turbulent Flow," Proc. Roy. Soc. London, A317 (1970) pp. 417-33.

39. Sami, S., Carmody, T. and Rouse, H., "Jet Diffusion in the Region of Flow Establishment," J. Fluid Mech., (1967) vol. 27, part 2, pp. 231-52.

40. Sharp, J. J., "Spread of Buoyant Jets at the Free Surface," Proc. ASCE J. Hyd. Div. 95 HY4, (May 1969), pp. 811-25.

41. Staniszewski, B., "Wymiana Ciepla - Podstawy Teoretyczne," Panstwowe Wydawnictwo Naukowe, Warszawa, 1963.

42. Tchen, C. M., "On the Spectrum of Energy in Turbulent Shear Flow," J. of Research of Natl. Bur. Standards., 50, 51 (1953).

43. Tchen, C. M., "Transport Process as Foundations of the Heisenberg and Obukhoff Theories of Turbulence," Phys. Rev., 93, 4 (1954).

44. Tulin, M. P., and Schwartz, J., "Hydraulic Aspects of Waste Discharge," AIAA Paper No. 70-755, (July 1970).

45. Von Karman, Th., and Lin, C.C., "On the Statistical Theory of Isotropic Turbulence," Advances in Applied Mechanics, vol.II, (1951).